REMOVAL OF MERCURY (II) FROM WATER USING BIOSYNTHESIZED SILVER AND IRON NANOPARTICLES

BY

SALAWU OMOBAYO ADIO

A Thesis Presented to the
DEANSHIP OF GRADUATE STUDIES

KING FAHD UNIVERSITY OF PETROLEUM & MINERALS

DHAHRAN, SAUDI ARABIA

In Partial Fulfillment of the
Requirements for the Degree of

MASTER OF SCIENCE

In

ENVIRONMENTAL SCIENCE

MAY, 2016

KING FAHD UNIVERSITY OF PETROLEUM & MINERALS

DHAHRAN- 31261, SAUDI ARABIA

DEANSHIP OF GRADUATE STUDIES

This thesis, written by **SALAWU OMOBAYO ADIO** under the direction of his thesis advisor and approved by his thesis committee, has been presented and accepted by the Dean of Graduate Studies, in partial fulfillment of the requirements for the degree of **MASTER OF SCIENCE IN ENVIRONMENTAL SCIENCE.**

Dr. Basheer Chanbasha
(Advisor)

Dr. Abdulaziz M. Al - Shaibani
Department Chairman

Dr. Bassam Tawabini
(Member)

Dr. Zafarullah Khan
(Member)

Dr. Salam A. Zummo
Dean of Graduate Studies

29/5/16
Date

© Salawu Omobayo Adio
2016

This work is dedicated to the memory of my mum, whose love and care continue to light my way in dark places when all other lights go out.

And

To my son, Sultan Hamdan Omotayo Salawu

ACKNOWLEDGMENTS

All praise be to Allah, the author and finisher of my faith. I am most grateful to my supervisor, Dr. Basheer Chanbasha who believed so much in me that he gave me the opportunity to explore and guided me when I faltered. I wish to acknowledge the efforts of Dr. Bassam Tawabini in mentoring me throughout my studies and during my thesis. Dr. Zafarullah Khan provided insightful comments and constructive criticisms where necessary. I am sincerely grateful to him.

My profound gratitude goes to King Fahd University of Petroleum and Minerals (KFUPM) for providing me with the opportunity to pursue my masters. I will also like to appreciate the members of Dr. Basheer research group and Centre for Environment and Water. I am sincerely grateful to the Deanship of graduate studies, Geosciences department, Chemistry department and Centre for Excellence in Nanotechnology for their inputs in this work.

I am grateful to the following people who made my stay in KFUPM memorable; Abduljamiu Amao, Mustapha Animashaun, Taoreed Lawal, Gaddafi DanMaliki, Mohammed O. Hussein, Tajudeen O., B. Akeem, A. Mahfouz, Saravanna, Rajan, Musah A., A. Abdi, Abdulrazaq A., S. Solikan.

I wish to express my gratitude to my dear friends; David Alaka, Aisha Adeyemi, Tobiloba Olusanya and Mustapha Kabiru for their love and care always.

Most importantly, none of this would have been possible without the love and support of my immediate family. I am forever indebted to Dr. and Mrs Salawu Omotayo.

To those whose name I have unintentionally omitted in this acknowledge, you are appreciated and I intend to make a comprehensive list in subsequent work.

I owe my gratitude to all those people, mentioned or not, who have made this thesis a success.

TABLE OF CONTENTS

LIST OF TABLES

LIST OF FIGURES

LIST OF ABBREVIATIONS

AgNP	-	Silver nanoparticles
BET	-	Brunauer–Emmett–Teller
EDX	-	Energy dispersive spectroscope
Fe_2O_3	-	Iron oxide nanoparticles
FE-SEM	-	Field emission scanning electron microscopy
nZVI	-	Nanoscale zero valent iron
TGA	-	Thermogravimetric analysis
mg/L	-	Milligram per Liter
mg/g	-	Milligram per Gram
µg/	-	Microgram per Liter

ABSTRACT

Full Name : [SALAWU OMOBAYO ADIO]

Thesis Title : [Removal of mercury (II) from water using biosynthesized silver and iron oxide nanoparticles]

Major Field : [Environmental Science]

Date of Degree : May, 2016]

This research demonstrates the ability of biosynthesized nanoparticles to be used as colorimetric sensor and as adsorbents. Biogenic synthesized silver nanoparticles were used to sensitively and selectively detect the presence of mercury cation (Hg^{2+}) in water. The effects of various factors such as broth concentration, precursor concentration, temperature, contact time and pH on the synthesis of the nanoparticles were studied. The synthesized silver nanoparticles were then used in the colorimetric detection of Hg^{2+} in water. Result showed that as-prepared AgNPs has high selectivity to detect Hg^{2+} alone compared to other cations and high sensitivity at different concentration of Hg^{2+}. The limit of detection for Hg^{2+} was as low as 6.25×10^{-8} mol L^{-1} indicating that these biogenic synthesized silver nanoparticles represent a highly sensitive Hg^{2+} detection tool. Subsequently, Silver nanoparticles (AgNP), Iron oxide nanoparticles (Fe_2O_3) and Nanoscale zerovalent iron (NZVI) synthesized using plant extract of Basil, Myrtle and Aloe Vera respectively were used for the removal of Hg^{2+} in water. The biosynthesized nanoparticles were characterized using field emission scanning electron microscopy (FE-SEM), energy dispersive X-ray spectroscopy (EDX), x-ray diffraction spectroscopy (XRD), Brunauer–Emmett–Teller (BET), Thermogravimetric analysis and Fourier transform infrared spectroscopy (FTIR). The removal process was investigated using batch mode. Results of the study revealed that

the adsorption efficiency increased with time and agitation speed. The adsorption efficiency also increased when pH of the solution increased from 4 to 7 but decreased when pH of the solution increased to 8 and 9. Increase in the dosage of the adsorbent also affected the percentage removal of Hg^{2+}. Langmuir and Freundlich isotherms were used to explain the adsorption process. Silver nanoparticle having showed the highest maximum adsorption capacity was dispersed in polyacrylonitrile and electrospun. A nanofiber was prepared and fitted in a filter cartridge and used in column studies for the removal of Hg^{2+}.

ملخص الرسالة

الاسم بالكامل : سالاو أوموبايو أديو

عنوان البحث: أزالة كتيون الزئبق II من الماء باستخدام جسميات الفضة واكسيد الحيديد النانوية المحضرة بولوجيا

التخصص: علوم بيئية

تاريخ نيل الدرجة: أبريل ، 2016

هذا البحث يشرح فعالية الجسيمات النانوية المحضرة بطريقة بيولوجية والتي تم استخدامها كحساس ضوئي و مادة ادمصاص. جسميات الفضة النانوية المحضرة حيويا استخدمت للكشف عن كاتيون الزئبق II في الماء بحساية وانتقائية جيدة.تمت دراسة عدة عوامل على الجسيمات النانوية كتركيز الخليط (خليط مستخلص النبات ونترات الفضة) ، تركيز المادة البادئة، درجة الحرارة، زمن الأتصال و الرقم الهيدروجيني. بعد ذلك تم استخدام الجسيمات النانوية المحضرة في الكشف الضوئي لكاتيون الزئبق II في الماء.

أضهرت النتائج ان جسيمات الفضة النانوية لها انتقائية عالية تجاه كاتيون الزئبق II عندما يكون لوحدة مقارنة مع كاتيونات اخرى ولها حساسية عالية مع تراكيز مختلفة ل كاتيون الزئبق II. حد الكشف لكاتيون الزئبق II كان صغيرا وكان 6.25×10^{-8} مول لكل لتر وهذا يدل ان جسيمات الفضة النانوية تمثل اداة كشف ذات حساية عالية للكشف عن كاتيون الزئبق II. بعد ذلك تم تحضير جسيمات الفضة النانوية، جسيمات اوكسيد الحديد النانوية و الحديد صفر التكافؤ النانوي باستخدام طريقة كيميائية خضراء باستخدام مستخلص نبات الريحان، الاس و الصبار وتم استخدامهم لازالة كاتيون الزئبق II من الماء.

تم تشخيص الجسيمات النانوية المحضر حيويا باستخدام المجهر الماسح الضوئي، الاشعة السينية متشتتة الطاقة، مطيافية الاشعة السينية, محلل .Brunauer–Emmett–Teller (BET) ، تحليل الثقل النوعي الحراري و مطيافية الاشعة تحت الحمراء. تم التحقق من عملية الأزالة باستخدام الأسلوب الدفعي، واظهرت النتائج ايضا ان فعالية الادمصاص

تزيد بزيادة الزمن و سرعة التحريك. تمت زيادة فعالية الادمصاص عند رفع الرقم الهيدروجيني من 4 الى 7 ولكنها نقصت عندما وصول الرقم الهيدروجيني الى 8 و 9. زيادة كمية المدمص ايضا اثرت على نسبة فعالية ازالة كتيون الزئبق.

تم استخدام ايزوثيرم لانجمور و فراوندلش لتفسير عملية الأدمصاص. و أضهرت جسيمات الفضة النانوية اعلى سعة ادمصاص وتم تشتيتها على بولي اكربلونترايل بوليمر واستخدام طريقة الغزل الكهربي. تم تحضير الياف نانوية مبدئية واستخدامها في خرطوشة مرشحة واستخدمت في دراسات العمود لأزلة متيون الزئبق II

CHAPTER 1

INTRODUCTION

1.1 Background

The need for potable water, in the wake of increasing human population and industrial growth, is headed for an upsurge. The increasing demand for water cuts across various industrial and domestic sectors and it suitability for use depends on its quality; the quality of available water primarily for drinking is decreasing rapidly.

The availability of potable water has become an issue globally and in some areas, has resulted in water scarcity, especially in the face of climate change. It has been reported that over 1 billion people lack access to potable water while millions die annually as a result of water-borne diseases (Malato et al., 2009). In the quest to sustain the demand resulting from growing human populations and to support technological advancement, anthropogenic activities such as mining, agriculture, and other industrial activities have resulted in high pollution of available water bodies. Chemical pollutants such as organic elements and chlorides, inorganic and heavy metals can be released into water bodies either intentionally or accidentally. This affects human populations, either directly, resulting in outbreak of disease peculiar to unhygienic environments or through bio-accumulation in living organisms. In the latter case, it may result in changes in the natural ecosystem or in disease outbreaks in humans after consumption.

For regions such as arid ones where water is a non-renewable resource, adequate wastewater treatment and desalination have been the two most promising water recycling techniques (Gutub et al., 2013). The need for better wastewater treatment techniques has become even more challenging and a necessity due to the growth and expansion of industries that uses toxic chemicals and pollutants in their production process and hence releases these toxic pollutants into marine, surface and groundwater bodies.

1.2 Heavy metal removal technologies

Heavy metals pollution plays a major role in the reduction of water quality in available water resources and the increase in the cost of wastewater recycling. Large quantities of industrial metal-containing waste water are released to water bodies (Al-Saad et al., 2012). This poses danger to aquatic organisms and reduces water quality for domestic use. Different techniques have been applied in the removal of heavy metals from wastewater. The technique selected depends largely on it efficiency in the removal of the heavy metal under study. Some of the techniques that have been used include;

1.2.1 Flotation

Flotation process involves producing small air bubbles, of sizes less than 0.1mm, as attachments to remove heavy metals from water. The application of flotation in waste water treatment was adopted from mineral processing (froth flotation) where it is used to separate different minerals from each other. Flotation can be dissolved air flotation, precipitate flotation, electrolytic flotation, ion flotation, dispersed air flotation. The main types of flotation applied for the removal of heavy metals in waste water treatment include;

Dissolved Air Flotation involves the formation of an agglomerate of particle and small air bubbles with a density lower than the density of water. The lower density of the agglomerates ensures that they float and accumulate on the surface of the water where they can be easily removed by skimming. The efficiency of dissolved air flotation depends on the number of bubbles generated, nature and size of the particles to be removed, the presence of dispersive agent in the water to be treated. Although the application of dissolved air flotation as a stand-alone technique in waste water treatment has been studied in the past, recently it use has been in combination with other waste water treatment technique or with a slight modification to enhance the efficiency of heavy metal removal. Al Zoubi *et al*., (2015) used different commercial polymers as collectors in enhancing dissolved air flotation process for the removal of cadmium, nickel, manganese and lead from water. Santander and Valderrama (2015) removed arsenic from synthetic effluent using adsorbent particle flotation and dissolved air flotation. Coagulation and dissolved air flotation has also been combined for the removal of chromium (VI) from water using ferric chloride and polyaluminium chloride as coagulant (Esmaeili *et al*., 2014).

Ion Flotation has been applied for the removal of heavy metals from waste water. In this process, the heavy metals present in water is rendered hydrophobic by the addition of surfactant and subsequently removed by bubbling air in the water. The method was developed by Sebba and published in 1959.

Precipitation Flotation is the removal, by air bubbles, of precipitates formed in water. It involves the addition of chemical compounds Precipitate flotation can be of the first kind or second kind. In the first kind precipitate flotation, the ion of interest is precipitated in solution by the addition of a precipitating (a non-surface active) agent and subsequently

made hydrophobic by the addition of a surfactant. The second kind precipitate flotation is in contrast to the first kind and as such does not involve the addition of a surfactant. The agglomerate formed as a result of the interaction of the ion of interest and the precipitating agent is hydrophobic. Precipitation of heavy metals in water solution is usually done by the addition of alkali.

1.2.2 Chemical precipitation

The application of chemical precipitation technique in waste water treatment involves separation of precipitated solids formed due to the addition of chemical reagents from water. Most heavy metals are known to form precipitates of metal hydroxides or metal carbonates at alkaline pH, as such, the addition of chemicals which raises the pH of waste water and enhances the formation of these precipitates have been exploited as a waste water treatment technique. Some of the chemicals so far used include caustic soda, ash, limestone and lime.

Chemical precipitation is a widely used water treatment technique especially in industries because of its simplicity in operation. It is also a cheap waste water treatment technique and is non-metal selective. However, it is known to generate huge amount of sludge that requires extra cost to dispose as waste. It is also ineffective in the treatment of water with low concentration of heavy metals.

Chemical precipitation in waste water treatment is the formation of insoluble substances by the addition of a chemical reagent to the water. Chemical precipitation is an easy and low-cost treatment technique used in the removal of heavy metals from wastewater. Chemical precipitation of heavy metals can be hydroxide, sulfide or carbonate.

Hydroxide precipitation is the addition of an alkaline substance to wastewater to precipitate heavy metals in the solution by the formation of metal hydroxides. Metal hydroxides are sparingly soluble at high pH, as such the addition of alkaline substances increases the pH of the solution thereby precipitating the heavy metals which are subsequently removed by physical methods such as sedimentation and decantation or filtration.

Sulfide precipitation is a similar process to hydroxide precipitation. Hydrogen sulfides and sodium sulfides are mostly used to form insoluble heavy metal sulfides. Precipitates of metal sulfides are more insoluble when formed compared to precipitates of metal hydroxides within the same pH range.

1.2.3 Ion exchange

Dissolved water impurities dissociate to form ions. The exchange of an ion, temporal holding of the ion and release of the ion to a stronger regeneration solution characterizes an ion exchange process in water treatment. In most cases, the impurities are removed from water by exchanging them with another ion. Ion exchange is carried out to soften, deionize, de-alkalize, or disinfect water. It can also be applied for mixed bed polishing, nitrate removal or the selective removal of different contaminants. The exchange medium can be made up of montmorillonite, clay, zeolites, polymers (exchange resin), synthetic organic resins and clay or humus soil. Typical ion exchangers are cationic, anionic or amphoteric.

1.2.4 Electrochemical treatment

Electricity has been used for water treatment since 1889 when it was first used in the United Kingdom. It is efficient and preferred to most other water treatment technologies because it does not result in the generation of sludge and can be fully automated. However it is

capitally intensive because it requires the generation of continuous electric supply. As a result of this, it has not been widely accepted like other conventional water treatment techniques. There are different types of electrochemical treatment used in water treatment. Some examples of electrochemical treatment processes are; electrocoagulation, electroflotation, electrodisinfection, electrooxidation, electrodeposition and electrophotooxidation.

In electrocoagulation, hydrogen gas generated at the cathode is used to float the contaminant of interest (Chen, 2004). Coagulants and metal ions are generated at the anode by the electrolytic oxidation of an anode material. The metal of concern is removed from solution when it react with ion of opposite charge or a metallic hydroxide floc generated within the effluent (Mollah *et al.,* 2001). Electrode arrangement in a typical electrocoagulation set up may be monopolar or bi-polar.

The removal of Cu, Ni, Zn and Mn have been demonstrated using monopolar – Iron electrodes with high efficiency especially for Cu, Ni and Zn and at high pH (Al-Aji *et al.,* 2012). The removal of As (III) and As (V) is affected by the type of electrode used and the current density (Kumar *et al.* 2004). In Arsenic contaminated water, the removal of the contaminants by electrocoagulation can be due to the oxidation of As (III) to As (V) accompanied by adsorption/complexation (Kumar *et al.,* 2004).

Different studies have been carried out aimed at reducing the cost of running an electrochemical treatment process in water treatment. Soliso et al (1999) and Marco et al. (1999) compared the use of simple platinum and stainless steel AISL 904L plate as cathode in place of three dimensional electrodes for the treatment of copper II from industrial effluent. While copper foam is expensive alternative, it was discovered that it performs

better in the removal of copper (II) because they have high surface area and supply better performances. Electrochemical reactions take place on the high surface area of three dimensional electrodes thereby decreasing the current density (Exposito, 1999). Stainless-steel sheets and Ruthenium oxide coated titanium have been used as cathode and anode respectively to treat Cu2+, Cr^{6+} and Ni^{2+} in wastewater (Hunsom et al., 2005). The method proved to be very efficient and requires low consumption of energy and is cost effective. Electrochemical water treatment process can also be combined with other techniques in the removal of heavy metals.

1.2.5 Coagulation/Flocculation

Coagulation and Flocculation are simple and cheap water treatment techniques that have been applied for centuries for the removal of dissolved and suspended particles in water. Suspended particles in water are made up of negative charges which creates a repulsive force between them and hinders the formation of removable clumps. Coagulation, the addition of coagulants, overcomes the opposing forces; enhancing particle collision, growth of flocs and formation of large agglomerates (microflocs), which are subsequently removed by sedimentation and/or filtration. Temperature and sequence of chemical addition affects a coagulation process. Coagulation in water treatment follows three consecutive steps; addition of coagulants, destabilization of particles and agglomeration of destabilized particles. Chemical coagulants are of three types; Organic polymers, inorganic electrolytes and synthetic polyelectrolytes. Inorganic electrolytes are mainly compounds of aluminum and iron such as ferric chloride, ferrous sulfate, aluminium sulfate, aluminum chloride. Hydrated lime and magnesium carbonates have also been used in coagulation process. Synthetic polyelectrolytes coagulants are functional groups of anions and cations.

Flocculation process clarifies water as a result of the formation of precipitate which is then removed by physical methods. While flocculation does not involve overcoming particle charges, polymers of high molecular weight are added to water in a flocculation process to clump particles together into microflocs and as such enhance their removal.

Coagulation-Flocculation process is sometimes combined with other conventional water treatment techniques to aid the removal of heavy metals. Machado et al., (2008) applied bioremediation-flocculation and sedimentation in the removal of Cu^{2+}, Ni^{2+}, Zn^{2+}, Cd^{2+} and Cr^{3+} from synthetic effluents. Brewer's yeast strain was applied as a flocculant. The flocculating ability of the yeast strain was also studied in the removal of Cu^{2+} from water (Soares, 2002). Charerntanyarak (1999) applied lime and polymer in a combined chemical coagulation and precipitation process for the removal of Zn, Cd, Mn and Mg from synthetic waste water.

1.2.6 Membrane Technologies

Different membranes have been applied in water treatment. It involves the use of thin porous materials for the removal of water impurities. Some main membrane technologies used in water treatment so far include;

1.2.6.1 Ultrafiltration

Ultrafiltration is a type of membrane filtration in which hydrostatic pressure or concentration gradient is used to force a liquid through a semi-permeable membrane. Ultrafiltration is an accepted technique in industrial waste water treatment for the removal of macromolecules from water. It is readily applied for the removal of suspended solids and solutes of high molecular weights. For an enhanced removal of heavy metals,

ultrafiltration can be modified by the addition of polymer or surfactant. Based on this, ultrafiltration is divided into two; polymer enhanced also known as complexation-ultrafiltration or micellar enhanced. Complexation-ultrafiltration is the use of water soluble polymers to increase the size of metal ions. When these polymers are added, a macromolecule of higher molecular weight and large enough to be trapped when the water passes through an ultrafiltration membrane is formed. The efficiency of a polymer enhanced ultrafiltration process is affected by pH, the presence of other metal ion in the solution to be treated, the ratio of metal to polymer, the type of polymer used and the metal to be treated. Micellar enhanced ultrafiltration is the addition of surfactant to water such that the concentration of the surfactant exceeds the critical micelle concentration. Micelles formed in the process bind metal ions and form an aggregate of metal and surfactant that are large enough to be trapped in an ultrafiltration membrane. The use of micellar enhanced ultrafiltration in the removal of heavy metals from water is affected by membrane type pore sizes of membrane used, surfactant concentration, temperature, competing metals, pH, co-presence of organics and heavy metals, salt concentration, the use of non-ionic surfactant, operating pressure and additives (Bade and Lee, 2011). Heavy metal removal using ultrafiltration is simple and relatively chemical free. It produces less sludge and hence lower cost of sludge disposal, requires less attention of the operator and is effective.

The application of ultrafiltration in heavy metal removal has been studied extensively (Zhang et al., 2015, Libya et al., 2015, Ferella et al., 2007 Bade et al., 2007, Aoudia et al., 2003). Carboxy methyl cellulose and Polyethersulfone (FUS 0181) were used as metal complexing agent and ultrafiltration membrane respectively for the removal of Cu (II), Ni (II), and Cr (III) from wastewater (Barakat et al., 2010). The process was found to be pH

dependent and requires low energy. Plyehtersulfone was also found to be highly selective for the metal ion considered. Maleic acid and acrylic acid (PMA-100) used as copolymers also produced very high efficiency in the removal of Cu (II), Zn (II), Ni (II) and Mn (II) from water at pH 6 (Qiu and Mao, 2013). The copolymers were chosen as an attempt to reduce the dosage of polymer used and thus enhance the economic potential of their use in the treatment process. They are known to contain high carboxyl group content that could correspond to high metal ion capacity. They are also water soluble, non-toxic and stable under high temperature. Cetyltrimethylammonium bromide (CTABr) use as a surfactant in micellar enhanced removal of hexavalent chromium revealed that chromium adsorption capacity on the surfactant increased its concentration and pH and decreased with temperature rise, adsorbent dosage and the concentration of other ions in the solution (Sadaoui, 2009). Other surfactants that have been used include, sodium dodecyl sulfate (SDS) for Cd (II) and Zn (II) removal (huang et al., 2010), cetylpyridinium chloride for the removal of arsenic (V) (Gecol et al., 2004) sodium dodecyl sulfate and monoalkylphenol polyetoxilate, anionic and non-ionic surfactant respectively, for the removal of Ni (II) from water (Yurlova et al., 2002). Combined cetyltrimethylammonium bromide (CTAB) and cetylpyridinium chloride (CPC) for the removal of Cr (VI) (Kamble, 2005).

1.2.6.2 Reverse osmosis

Water treatment using reverse osmosis technique is achieved by passing contaminated water through a semi-permeable membrane under the influence of pressure. The principle of treating water by reverse osmosis is a reversal of a simple osmosis process. Water has the tendency to move from a region of lower salt concentration to that of higher salt concentration when both regions are separated by a semi-permeable membrane (osmosis).

In order to reverse this process, a pressure high enough to counter the normal osmotic pressure and force the water to move in the opposite direction to its normal flow is exerted. When water flows in the opposite direction through the membrane, some of the ions, dissolved salts and micro-organisms are trapped in the membrane. One advantage of reverse osmosis is that cross filtration is employed in the water treatment process. Cross filtration ensures that while treated water passes through the membrane to the pure water outlet, the contaminants in the untreated water goes in a different direction instead of clogging on the membrane. Turbulence around the membrane ensures that it is kept clean and free from contaminants. Diffusion governs water movement across the semi-permeable membrane used in reverse osmosis and illustrated in equation 1.

$$J_w = A\ (\Delta P - \Delta\pi) \qquad (2.1)$$

Where J_w is water flux across the membrane, A is the water permeability coefficient; ΔP and $\Delta\pi$ are difference in pressure and difference in osmotic pressure across the membrane respectively.

Reverse osmosis is a well-accepted technique in water desalination. It has also been adopted in the treatment of dissolved solids, organic and inorganic contaminants. Copper, nickel and zinc has been removed from water using reverse osmosis with polyamide thin-film composite membrane TW30-181 as semi-permeable membrane (Bakalár et al., 2009). While ion rejection is affected by applied and osmotic pressure, chelating agents has been used to enhance ion rejection and thus increase the overall efficiency of a reverse osmosis process in heavy metal removal (Mohsen et al., 2007). EDTA is a reliable chelating agent that supports heavy metal removal at different pressures (Ujang and Andersoon, 1996).

Other factors that affect ion rejection include feed pressure, feed pH and concentration of other ions present in contaminated water (Ozaki et al., 2002).

1.2.6.3 Nano-filtration

Nanofiltration is a relatively new and promising water treatment technique. It is mostly applied for the treatment of low total dissolved solids, polyvalent cation and disinfection by products precursors in water. Nanofiltration process is easy to use, requires low operation pressure, consumes low energy, has high efficiency in the removal of pollutant of interest and reliable. Nanofiltration process involves the use of nano-porous membranes of sizes within 1-10nm. It has divalent ion rejection and low monovalent ion rejection. It is also made up of higher flux membrane than those used in reverse osmosis. It is considered to have properties between reverse osmosis and ultrafiltration. Nanofiltration processes can either be used to treat organics and metals either in wastewater, ground water or surface water or as a pretreatment procedure for water desalination. One major drawback in nanofiltration use is fouling.

1.2.7 Adsorption

Adsorption process is the physical or chemical binding of a fluid (liquid or gas) also known as adsorbate to the surface of a material (adsorbent). It may also be referred to as material enrichment or the increase in fluid density in the vicinity of an interface. Adsorption of a solute on a particular solid surface depends on the porosity of the surface, the presence of unsaturated intermolecular forces of attraction within the surface. Adsorption is a simple, efficient, widely used and technically feasible water treatment process. The reversible nature of adsorption processes offers an opportunity to regenerate used adsorbents simply by desorption. This has increased it cost effectiveness and made it socially and

economically acceptable. It can also be used to remove contaminants at very low concentration and generates only little sludge as such does not require addition waste management.

The adsorption of an adsorbate to an adsorbent is completed in three steps; movement of the adsorbate from the solution to the adsorbent, adsorption on the adsorbate and movement within the adsorbent surface.

The interaction between contaminants with adsorbents is studied using adsorption isotherms. Adsorption isotherms describe the phenomenon governing the retention, distribution or mobility of the adsorbate from a liquid or gaseous medium to the adsorbent at constant conditions of temperature and pH. They are important for the optimization of adsorption mechanism pathways. They also provide an investigation of surface properties of different materials for use as adsorbents, adsorption capacities of the adsorbents and hence the comparison of the use of different adsorbents. Adsorption isotherms can be two parameter, three parameter or multilayer physisorption. Some notable examples of isotherms are shown in Figure 1. Langmuir and Freundlich are the most used adsorption isotherms especially in water treatment. Langmuir adsorption isotherm assumes homogeneous and monolayer adsorption. Monolayer adsorption means the adsorbed layer has one molecule in thickness. Freundlich adsorption isotherm does not assume monolayer adsorption and as such can be applied to multilayer adsorption and varying conditions of adsorption heat over a heterogeneous surface.

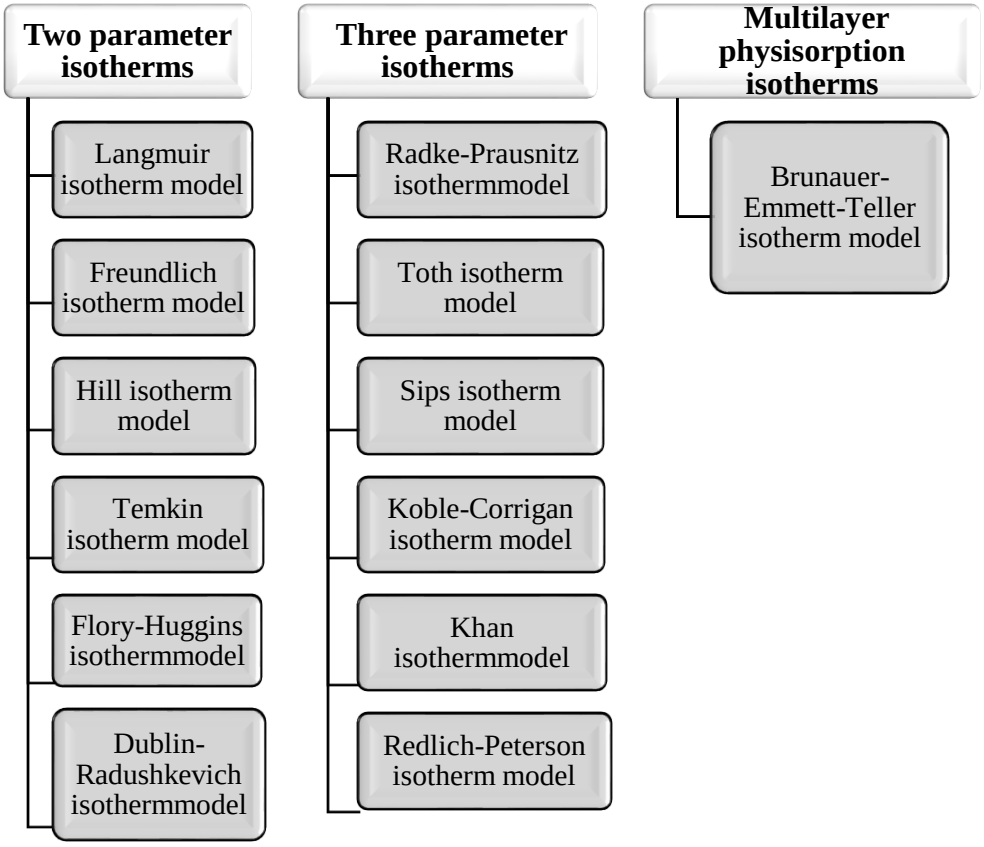

Figure 1: Classification of adsorption isotherm models

Adsorption kinetics are also used to determine the performance, mechanism and pathways involved in an adsorption process. Knowing the kinetic performance of a sorbent is imperative for it future use and for the purpose of scaling up. The rate of solute uptake, a function of the time required to complete an adsorption process, is determined from kinetics study.

The efficiency of an adsorption process in the removal of heavy metals from water depends to a greater extent on the adsorbent used. Different adsorbents have been used in the removal of heavy metals.

1.3 Mercury as a pollutant

Mercury pose the greatest concern of all heavy metal pollutants globally due to its ability to accumulate easily in the food web and its high persistence in the environment, circulating for centuries to millennia (Bernalte et al., 2011; Selin, 2009; Zahir et al., 2005). Mercury contamination may be as a result of natural processes such as volcanos and erosion of natural deposits of mercury or as a result of human use of mercury compounds in agricultural, industrial, pharmaceutical or mining activities (Holmes et al., 2009). Mercury is widely used in pesticides and fungicides, in paper milling industries, and is generated from coal burning, waste incineration and mining and processing of metals. The main sources of mercury are shown in Figure 2.

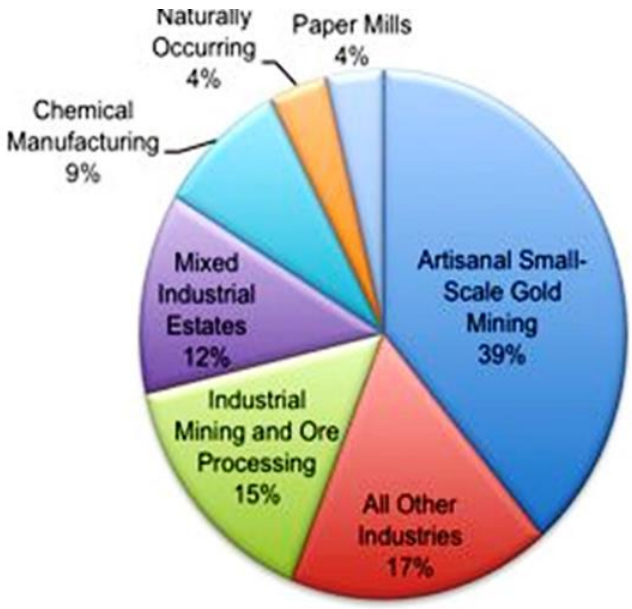

Figure 2: Main mercury sources

The properties, chemical behaviour and path way of mercury in environment depends on the type of mercury involved and its oxidation number. Mercury can exist as elemental or metallic mercury, in oxidized state as inorganic mercurial or mercuric ion, and as organic

alkyl species (Crespo-López et al., 2009; Sumesh, Bootharaju, Anshup, & Pradeep, 2011). Mercury cycle or pathway in the environment is represented in Figure 3. Organic mercury has been reported to pose more significant toxic effects due to its high solubility and diffusivity into cell membranes (Crespo-López et al., 2009). It exist as a result of the combination of mercury with organic compounds containing carbon. Once in the environment, It can bio-accumulate and bio-magnify along the food chain. Inorganic mercury exist in water in an oxidation state of +2 (Lisha & Pradeep, 2009).

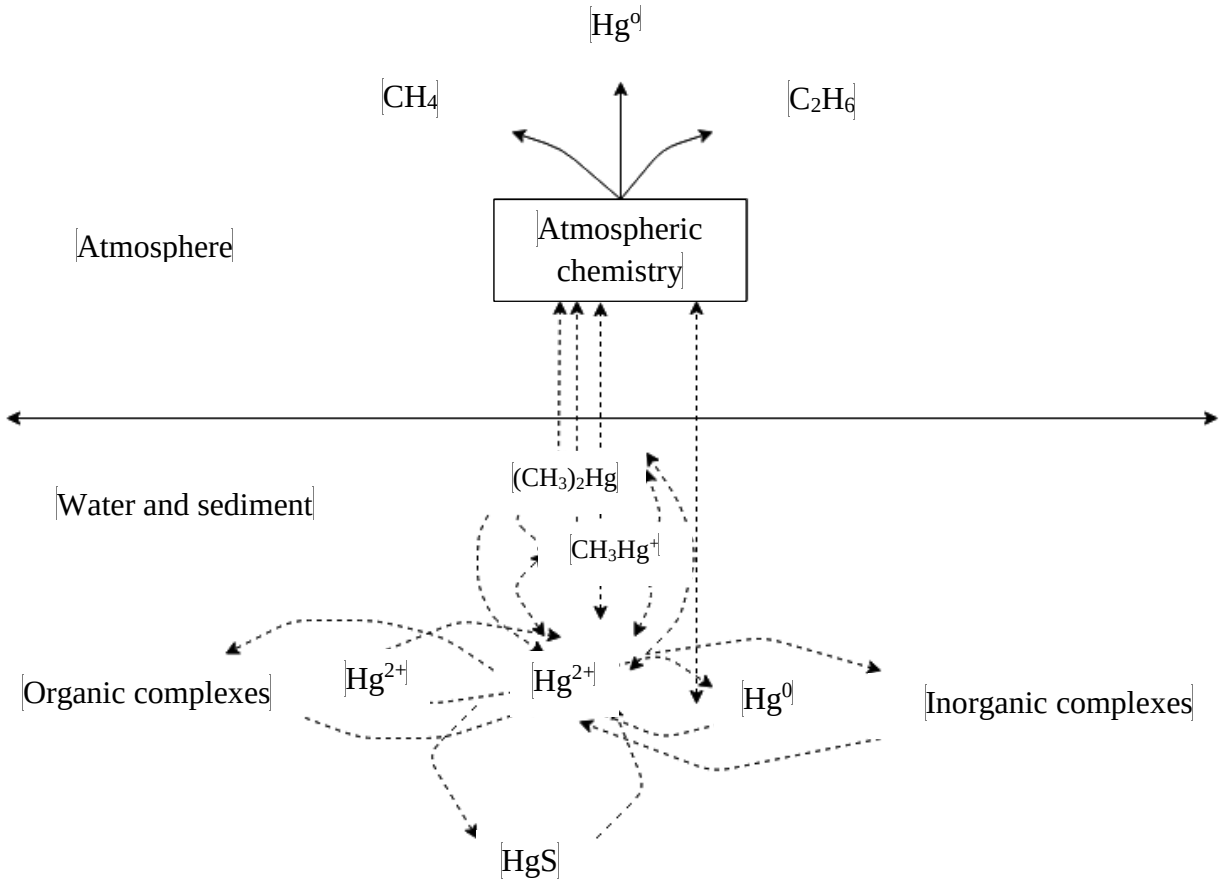

Figure 3: The pathway of mercury in the environment

1.4 Effect of Mercury

Mercury, irrespective of its form, has been reported to be toxic to humans and the ecosystem. It toxicity is worsen by its persistency and ability to bio-accumulate (Miretzky and Cirelli., 2009). Mercury can be liberated either from ores, fossil fuel or mineral deposits. It is sometimes released as a result of volcanic eruption, weathering of rocks and human activities. Once in the environment, it can remain and cycle between the atmosphere and other spheres. For instance, the contamination of water bodies by mercury has generated concern in affected areas since the Minamata bay incidence in 1953 to 1960. Long-time exposure to any form of mercury is known to disrupt different human systems especially the nervous system. Even at low levels of contamination, exposure to mercury of any form may result in kidney damage and negative effect on renal, immune, reproductive and cardiovascular systems (Zahir et al., 2005). Some symptoms of neurological and behavioural disorders caused by exposure to mercury include tremors, insomnia, memory loss, headaches and cognitive and motor dysfunction

The most toxic form of mercury, methyl-mercury (Leopold, Foulkes, & Worsfold, 2010), is basically formed in aquatic environments as a result of the formation of soluble monomethylmercury ions and volatile dimethylmercury by the action of anaerobic bacteria (Manahan, 2004).

1.5 Statement of problem

Mercury (II) enters the environment due to its wide application in different industries notably petrochemical, mining, medical and automobile industries. It is also released from the burning of mercury containing fuels in vehicles. Once in the atmosphere, it combines

with particulates and settles in water bodies such as marine, well, ground water and other exposed water channels. It toxicity in the ionic state and possibility to form even more toxic compound in methyl-mercury has always been a source of concern. Contamination of the environment with mercury is known to bioaccumulate in organisms and may result in a major health disaster.

Saudi Arabia's dire need to conserve its limited water resources and safeguard the health of its increasing population and biota may involve adopting effective and environmentally friendly wastewater treatment techniques. The assessment and subsequent treatment of contaminants such as mercury (II) from water is considered paramount. Prior to 1995, few literatures have reported the contamination of water bodies with mercury within the Kingdom. However in 1995, Kutty et al., reported the presence of mercury in product water from sea water desalination plant. Hussein et al., (2011) also reported the presence of mercury in ground and well waters in western province. They reported the bioaccumulation of mercury in liver, kidney and residues of chicken. Both authors attributed the presence of mercury above the legal limit to occasional pollution from industrial activities.

1.6 Significance of study

The demand for clean and potable water in Saudi Arabia has never been more pressing. Water in Saudi Arabia is considered a scarce and rather valuable resource due to the climatic conditions and location. The continuous boost in economic development, industrialization and increase in population has resulted in the subsequent increase in the net water requirement both for industrial, domestic and economic application. In order to meet the increasing demand for water and ensure the sustenance of her economic and

industrial growth, the kingdom needs to supplement its current water sources; ground water and desalinated water (Gutub et al., 2013). This places an emphasis on wastewater treatment. Waste water treatment not only increases the availability of water directly but also reduces pollution of available water bodies; since the quantity of wastewater generated from industrial and domestic application has increased as a result of industrialization and increase population. Also of paramount importance is the need to safeguard the health of organisms and their environment affected by water pollution.

Mercury contamination is one of the factors that hinders the availability of potable water and possesses significant effect to the environment. Contamination of the environment with mercury is bio-accumulates in organisms and may result in a major health disaster if not checked. Continuous industrialization, especially increase in growth of mining, medical, battery manufacturing, pesticides, metal processing and petrochemical refining industries have been known to lead to the production of more mercury-containing wastewater. Mercury exists in different forms. While methyl mercury may be the most toxic form of mercury, it has been confirmed that mercury (II) is immensely toxic to components of the environment and very reactive. The formation of methyl-mercury occurs by conversion of inorganic mercury (Hg^{+1} and Hg^{+2}) by micro-organisms in aquatic media.

One of the most applied mercury treatment technique is the use of adsorbent to sorb the contaminants from solution. The use of nanoparticles as adsorbent has recently become widely accepted as a result of their unique properties; unusual crystal shapes and lattice order and reactivity.

Chemically synthesized nanoparticles have been adopted as adsorbents in the removal of mercury (II) from water, though effective, its use is limited as a result of the effect it poses to the environment after use. Biosynthesized nanoparticles offer a likely solution to this. It is known to be more environmentally benign and easier to synthesize compared to chemically synthesized nanoparticles. The availability of plants, to be used as adsorbents, also offers a cost effective alternative to the use of other commercial adsorbents and other techniques for treatment of mercury contaminated water.

This study focuses on the use of biosynthesized nanoparticles which have been regarded as environmentally friendly to remove reactive mercury (II) from water. The use of plant extract in the synthesis is in compliance with environmental sustainability goals and an effort to produce cheap adsorbent. The study aims to contribute to efforts in improving the availability of clean water and the reduction of mercury contamination.

CHAPTER 2

LITERATURE REVIEW

Mercury is considered one of the major inorganic water contaminants (Tawabini et al., 2012). In all forms, the presence of mercury in water is toxic and possesses significant risk to aquatic biota (Skubal & Meshkov, 2002). In humans, mercury is neurotoxic and may cause impairment to the central nervous system or disrupt the proper functioning of the kidney and pulmonary system (Fu & Wang, 2011).]. Due to its high toxicity, the permissible limit of mercury in drinking water according to the United State Environmental Protection Agency (US EPA) has been set as low as 2 ppb (Bothra et al., 2013). Mercury is released into the environment as a result of anthropogenic activities such as trash incineration, industrial activities and coal burning (Zhang et al., 2004). It exists in three main forms; elemental mercury (Hg°), inorganic mercurous and mercuric forms (Hg (I) and Hg (II)) and organic alkyl mercury. Hg (II) has been described as the most toxic form of mercury due to its high reactivity (Miretzky et al., 2009). It contributes to element alkylation in aquatic mediums (Bodaly et al., 1998).

2.1 Colorimetric detection of mercury in water

Colorimtric sensing involves the determination of the concentration of a contaminant in a solution by comparing with the color of a standard solution of the contaminant. Colorimetric methods have been widely accepted as a result of their simplicity and ease of detecting contaminants. They are easily read out by the use of naked eye and provide an

alternative for instrumental use especially on field where instrumental analysis may be far from reach.

The colorimetric detection of mercury in aqueous solution has been well reported. The sensing systems have been based on the use of polymers (Zhao et al., 2006; Liu et al., 2007; Kim et al., 2006), organic compounds (Yoon et al., 2005; Huang et al., 2006; Chen et al., 2007), chromophores or fluorophores (Coronado et al., 2005; Zhu et al., 2006; Ros-Lis et al., 2005), DNA (Liu et al., 2007) and recently nanoparticles (Lee et al., 2007; Zheng et al., 2007; Rex et al., 2006). Nanoparticles are particularly attractive for use in the colorimetric detection of mercury. The have controlled size and the color change they exhibit when used as colorimetric sensor is associated with surface plasmon resonance (Aslan et al., 2004). For instance, Bothra et al., (2014) developed a nanosensing system made from the functionalization of silver nanoparticles using β – alanine dithiocarbamide. The system was efficient in the selective detection of Hg^{2+} and Fe^{3+} in the presence of anions. In a similar study (Bothra et al., 2013), although using p-phenylene diamine for fucntionalization, AgNP was applied for the sensing of metal ions in water.

2.2 Mercury removal in water

Due to the toxicity of mercury and hazards caused by it pollution of water bodies as noted above, research aimed at removing mercury has always been of high priority. Various techniques such as volatilization, mechanical filtration, bioremediation, chemical precipitation, adsorption, and photochemical methods (Pacheco et al., 2006) have been adopted for removing mercury from both surface and ground water bodies. These techniques include the use of activated carbon developed from organic sewage sludge to

remove mercury (II) from wastewater (Zhang et al., 2005), and combined use of titanium dioxide and modified sewage sludge carbon in the photocatalytic removal of ionic mercury (Zhang et al., 2004). Other methods include the use of plant (phytoremediation), bioremediation, ion exchange resin (Chiarle et al., 2000) etc. However none of these technique have been used for commercial scale mercury removal (Mazyck et al., 2009). Adsorption process has been reported as the most preferred mercury removal technique especially for concentrations below 100 ppm (De Clercq, 2012). However, while selecting adsorption techniques, it is important to consider the efficiency, cost, time, applicability and ultimately the environment in adopting suitable adsorbents. The use of adsorption by commercial activated carbon and other low cost adsorbents have been widely practised, they have either not achieved the desired low concentration low standards or have been too expensive to commercialize (Mazyck et al. 2009).

2.3 Adsorbents

Adsorbents are the surface on which contaminants of interest are attached. The attraction and subsequent deposition of a contaminant on a solid surface is governed by physical and chemical forces (Rouquerol et al., 2014). Forces such as dipole, dispersive, polarization and electron interaction are responsible for the attachment of adsorbate on adsorbents. The efficiency of an adsorption process often depend on the type and quantity of the adsorbent used. Different materials have been used as adsorbents especially in the removal of mercury from water. Adsorbent materials used for this purpose or for any other water contaminant removal are required to have high surface area for sorption of contaminants, high mechanical and thermal stability and possess high affinity for the contaminant in question (Czaja et al 2009). The removal of mercury from water has been carried out using

both conventional and unconventional adsorbents. Adsorbent classified either as activated carbon (Rao et al.., 2009; Zhang et al., 2005), carbon nanotubes (Mohan et al., 2001), low-cost carbon (Shadbad et al., 2011) or bio-adsorbents (Meena et al., 2004; Banerjee et al., 2012; Jamil et al., 2009) have showed great affinity for mercury removal.

2.3.1 Activated carbon

Activated carbon possesses large surface area and microporous nature; properties which made it suitable for use as an adsorbent. It has been particularly adopted in the removal of most heavy metals including mercury. It modification by sulfuration, ammonification, oxidation and coordinated anchorage gas even increased it suitability for sorption of contaminants (Rivera-Utrilla et al., 2011). Activated carbon produced from different materials has been used in the removal of mercury from water. Yardim et al., (2003) used activated produced from furfural to remove mercury (II) from aqueous solution. The activated carbon was produced by carbonization and subsequent activation of the polymer material with vapor at high temperature. This preceded the polermization of the furfural. They recorded very high adsorption capacity (174 mg/g). Zhang et al., (2005) also prepared activated carbon from sewage sludge and applied it in the removal of mercury (II). The activated carbons were produced from organic sewage sludge (SS) using H_2SO_4, H_3PO_4 and $ZnCl_2$ as chemical activation reagents. They reported that $ZnCl_2$ activated carbon had the highest removal efficiency of the activated carbon produced using other activation agents. However, the use of activated carbon can be expensive especially at commercial scale.

2.3.2 Metal Organic Frameworks

Metal-organic frameworks (MOFs), Figure 4, are emerging inorganic– organic solid-state materials. They have gained research prominence as a result of their chemical and physical properties. They are crystalline in nature and are synthesized by connecting metal ion or metal clusters with carboxylates as multidentate organic ligands (wang et al., 2009). They also have large surface area, are very porous and easily tunable (Khan et al., 2013). The surface area, pore size and framework topology can be tuned by using different organic building blocks and metal ions (Wang et al., 2009). MOF can be synthesized using conventional hydro/solvothermal reaction with different organic building blocks and metal in various organic solvents (Du et al., 2006). They can also be synthesized using various metal ion and organic linkers (Perry et al., 2009). Ke et al., (2011) used thiol-functionalized [Cu3(BTC)2]n and unfunctionalized HKUST-1 to remove mercury (II) in water. While the former showed high affinity for the sorption of mercury (II), the latter showed no mercury adsorption at similar conditions.

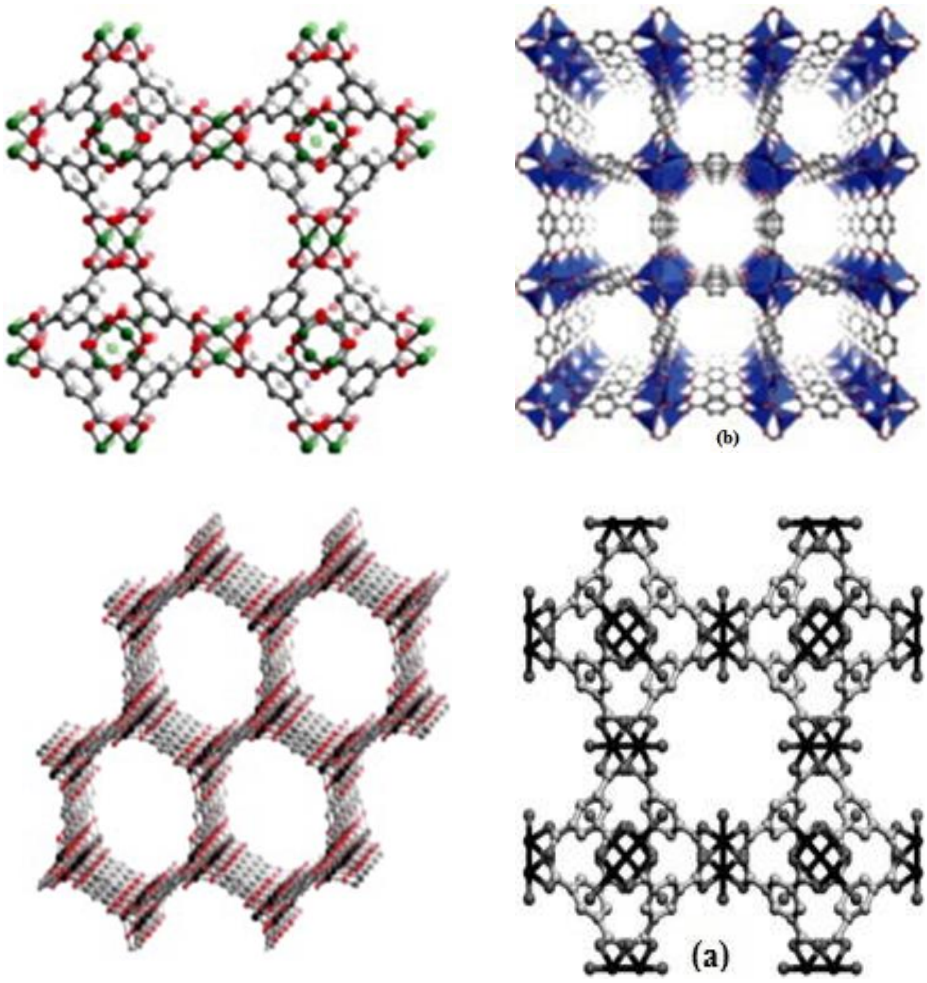

Figure 4: Structure of some metal organic frameworks.

2.3.3 Nanomaterials

Different nanomaterials exist for use as adsorbents in water treatment. The development of cost-effective and novel nanomaterials for adsorption and water treatment has attracted considerable attention in recent years. The unique properties of nanomaterials such as nanocarbon, nanometallic particles, and polymer-supported nanoparticles increase their adsorption capacity and selectivity for use as adsorbents. Nanosized metal oxides such as cerium oxides, manganese oxides, magnesium oxides, ferric oxides, zinc oxides, aluminum

oxides, and titanium oxides provide high surface area and specific affinity for heavy metal removal from aqueous solutions (Hua et al., 2012).

The superparamagnetic properties of iron nanoparticles based nanomaterials have made it a widely used adsorbent for water treatment. They also possess favourable physiochemical properties

2.3.3.1 Carbon nanotubes

Carbon nanotubes are made up of graphene sheets that exist as seamless cylinder folds Figure 5. They were first discovered by lijima (Rao et al., 2007). They exhibit unique electronic, structural, optoelectronic, mechanical, chemical and physical properties (Rao et al., 2007). Carbon nanotubes can be single walled or multi-walled. They can be synthesized arc-discharge, laser ablation and chemical vapor desposition methods. Hadavifar et al., (2014) used functionalized mutli-walled carbon nanotubes as adsorbent in the removal of mercury (II). The functionalization was carried out to equip the nanotubes with thiol functional groups and amine.

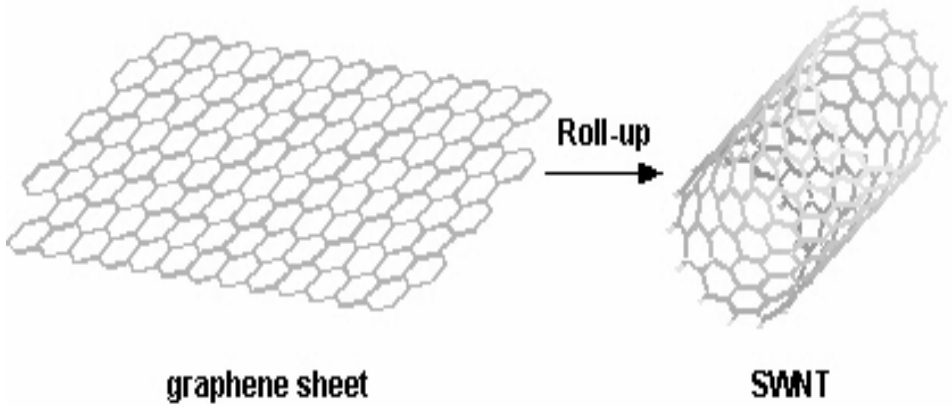

Figure 5: Single walled carbon nanotubes formed by folding graphene sheet

2.4 Nanoparticles

The physiochemical, optoelectrical, mechanical and magnetic properties of nanoparticles are distinct as a result of their confined quantum, surface plasmon resonance and paramagnetic nature (Buzea, Pacheco, & Robbie, 2007; Murali Sastry, Absar Ahmad, 2003; Prathna T.C., 2010). Nanoparticles exist both as organic and inorganic materials. As organic materials, they exist either naturally or are synthesized from organic molecules. In both cases organic nanoparticles are mostly solid particles made up of organic compounds between 10nm and 1µm (Allouche, 2013). Organic nanoparticles can be polymeric or solid lipid (Allouche, 2013). They are formed by chemical binding or self-organization of several organic molecules. (Jesus M. de la Fuente, 2012). However more attention has been given to inorganic nanoparticles as a result of their versatility and superordinate material properties (Prathna T.C., 2010). Inorganic nanoparticles are mostly formed from the precipitation of inorganic salts (Jesus M. de la Fuente, 2012). Inorganic nanoparticles can be classified into noble metals, semiconductors and magnetic nanoparticles (Prathna T.C., 2010)

2.4.1 Methods of synthesizing nanoparticles

Broadly, nanoparticles can be synthesized physically, chemically or biologically. Some of these methods include heat decomposition of compounds, solution reduction, chemical and photochemical reactions in reverse micelles, irradiation, electrochemical, microwave-assisted process, tollen method, polyoxometalates methods and polysaccharide methods (Geethalakshmi & Sarada, 2010), (Sahayaraj & Rajesh, 2011). Physical and chemical methods require the use of reducing or protective agents which are toxic and are not

environmentally benign (Sahayaraj & Rajesh, 2011). The main method of synthesizing nanoparticles is represented in Figure 6.

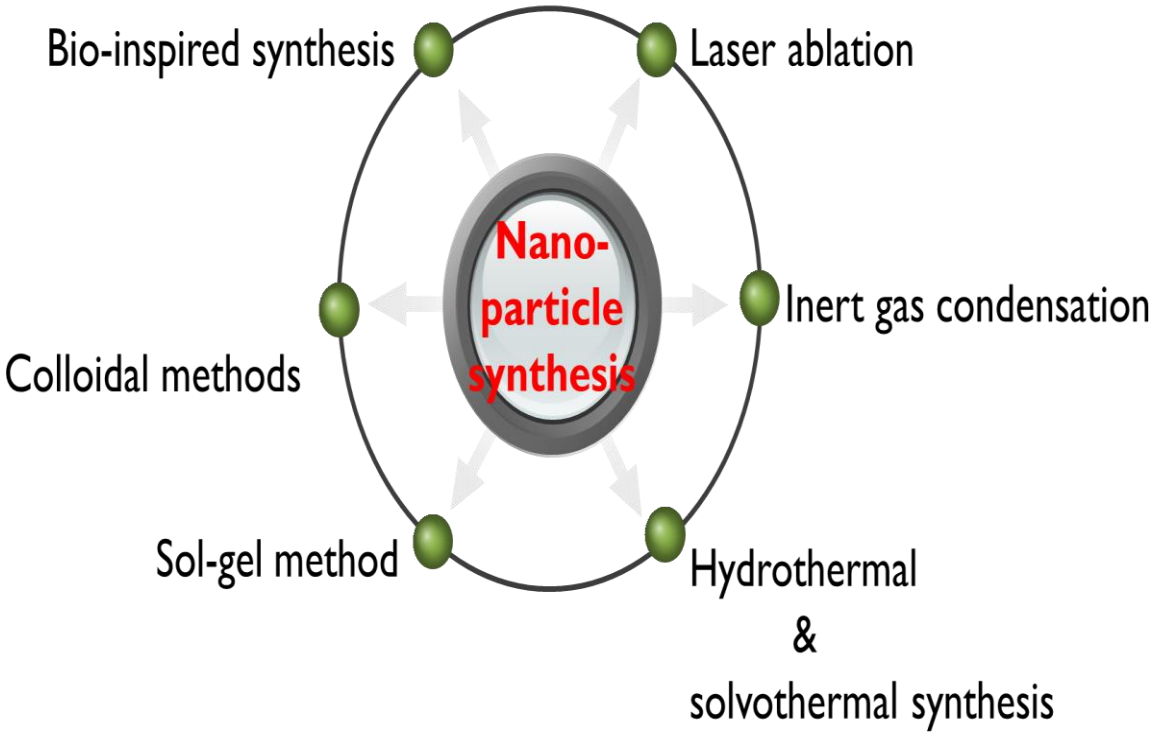

Figure 6: Different nanoparticle synthesis methods

2.4.2 Biosynthesis of nanoparticles

The application of biomaterials in synthesizing nanoparticles, especially inorganic nanoparticles, has been a high focus of research in nanotechnology recently. Previously synthesized using physical and chemical methods, the need to produce environmentally friendly nanoparticles have become paramount. This has resulted in the recent use of biological organisms and plants in the production of inorganic nanoparticles such as silver and gold nanoparticles. Thus, it has been reported that the production of nanoparticles using biological means are more rapid and cost efficient (Ashok, 2012). Basically, two bio-sources have been utilized so far in the reduction of the metallic salt to nanoparticles. These

include microorganisms such as fungus; *Cladosporium cladosporioides* (Balaji et al., 2009), *Fusarium oxysporum* (Durán et al., 2005), and plant extracts such as; *Parenthum Hysterophorus* (Ashok, 2012), Carob leaf (Awwad, Salem, & Abdeen, 2013), *Ananas comosus* (Basavegowda et al., 2013), *Magnolia Kobus* and *Diopyros kaki* (Song et al., 2009), *Trianthema decanda* (Geethalakshmi & Sarada, 2010), *Pinus eldarica* bark (Iravani & Zolfaghari, 2013), *Mentha pipenta* (*Lamiaceae*) (MubarakAli et al., 2011). However, plant extracts have been reported to be more energy efficient, require less purification, are less hazardous, and demand no culturing or cell maintenance processes which are sometimes too elaborate (Awwad et al., 2013), (Basavegowda et al., 2013).

2.5 Biosynthesis of nanoparticles from plant leaves extract

Nanoparticles such as silver and gold have been synthesized using leaf extract from different plant sources (Mittal, Chisti, & Banerjee, 2013). Synthesis of silver nanoparticle from plant leave extract has been carried out using plant extract from carob (Awwad et al., 2013), Olive (M. M. H. Khalil, Ismail, El-Baghdady, & Mohamed, 2013), *Ocimum Sanctum* (Ramteke, Chakrabarti, Sarangi, & Pandey, 2013) and other plant sources. This principle is based on the reduction of the metal ion, in most cases silver ion, from silver nitrate to silver nanoparticle. The reduction rate of silver ion and hence nanoparticle formation, shape and size of silver nanoparticles formed from this process can be altered by change in pH (M. M. H. Khalil et al., 2013), substrate concentration, temperature (Iravani & Zolfaghari, 2013), time of reaction between extract and silver nitrate and the volume ratio of silver nitrate and plant extract (Amin, Anwar, Janjua, Iqbal, & Rashid, 2012).

2.6 The concept of mercury removal using silver nanoparticles

The concept of mercury removal via amalgamation has been used in different industries for millennia. However, this has recently been practiced using chemically synthesized nanoparticles which are less environmentally benign. It simply involves the reaction of mercury with silver to form mercury with zero valency. At the bulk scale, mercury II is known to react with silver to form mercury-silver amalgam (Katok et al., 2012). This property becomes even more pronounced as the size of the silver particle decreases, resulting in hyperstoichiometry where the ratio of mercury to silver changes from 1:2 to 1.125:1 with continuous size decrease (Katok et al., 2012). As a result, when mercury passes through a silver-containing medium, the mercury is trapped forming an amalgam.

$$Hg^{2+}_{(aq)} + 2\ A_{g(s)} = Hg_{(s)} + 2\ Ag^{+}_{(aq)}\ \text{(Katok } \textit{et al. 2012}\text{)} \qquad (2.2)$$

2.7 The concept of mercury removal using iron and iron oxide nanoparticles

The super-paramagnetic property of iron oxide has been exploited for the removal of different heavy metals in water. Both non-modified and modified iron oxide nanoparticles have been reported to remove chromium VI, cadmium, copper, arsenic III and Arsenic V from wastewater (Yantasee et al., 2007). This is possible because of the strong reactivity (super-paramagnetism) that exists between iron oxides and other metal species.

2.8 Nanomembrane filters for mercury removal

Cartridge filters with greater surface area should allow fewer clogs and easier maintenance. Exceptionally small in size, nanofibres of 50 - 250 nm in diameter will reduce the thickness of membrane tremendously and in turn result in less pressure. The characteristics of

interconnected pores result in nanofibres having high permeability and therefore appropriate for industrial cartridge filter applications. Replacement with fibres of size 100 nm results in ~ 100-150 times increase in surface area, a great improvement in filtration. Nanofibres are capable of processing substantially larger volumes of substances passed through them and ensuring large volume of retentate. Nanofibre filters will result in high flow rates. They also could hold a large amount of particulate material and retain a variety of microorganisms well. Larger surface area allows for different chemical treatments that may also adsorb different types of species such as viruses or gases/vapours. The capture efficiency of filter cartridge laced with nanofibers can be enhanced due to the larger surface area of nanofibers. Large surface area allows nanofiber filters to last at least twice as long as other commercial filters, resulting in fewer filter replacements and less compressed air usage. A schematic diagram of a filter cartridge made of a plastic casing and stocked with nanofibers is shown in Figure 7.

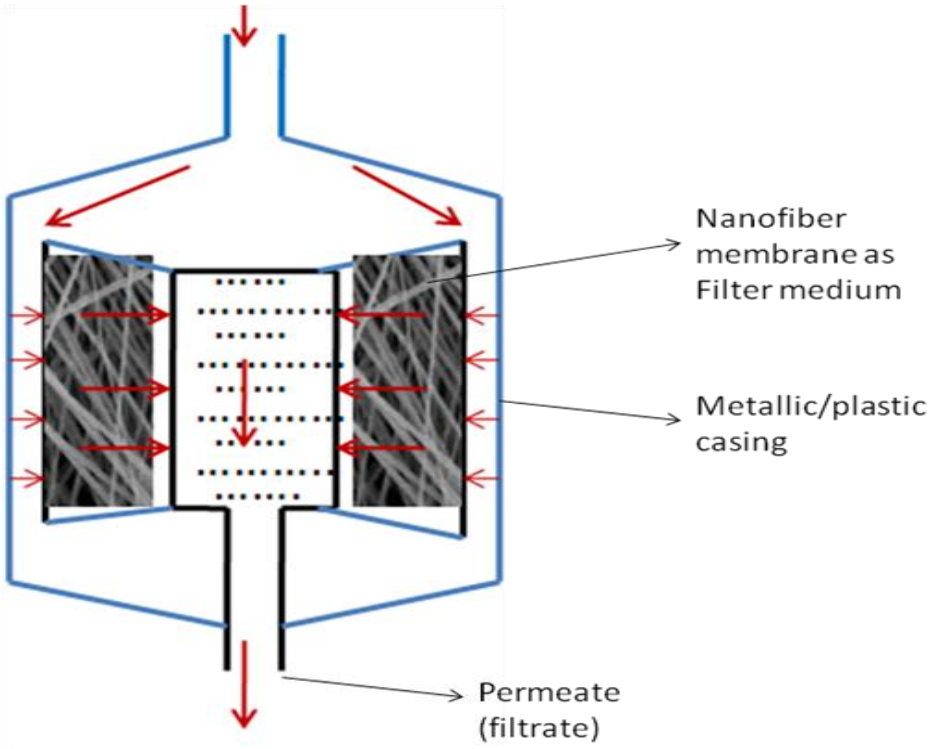

Figure 7: Different nanoparticle synthesis methods

2.9 Research objectives

The main aim of this research is to determine the adsorption efficiency of the removal of mercury (II) from water using biosynthesized silver and iron oxide nanoparticles. The specific objectives include:

1. To demonstrate the removal of mercury II from water using biosynthesized silver and iron oxide nanoparticles in batch adsorption processes;
2. To study the effect of solution conditions such as pH, contact time, mixing rate, mercury (II) concentration and biosynthesized nanoparticle dosage in the adsorption efficiency;
3. To design a filter membrane for the removal of mercury (II) from water;

4. To compare the efficiency of silver and iron oxide nanoparticles for use as an adsorbent for the removal of mercury II in water;
5. To appraise the adsorption isotherms and kinetics of the experimental data under optimum treatment conditions.

CHAPTER 3

MATERIALS AND METHODS

3.1 Solvents, chemicals and reagents

The chemicals used in this research work were of analytical grade and they include;

Silver nitrate (99.8% purity, $AgNO_3$, Merck, Germany)

Sodium chloride (NaCl, purity 99.5%, Merck Germany)

Calcium chloride ($CaCl_2$, 99.96%, Merck, Germany)

Barium chloride ($BaCl_2.2H_2O$, ≥ 97 %, Fisher Scientific Company)

Zinc nitrate hexahydrate ($Zn\ (NO3)_2.6H_2O$, Fisher Scientific Company 98% purity)

Nickel chloride ($NiCl_2.6H_2O$, 98%, Sigma Aldrich, St. Louis, Missouri, United States)

Managanese sulphate hydrate ($MnSO_4.H_2O$, Fisher Scientific Company ≥ 97 %)

Mercury chloride ($HgCl_2$, 99.5%, Aldrich, St. Louis, MO, USA)

Copper sulphate ($CuSO_4.5H_2O$, ≥ 99% Sigma-Aldrich, St. Louis, Missouri, United States)

Potassium chloride (KCl, Beijing Chemical Reagent)

Hydrochloric acid (HCl, 0.1 M, J.T. Baker Phillipsburg, NJ, USA)

Sodium hydroxide (NaCl, 0.1M, New Haven, CT, USA)

Nitric acid (HNO_3, ≥99% Sigma-Aldrich, St. Louis, Missouri, United States)

Iron III chloride hexa-hydrate ($FeCl_3 \cdot 6H_2O$, 99%, Loba chemie, India)

All solutions were prepared using Milli-Q water from Millipore (Bedford, MA, USA).

3.2 Instrumentation

The following instruments were used for characterization and analysis of the research work.

3.2.1 Field emission scanning electron microscopy (FE-SEM) and energy dispersive spectroscopy (EDX)

The surface morphology, shape and size of the as-prepared nanoparticle were analyzed using field emission scanning electron microscopy (Lyra3 TESCAN FESEM), Figure 8. The Field Emission Dual Beam (Electron/ Focused Ion Beam) system combines a high-end field-emission scanning electron microscope (FESEM) and a high-performance focused ion beam (FIB) system in one chamber. It is made up of electron guns which produces a fine and controlled beam of electrons that are focused at the specimen surface. The electron gun omits electrons from field-emission gun to produce the image and number of other characteristics.

The FESEM used was also equipped with an energy-dispersive X-ray spectroscope (EDX) detector. EDX analysis reveals elemental analysis of specimens based on an interaction between an X-ray source and the specimen. The interaction between the X-ray source and the specimen is provided in terms of bombardment by an electron beam which results in

the emission of X-rays from the specimen. The emitted X-ray which is unique with different elements is detected by the EDX technique.

The EDX analysis was used to determine the elemental composition of the as-synthesized nanoparticles and the spun membranes. It also produces a map view of the nanoparticle incorporated membrane showing the elemental distribution of the embedded nanoparticles. The sample was prepared by adding 2 mg of the nanoparticles in 8 ml of water and 5 ml of isopropanol. The mixture is sonicated for 15 minutes and a blob dropped on a foil. The drop is allowed to dry and is gold coated. The coated set-up is analyzed by the FESEM.

Figure 8: Image showing Field emission scanning electron microscopy set-up

3.2.2 Fourier transform infrared spectroscopy (FT-IR)

The FT-IR analysis provides spectrum which represents the molecular absorption and transmission, a unique characteristics of the sample under analysis. FT-IR analysis of the sample was done using Nicolet 6700 FT-IR (Thermo Electron Corporation), Figure 9. The instrument has a resolution of 2.0 cm^{-1} and is equipped with an OMNIC program and a deuterated triglycine sulfate detector. Each sample was grounded into powder and mixed with KBR to make KBR pellets before being analyzed. The spectra were obtained by adding 64 scans and corrected for background noise. The spectra were further recorded in transmission mode and at wavelength range 4000 – 500cm^{-1}. The spectra of the plant used in the various biosynthesis process, the biosynthesized nanoparticles before use and after use were collected.

Figure 9: Image of a Fourier transform infrared spectrophotometer

3.2.3 X-ray diffraction spectroscopy

X-ray diffraction analysis is use to determine the composition, crystallinity and average particle size of the biosynthesized nanoparticles.

X-ray diffraction analysis was done using Rigaku Miniflex II desktop X-ray diffractometer with tube output voltage of 30kV and 200mA current (Figure 10). The diffractometer produces a Cu-Kα radiation, while data were collected at angels between 20 and 80°C at a scan rate of 4°C/min. The samples were grinded lightly to powder and smeared on a silicon-made zero-background holder before being fed into the diffractometer for analysis (Dubey et al., 2013).

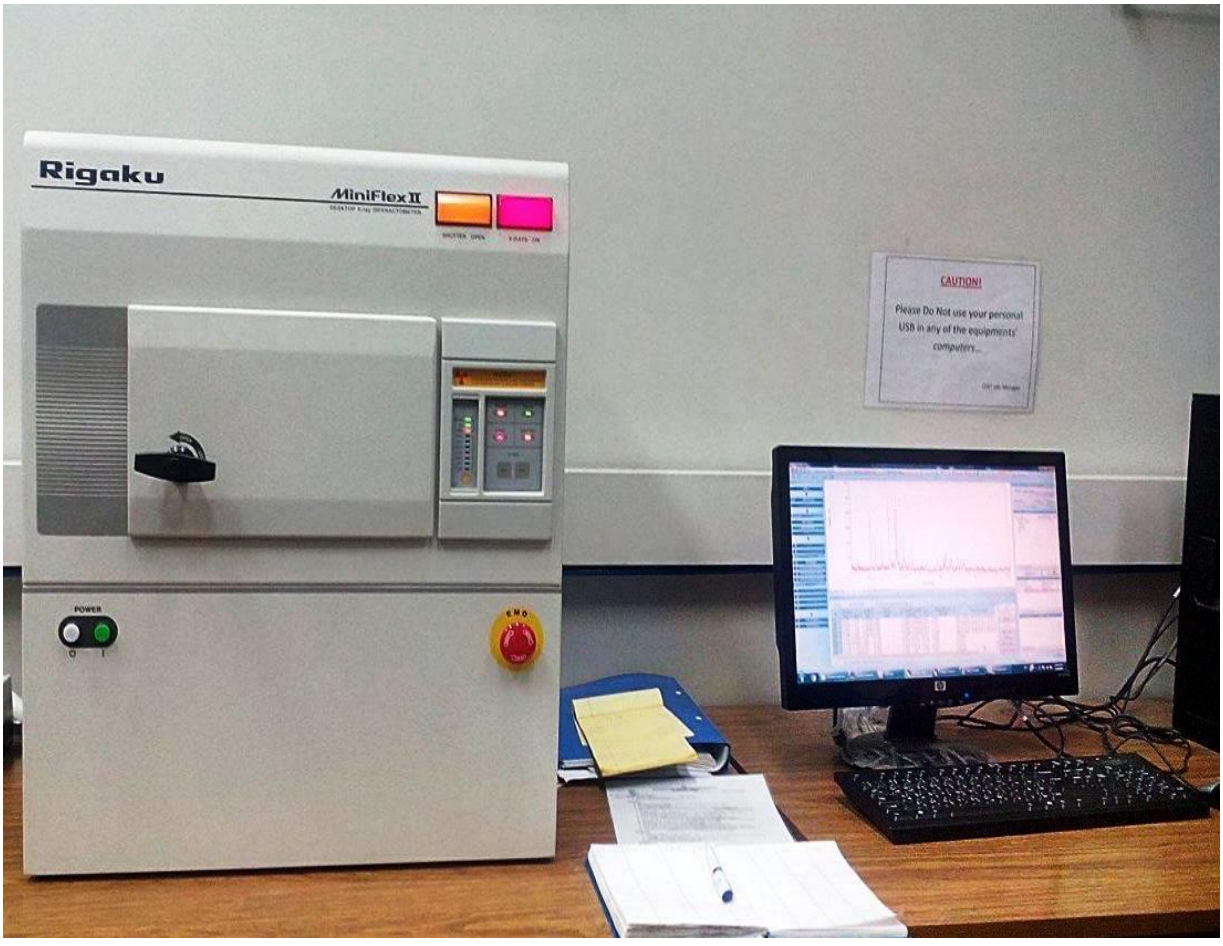

Figure 10: Image of a Rigaku Miniflex II desktop X-ray diffractometer

3.2.4 Thermogravimetric analysis

The physical and chemical properties of materials with respect to change in temperature are determined using TGA analysis. The mass of the material is monitored as the temperature, in which the material is subjected to, is varied.

Thermal stability of the synthesized nanoparticles was determined by heating 15mg of the nanoparticles from 100°C to 600°C at 20C/min. The heating is done in N_2 atmosphere with a purge rate of 100 ml/min. A typical TGA instrument is shown in Figure 11.

Figure 11: Image of a TGA analyzer

3.2.5 Atomic Force Microscopy measurements

AFM measurements were carried out using PicoSPM described Agilent 5100 SPM system (Figure 12). The system is controlled by a magnetic AC (MAC) mode module which is interfaced with a controller PicoScan. The measurements were done by scanning the surface at 1-3 lines per second at room temperature. The samples were prepared by adding 5 mg of the nanoparticles to 10 ml each of water and ethanol solution. The suspension is ultrasonicated for 20 minutes and afterwards, a drop of the suspension placed on mica and allowed to dry at room temperature. This analysis is carried out to confirm the average particle size of the synthesized nanoparticles.

Figure 12: Image of an Agilent 5500 AFM/SPM microscope

3.2.6 Brunauer, Emmett and Teller (BET) surface area analysis

The specific surface area of the as-synthesized nanoparticles is determined by BET analysis. This analysis evaluates the material by nitrogen multilayer adsorption. The adsorption/desorption of nitrogen at -196°C provides the porous structure of the nanoparticles. The analysis is carried out using a Micromeritics ASAP 2020 surface area and porosity analyzer (Figure 13). Some of the parameters obtained from the equipment include pore volume, BET surface area and pore size distribution of the as-synthesized nanoparticles.

Figure 13: Micromeritics ASAP 2020 surface area and porosity analyzer.

3.2.7 UV – Vis spectroscopy

The reduction of $AgNO_3$ by the plant extract was confirmed using Specord 50 single beam UV spectrophotometer at a resolution of 1nm set to scan within 300 and 800nm. The UV-vis analysis was carried out on a mixture diluted 10×. The UV-Vis spectroscopy was employed in the determination of the effect of physico-chemical parameters on the biosynthesis of silver nanoparticles. The colorimetric detection of mercury (II) in aqueous solution was also done using the same instrument.

UV-visible absorption spectroscopy analyses were carried out using a single beam, Specord 50 UV-vis spectrophotometer (Analytik Jena) with a 1.0 cm quartz cell (Figure 14).

Figure 14: Specord 50 UV-vis spectrophotometer

3.3 Biosynthesis of nanoparticles

3.3.1 Plant selection

Plant availability in the arid region of Saudi Arabia depends largely on their ability to withstand harsh weather conditions. However, the selected plants Basil (*Ocimum Basilicum*) and Myrtle are known to be well cultivated in this region and are therefore very available.

3.3.1.1Basil (*Ocimum basilicum*)

Basil (*Ocimum basilicum*), Figure 15, is a popular scented plant in various parts of the world. It is mostly perennial in arid regions although may be cultivated as an annual plant in temperate regions. It belongs to the Lamiaceae family and has been reported to have antibacterial and antioxidant properties and therefore used for medicinal purposes (A. Khalil, 2013). It is widely distributed in tropical Asia, Africa and south eastern Asia (Sarfaraz Khan Marwat, Muhammed Aslam Khan, Fazal-ur-Rehman, Abdul Hakim Akbari, Muhammad Shoaib, 2011). Different species of Basil has been applied in synthesizing nanoparticle (Ramteke et al., 2013), however the use of synthesized nanoparticles has been limited to antimicrobial activities.

(a) (b)

Figure 15: Images showing Basil (a) leaves and flowers (b) leaves

3.3.1.2Myrtle

Myrtle (Figure 16) is one of the most abundant shrubs within the environment of the King Fahd University of Petroleum and Minerals. Generally, it has different species and belongs to the Myrtaceae family. The species native to the Middle East region is *Myrtaceae commun*

(a) (b)

Figure 16 Images showing Myrtle (a) flowering part (b) leaves

3.3.1.3Aloe Vera

Aloe Vera is a succulent cactus-like plant species that grows in the tropics. It is well known for its medicinal values. It is also used as an ornamental plant in some part of the world. It has no stem and grows to 60 – 100 cm tall. A typical Aloe Vera plant is shown in Figure 17.

Figure 17: Images showing Aloe Vera plant

3.3.2 Silver nanoparticles (AgNP)

Basil (Ocimum basilicum) plant (Figure 15) was used in the biosynthesis of silver nanoparticles. It was obtained from King Fahd University of Petroleum and Minerals, Dhahran, Saudi Arabia. The 40g of the leaves and flowers were collected boiled in 300 mL of deionized water. The broth (plant extract) obtained is filtered and stored in the refrigerator at 4°C until further use. Different concentrations and volumes of plant extract and silver nitrate solutions were mixed at different temperatures to study the effects of various factors such as pH, temperature, broth concentration and precursor concentration

on the formation of silver nanoparticles. Plant extract solutions were added to the silver nitrate solution drop-wise and a change in the color of the mixture was observed. The reduction of the silver nitrate solution by the plant extract to form AgNPs was monitored using UV-vis spectrophotometry.

3.3.3 Iron Oxide Nanoparticles (Fe_2O_3)

Iron chloride hexahydrate ($FeCl_3 \cdot 6H_2O$, 99%) was used as the reagent to start the reaction. Myrtle plant (Figure 16) obtained from King Fahd University of Petroleum and Minerals nursery located within the campus was use to prepare plant extract. 40 g of well rinsed myrtle plant leaves were plucked and boiled in 400 ml of deionized water. The plant extract was stored in the refrigerator at 4C. In the preparation of Fe_2O_3 nanoparticles, the plant extract was mixed with 0.1M of $FeCl_3 \cdot 6H_2O$ in volumetric ration 1:1 for 30 minutes. The suspension formed is heated at 60°C for 4 hrs. It is subsequently cooled and centrifuged at 15000 rpm. The residue is collected and washed using deionized water and ethanol and dried at room temperature.

3.3.4 Nanoscale zero-valent iron (nZVI)

Aloe Vera (Figure 17) was used in the biosynthesis of nanoscale zero-valent iron. It was obtained from the surroundings of King Fahd University of Petroleum and Minerals was used as source of plant extract in the synthesis of nZVI. The aloe vera was cut and it spiked removed. It was washed thoroughly using de-ionized water to remove dust particles. 75g of rinsed Aloe Vera was cut into smaller pieces and boiled in 150 ml of de-ionized water for 10 minutes and allowed to cool to room temperature. An observed light green solution of plant extract containing Aloe Vera was filtered using Whatmann filter paper. The clear plant extract is stored at 4^{o}C. Iron III chloride hexa-hydrate ($FeCl_3 \cdot 6H_2O$, 99%) was

utilized as iron precursor in the oxidation of synthesized plant extract. The plant extract was mixed with 0.1M of $FeCl_3 \cdot 6H_2O$ continually for 30 minutes using magnetic stirrer in the ratio 1:1. The mixture is heated at 60°C for 4hrs, cooled and dried in an oven.

3.4 Characterization of biosynthesized nanoparticles

The biosynthesized nanoparticles were characterized using different instrumental methods. The methods used to characterize the as-prepared nanoparticles include field emission scanning electron microscopy equipped with an energy dispersive spectroscopy, x-ray diffraction spectroscopy, Fourier transform infrared spectroscopy, thermogravimetric analysis, BET surface area, particle size analysis. UV-vis spectroscopy was used to determine the response of as-prepared silver nanoparticles to UV-light.

3.5 Colorimetric studies

To demonstrate the detection of Hg (II) using the unmodified biosynthesized AgNPs, 1mL of as-prepared AgNPs was added to 9 mL of deionized water to make a 10× diluted solution. This was recorded as blank. This procedure was repeated three times for each solution containing a different concentration of Hg (II) ions in order to determine the detection limit of Hg (II) ions using unmodified AgNPs. Also to demonstrate the selectivity of the as-prepared AgNPs for colorimetric detection of Hg (II), the AgNPs were added to various metal solutions (Ca2+, Cu2+, Mn2+, Ni2+, Na+, Zn2+, Ba2+, K+) of the same concentration (1mM) and dilution rate. The analysis was carried out using a UV-vis spectrophotometry.

3.6 Batch mode adsorption experiment

Batch adsorption experiments were conducted. Different experimental conditions such as effect of pH, contact time, nanoparticle dosage and initial concentration on the removal of mercury was studied. De-ionized water was spiked with known concentration of the contaminant and known dose of the adsorbents. After treatment, aliquots of the samples were collected and the residual concentration of the contaminants was determined using a mercury analyzer. Data obtained were subjected to different adsorption models and kinetics.

3.6.1 Experimental design of batch adsorption studies

The experiments were designed to determine the effect of time, pH, contact time, nanoparticle dosage and initial concentration according to table 3.1 below.

Table 3.1 Summary of the experimental design

Adsorbent dosage (mg)	Contact time (hrs.)	pH	Temperature	Agitation speed (rpm)
10	1	3	15	Low speed
25	2	5	25	High speed
50	3	7	35	
75	4	9		

3.7 Design and fabrication of nanoparticle embedded membrane

The fabrication of membrane was done by electrospinning. Electrospinning is a method used to produce nanofibers as a result of the application of high electric voltage between the tip of a needle and a collector plate. A schematic diagram of the process is shown in Figure 19. The collector plate can either be stationary or rotating. NANON apparatus

(Mechanics Electronics Computed Cooperation Co. LTD. Japan, Figure 18) was used. It operates up to 30 kV and at distance of up to 150 mm between nozzle and collector. A syringe of known specification is filled with the polymer/polymer composite of interest and fitted inside the electrospinning chamber. The process parameters are set and the electrospinning process is started.

The Nanoparticle embedded membrane was prepared by adding known amount of the nanoparticles in dimethylformamide. The suspension is ultrasonicated at room temperature for 15 mins. Known amount of polyacrylonitrile pellets was added to the suspension and stirred at 85°C for 5 hours. The resulting polymer composite is filled in a syringe and fixed in the electrospinning chamber for electrospinning. The mat obtained mat is characterized before use in fixed bed adsorption experiment.

Figure 18: An electrospinning machine spins nanofibers

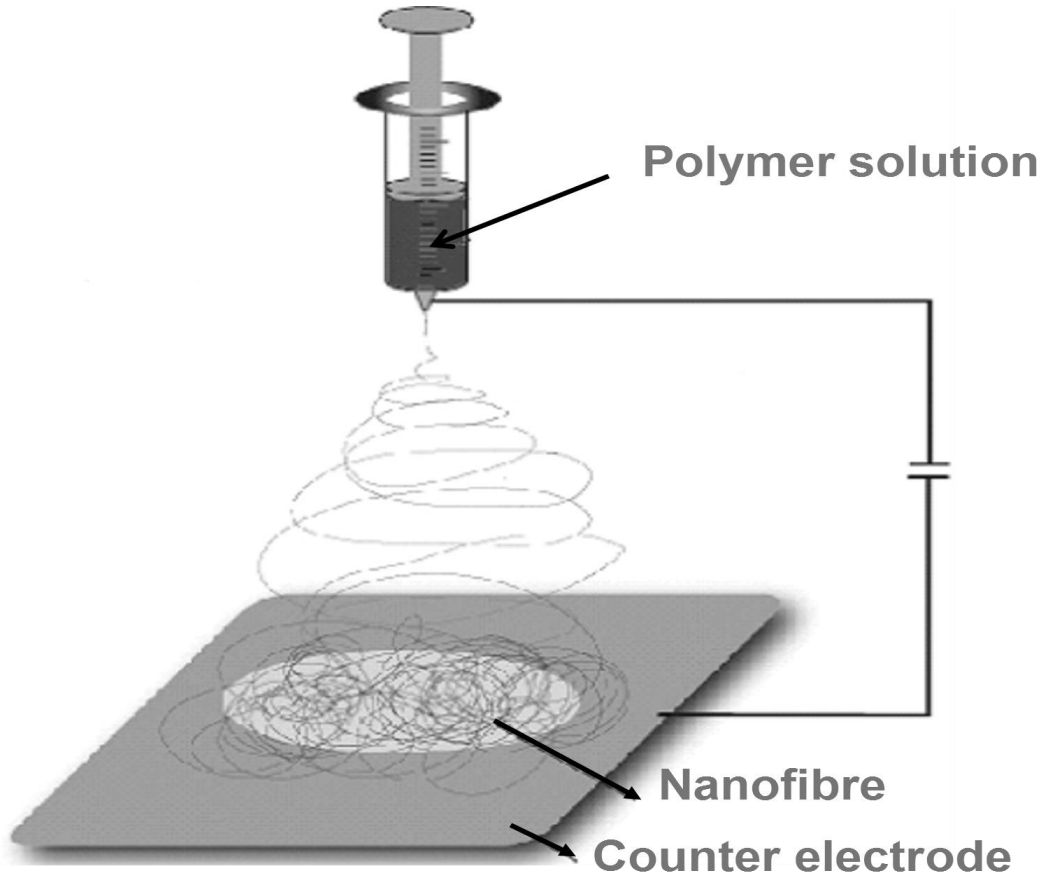

Figure 19: A schematic diagram of the electrospinning process

3.8 Fixed bed adsorption studies

Fixed bed adsorption experiments were carried out to examine the removal of contaminated samples using nanoparticle embedded membrane. The membrane synthesized was laid inside a small filter cartridge (Figure 20) and known concentration of mercury contaminated water is passed through the filter cartridge. The column bed adsorption studies was carried out by first designing the experiments using Minitab 16 statistical software. The factors whose effects are to be investigated where inputted into the software stating the low level and high level numerical values. The four factors investigated include; initial concentration of Hg (II) solution, the flowrate of the pump, the time of the experiment and the membrane loading, i.e. the dosage of the adsorbent in the polymer. The

experiment was carried according to the half factorial design option with 2-level factorial design. The response variable was the percentage removal of Hg (II) obtained according to the following equation;

$$\% \text{ removal of Hg (II)} = \frac{Ci - Ct}{Ci} \times 100 \qquad (3.1)$$

Where; C_i = initial concentration of mercury in the solution and C_t= concentration of mercury in the solution after time (t).

The volume of the solution was made constant at 100 ml while the pump flowrate, initial concentration, time of circulation and membrane loading were varied as summarized in table 3.2 below. The single head column studies was practised where the inlet and outlet of the tube are in the same beaker allowing for continuous circulation and more efficiency (Figure 21).

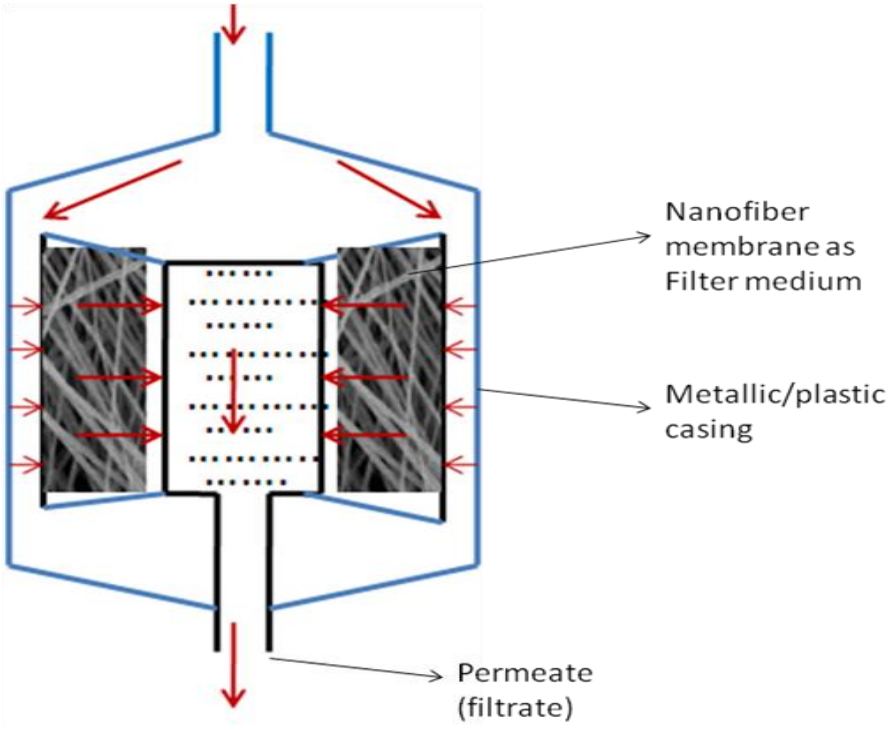

Figure 20: Schematic diagram of the filter cartridge with loaded electrospun membrane

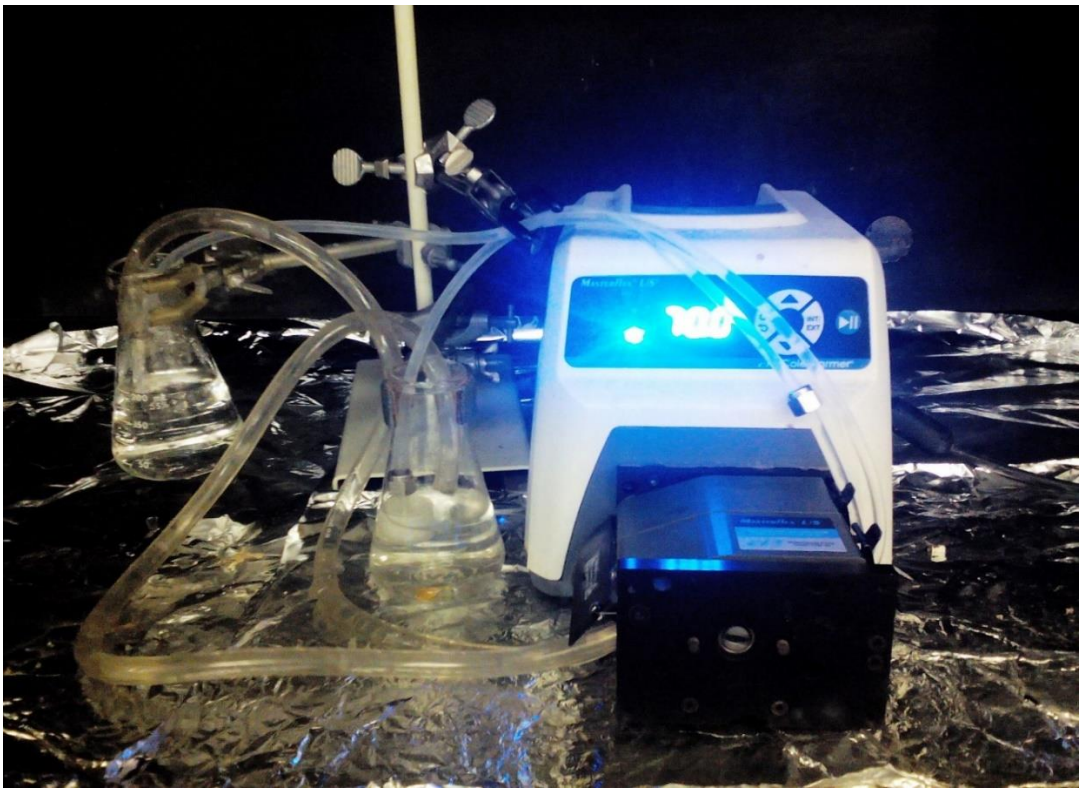

Figure 21: The column studies set-up

Table 3.2 Data sheet provided in the Minitab software

Initial conc. (ppb)	Flowrate (ml/min)	Time (mins)	Membrane loading (mg)
200	70	20	200
200	50	40	200
1000	70	20	100
1000	50	20	200
200	70	40	100
200	50	20	100
1000	50	40	100
1000	70	40	200

3.9 Mercury analysis

A mercury analyzer was used in measuring the amount of mercury (II) in the water samples. Mercury analysis can be carried out using cold vapor atomic adsorption spectroscopy, cold vapor atomic fluorescence spectroscopy, direct analysis by thermal decomposition and inductively coupled plasma with mass spectrometry. For the purpose of this work, the analysis was done using the direct analysis by thermal decomposition.

The cold vapor atomic absorption spectroscopy detects mercury at very low detection limit (parts per trillion). It also requires small volume of samples, less than 1 ml. it is fast and has a dynamic range of 2-3 orders of magnitude.

Fully-automatic thermal vaporization mercury analysis system (Mercury/MA-3000) was used throughout the duration of this work for determining the amount of mercury (II) in the samples. MA 3000 is an instrument built to operate based on cold vapor atomic absorption spectroscopy with gold amalgamation. It operates in compliance with US-EPA 7473, ASTM-6722-01, D-7623-10 test methods. The system is equipped with an in-built auto-sampler. Mercury compounds in the samples micro-pipetted into the instrument boats are heated and subsequently decomposed in the gases generated within the instrument. The interference-free mercury is collected in gold amalgam form ensuring that the mercury is totally pure. Purified mercury in the collection tube is heated to liberate mercury in gaseous form and the absorbance is measured at a wavelength of 253. 7 nm. The operating principle of the instrument is showed in Figure 22 below.

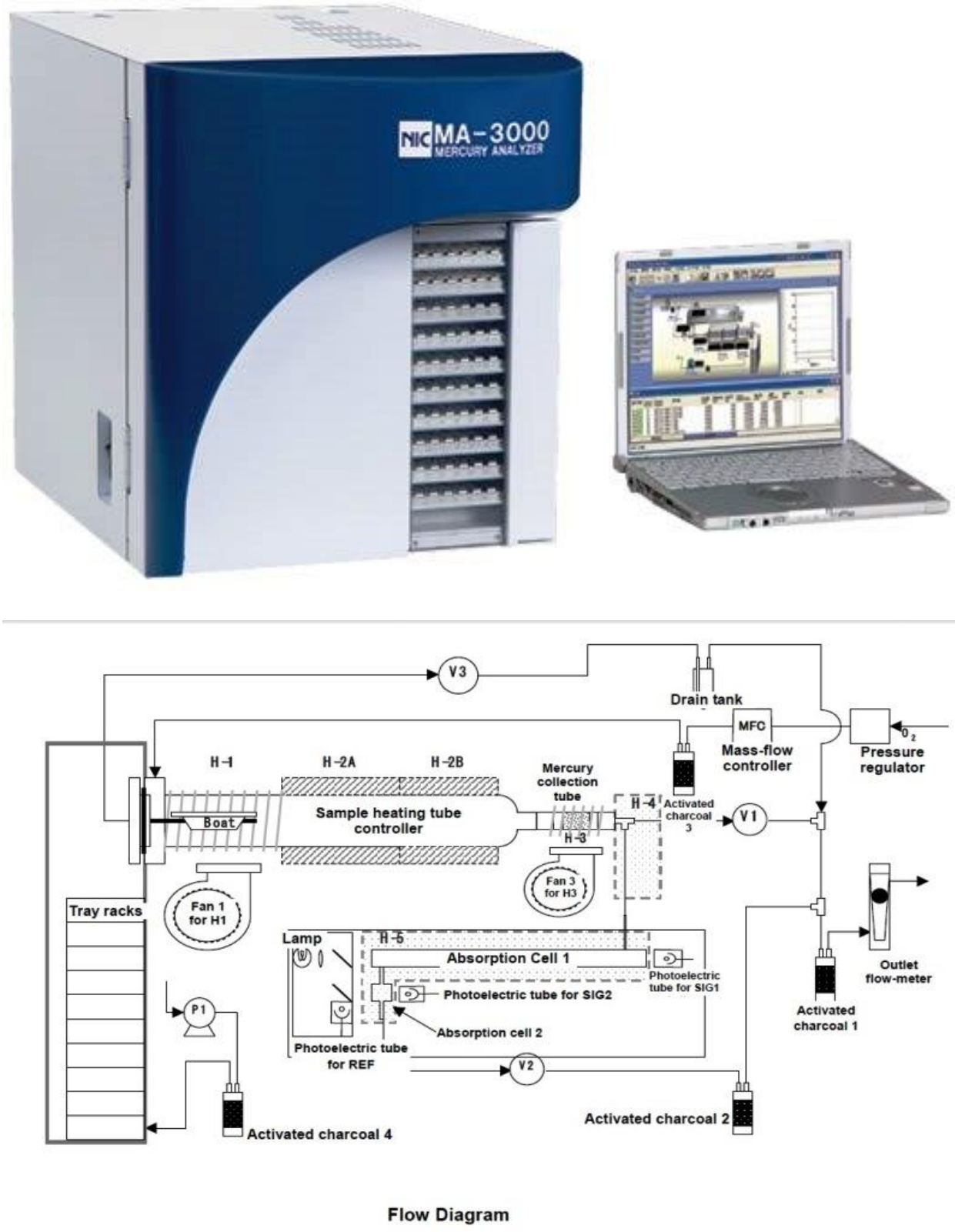

Figure 22: MA 3000 mercury analyzer and schematic diagram of its flow diagram

3.10 Adsorption kinetics

Adsorption kinetics are used to know the performance, mechanism and pathways involved in an adsorption process. Knowing the kinetic performance of a sorbent is imperative for it future application and for the purpose of scale-up. The rate of solute uptake, a function of the time required to complete an adsorption process, is determined from kinetics study. The adsorption kinetics of the biosynthesized nanoparticles were determined using the pseudo first order, pseudo second order and intraparticle diffusion models. The level of compliance between the experimental value obtained and the calculated values were also ascertained by obtaining the R-square values from plotted graphs.

3.11 Adsorption isotherms

Adsorption isotherms are mathematical models that describe the phenomenon governing the retention or distribution of a substance, the adsorbate, from a liquid to a solid phase, the adsorbent at constant conditions of temperature and pH. Different isotherms have been used to describe adsorption mechanism however, this study focuses on the use of Langmuir and freundlich adsorption isotherms.

Several models have been used to describe the process of adsorption, the isotherms of Freundlich and Langmuir have been widely used by several researchers (Nwabanne and Igbokwe, 2008; Kumar et al., 2008). Freundlich and Langmuir isotherms are widely used to understand the extent and degree of favorability of adsorption (Ding, 2008). For this research, Langmuir isotherm has been used.

CHAPTER 4

RESULTS AND DISCUSSION

4.1 Formation of biosynthesized silver nanoparticles

After adding plant extracts drop-wise into the prepared silver nitrate solution, the color of the mixture changes to that of the plant extract in an instant (brown) instantly and then becomes clearer (more transparent or colorless) indicating the start of the reaction. The color then changes with time as shown in Figure 23. The steady change of the solution color from brown to dark brown shows the continuous reduction of silver nitrate to AgNPs and hence an increase in concentration or formation of AgNPs in solution. The formation of AgNPs is characterized by excitation of surface plasmon resonance which introduces the color change. Surface plasmon resonance is the oscillation of conduction electrons at the interface between a negative and positive permittivity materials stimulated by color change.

Figure 23: From left to right, mixture of silver nitrate solutions and plant extracts at 0, 15, 30, 60, 120, 240 and 480 mins, respectively

4.2 Effect of various factors on biosynthesis of silver nanoparticles

4.2.1 Effect of reaction time

The effect of reaction time on the formation of AgNPs after mixing silver nitrate solution and plant extract at neutral pH and room temperature is shown in Figure 24. No visible peak was observed within the first 120 minutes of the commencement of the reaction. A pronounced peak became visible at 240 minutes. The observed peak increased from 240 minutes to 480 minutes. The gradual formation of the peak as shown may be attributed to the increase in the silver nanoparticles formed in the solution causing surface plasmon resonance vibrations. The difference in the peak formed at 240 minutes and 480 minutes was small, showing that the reduction reaction had almost reached completion at 240 minutes. The bands formed at 240 and 480 minutes were within the range 430 – 440nm, which gradually shift from above 450nm formed at shorter time. This shows the gradual reduction in the size of AgNPs formed over time.

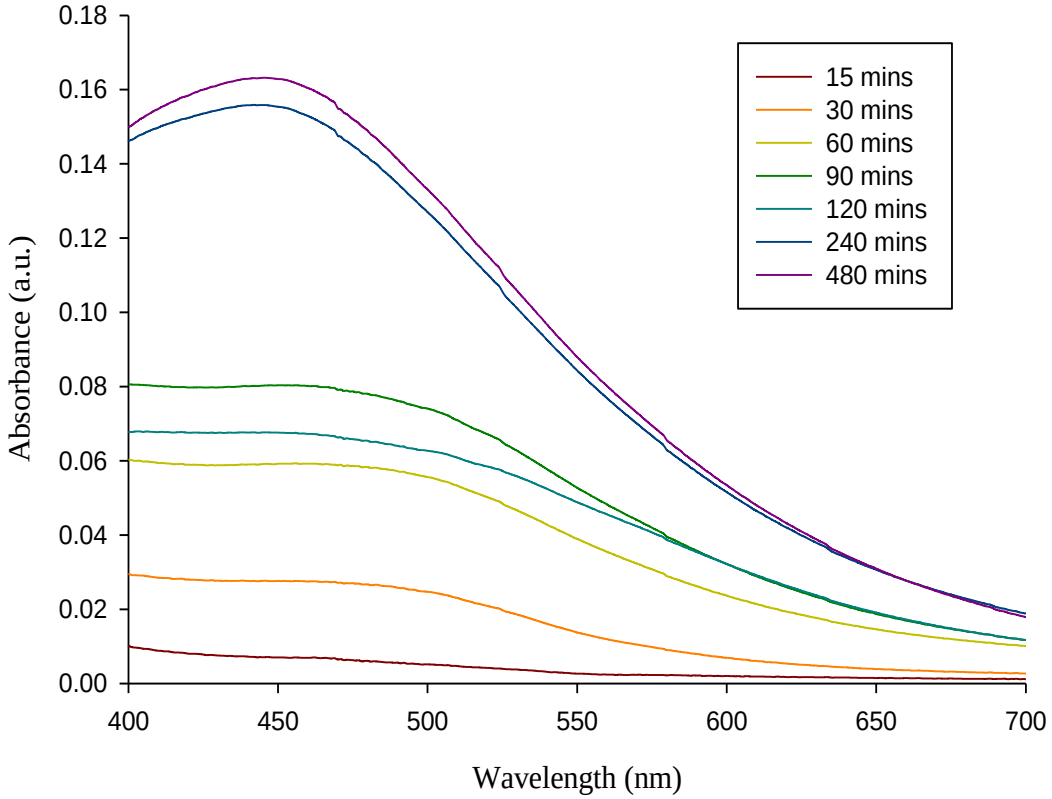

Figure 24: UV- visible spectra showing the effect of time on the formation of nanoparticles

4.2.2 Effect of broth concentration

The effect of broth concentration on AgNPs formation is shown in Figure 25 for different mixing ratios of plant extract and silver nitrate. The highest peak was observed at a ratio of 1:25 which shows that all the silver ions have reacted with the plant extracts. The complete reaction of $AgNO_3$ with the plant extract at this ratio therefore shows that the reduction of silver ion and hence the formation of AgNPs is optimum at this combination ratio.

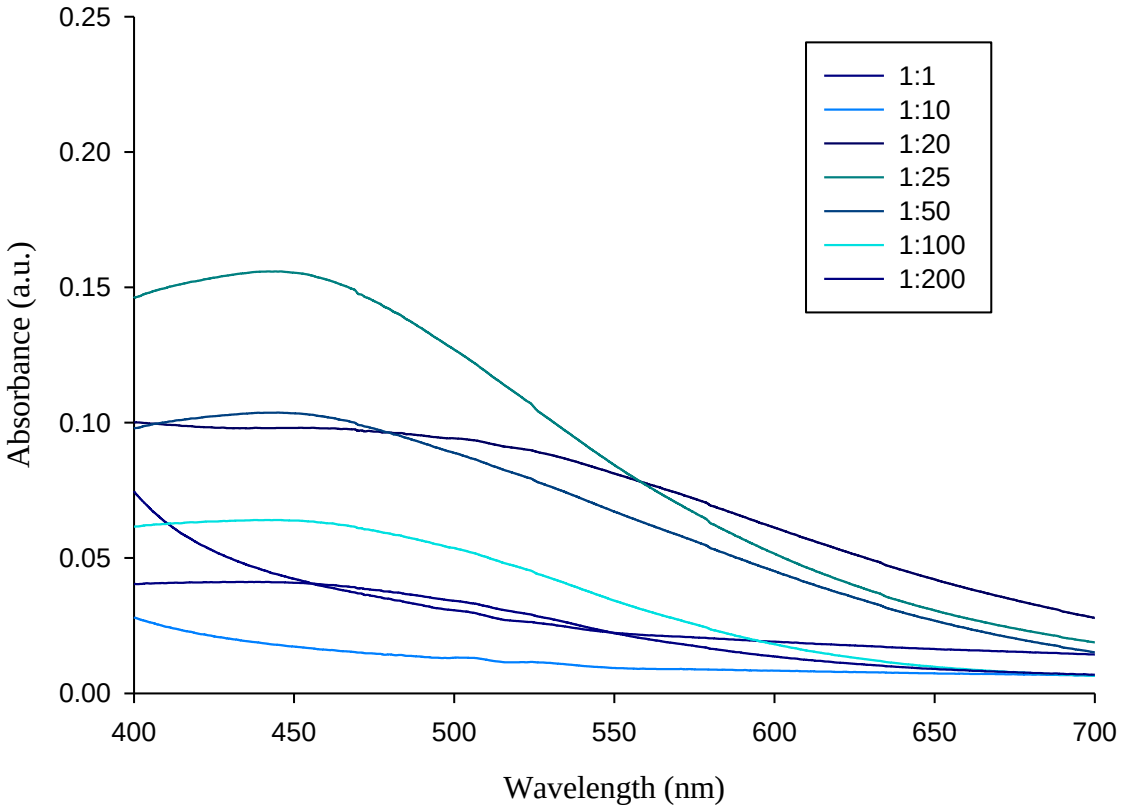

Figure 25: UV-Vis spectra for different concentrations in the formation of AgNPs

4.2.3 Effect of precursor concentration (Silver nitrate)

Figure 26 shows the effect of the precursor (silver nitrate) concentration at a constant time, temperature, pH and broth concentration. As the precursor concentration was reduced from 5 nM to 1mM, a shift in band closer to 400nm was observed. The peak absorbance was obtained at 2mM $AgN0_3$ indicating that the reaction is optimized at this concentration of the silver nitrate solution. The blue shift noticed may be attributed to the formation of Ag-Hg amalgam as well as changes in the refractive index of the particles (Sumesh et al., 2011).

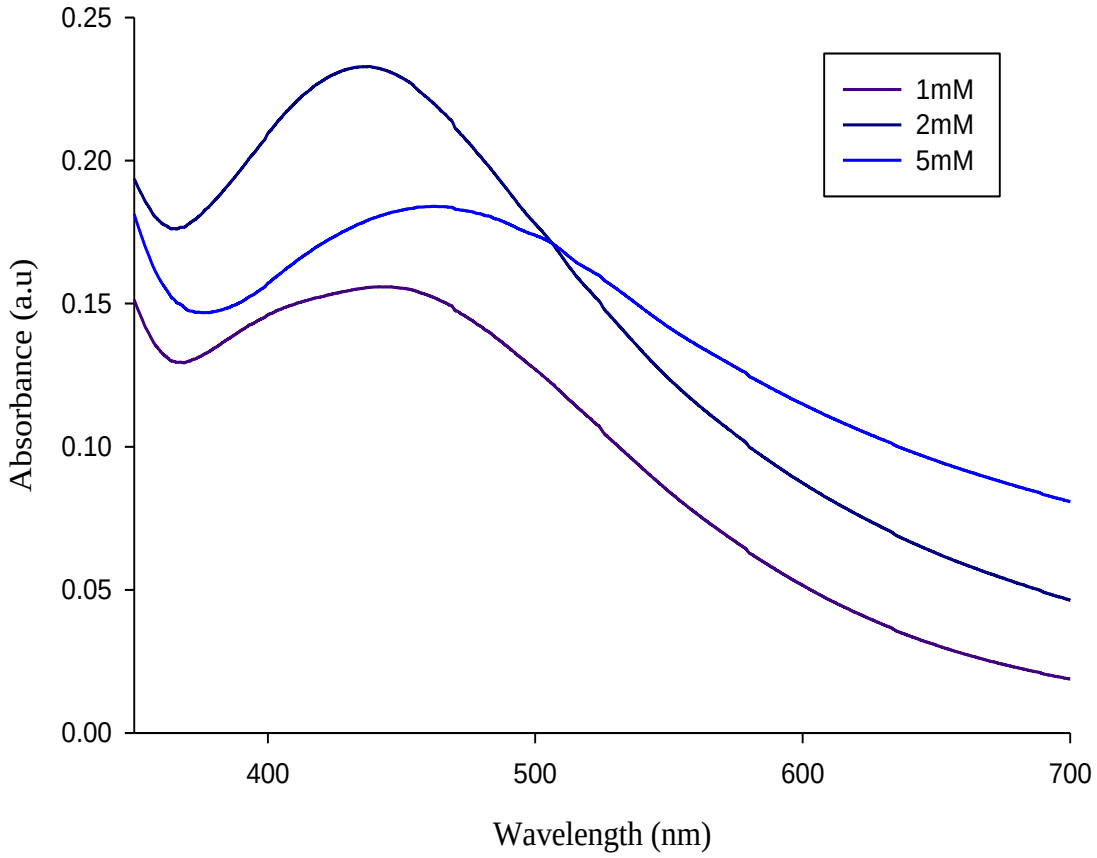

Figure 26: UV-Vis spectra at different precursor concentrations for forming AgNPs

4.2.4 Effect of temperature

The effect of temperature on nanoparticle formation was determined at a reaction time of 1 hour. Although the absorbance peak formed was not particularly pronounced, the value of the absorbance at a temperature of 70°C was the highest. This shows that the formation of silver nanoparticles increases with increase in the temperatures. This is due to the fact that an increase in temperature supports more effective collision of silver ion and biomolecules and also increases the rate of the reaction. The effect of temperature on

nanoparticle formation at constant conditions of pH, silver nitrate concentration and broth concentration is shown in Figure 27.

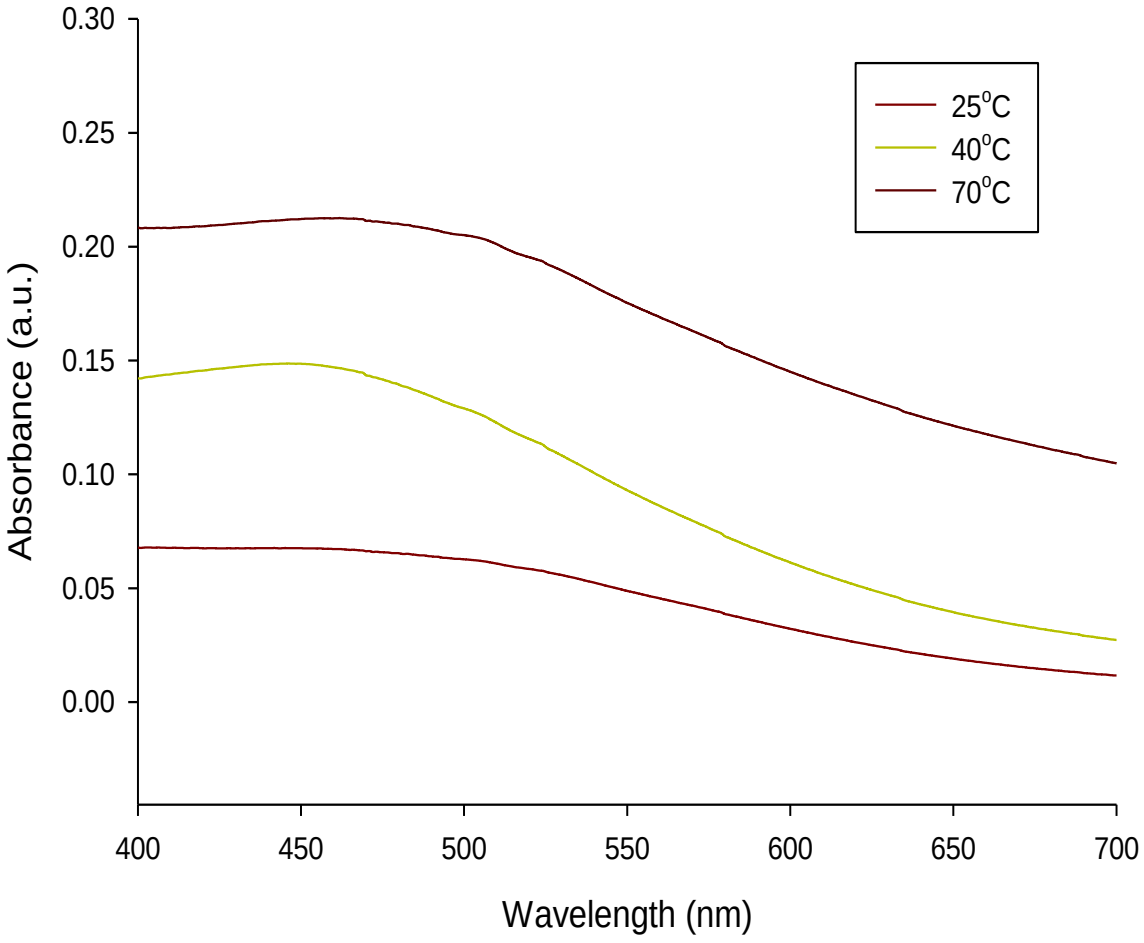

Figure 27: UV –Vis spectra for different temperatures in AgNPs formation

4.2.5 Effect of pH

The effect of pH on the formation of AgNP was also examined. Figure 28 shows the effect of pH on the formation of AgNPs. As evident from the figure, the bands obtained are closer to 400nm compared to the spectra obtained for other effects studied. Also, the absorbance readings are higher at pH 7, 8 and 10. However, in an acidic medium, the peak was not

obvious, signifying that the formation of AgNPs is not supported in acidic conditions. The peak increases with pH and as the solution becomes more alkaline with the highest absorbance obtained at pH 10 with a wavelength of 402 nm. This observation is consistent with Vanaja et al., 2013, who reported that the excitation of surface plasmon resonance is supported in alkaline media.

Alkalinity supports the reduction and capping of silver nanoparticles at specific facets and subsequent deposition of silver atom on these facets (Vanaja et al., 2013). They also cause electrostatic repulsion between the nanoparticles as they are formed. However, at acidic pH, the functional groups responsible for reducing the precursor to nanoparticles possess positive charges, due to high concentration of hydrogen ion, which in-turn lowers their reducing potential. Nucleation is also promoted at high pH as reported by Vanaja et al., (2013).

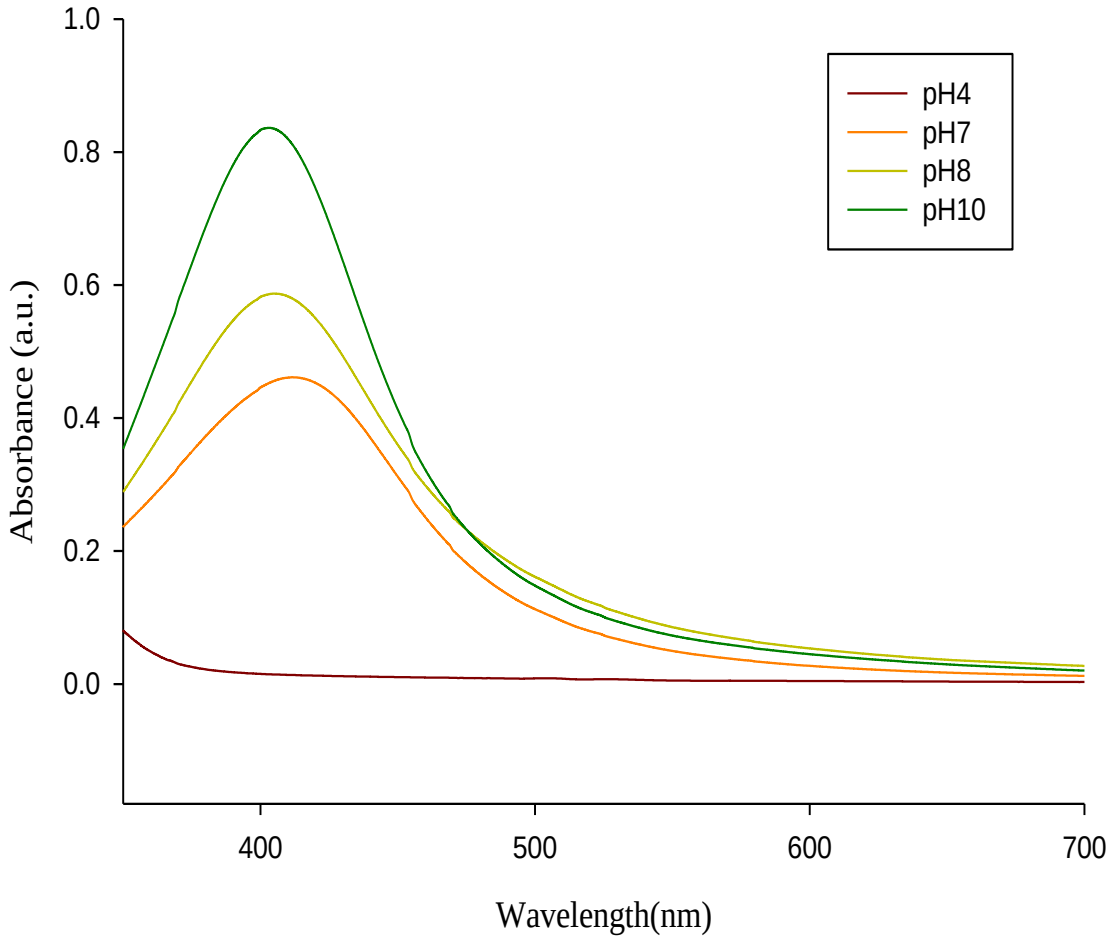

Figure 28: UV-Vis spectra showing the effect of pH in AgNPs formation

Having optimized the biosynthesis condition of silver nanoparticles, subsequent synthesis of the nanoparticles was done at pH 8 using 2mM silver nitrate solution at 40C. The plant extract and silver nitrate solutions were mixed at 1:25 volumetric ratio for 240 minutes.

4.3 Characterization of biosynthesized nanoparticles

After biosynthesizing the adsorbents, characterization was carried out to investigate their size, shape, surface morphology, elemental composition, crystallinity and the functional groups responsible for their synthesis. The results obtained provide an insight into the

properties and the adsorptive potentials of the biosynthesized nanoparticles for their use as adsorbents.

4.3.1 Field emission scanning electron microscopy (FE-SEM)

The as-synthesized nanoparticles were characterized using field emission scanning electron microscope (Lyra3 TESCAN FESEM) equipped with an energy dispersive spectroscope (EDS) detector. The FE-SEM images in Figures 29, 30 and 31 show the shape and morphology of biosynthesized AgNP, Fe_2O_3 and nZVI nanoparticles respectively. The Images also provide an estimate of the average size of the nanoparticles obtained. All the images show nanoclusters and agglomerates of spherically shaped nanoparticles with sizes ranging between 30 and 50 nm. The nanoparticles are also polydispersed.

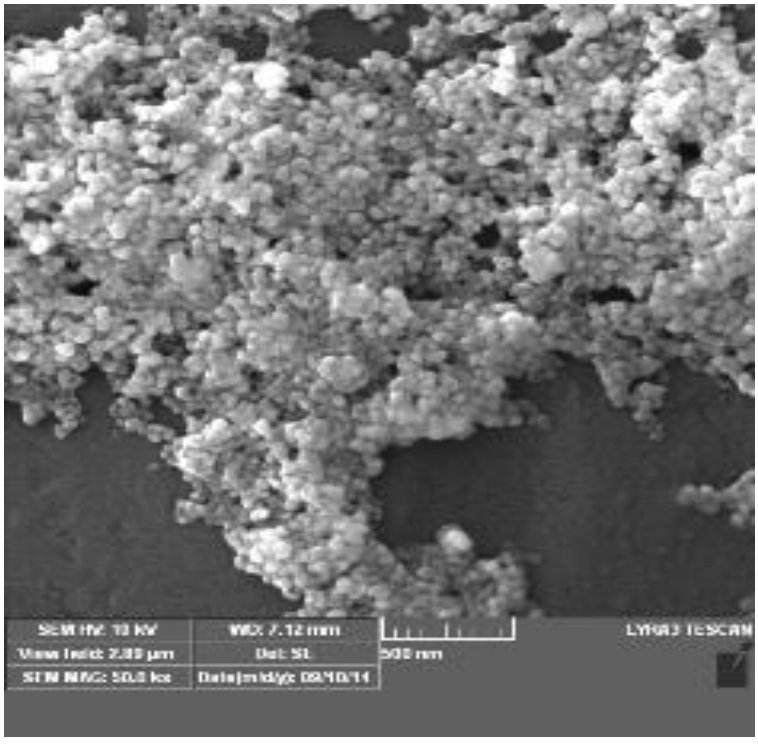

Figure 29: FE-SEM image of biosynthesized AgNPs

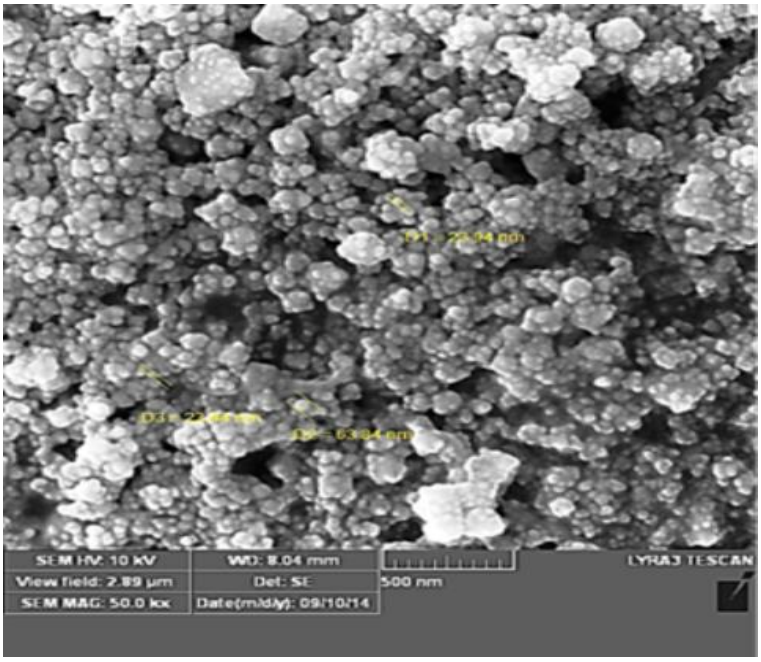

Figure 30: FE- SEM image of biosynthesized Fe_2O_3

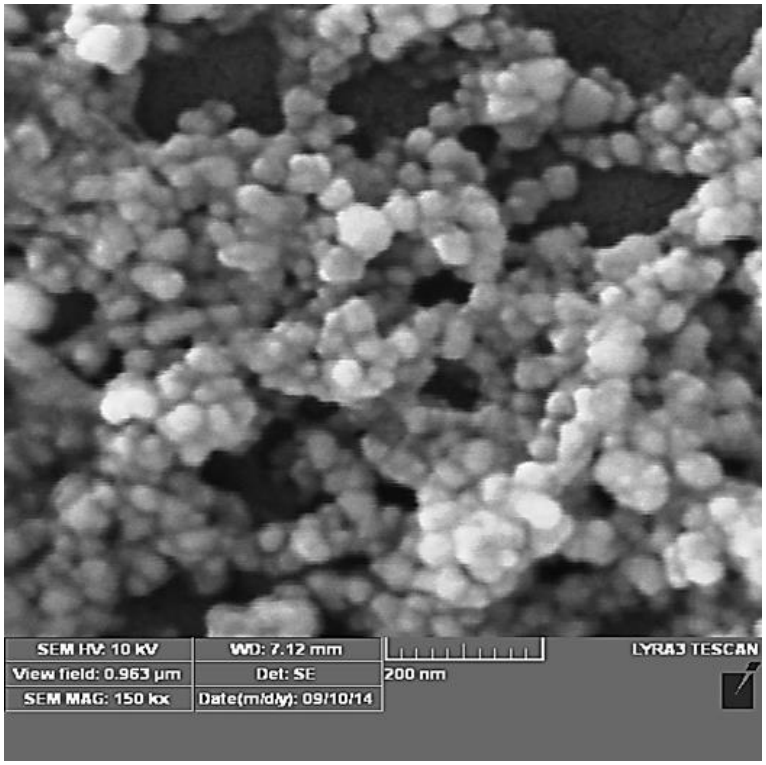

Figure 31: FE- SEM image of biosynthesized nZVI

4.3.2 Energy Dispersive X-ray (EDX)

The presence of the various metals in the biosynthesized nanoparticles was confirmed using EDX Figure 32, 33 and 34. Figure 32 shows biosynthesized AgNP mainly composed of silver with some impurities. Figure 33 and 34 show Fe_2O_3 and nZVI. The presence of oxygen can be observed in the Edx image of biosynthesized Fe_2O_3. The presence of impurities in all the Edx image may be as a result of the presence of remnants of biomolecules involves in the reduction of the metal precursors.

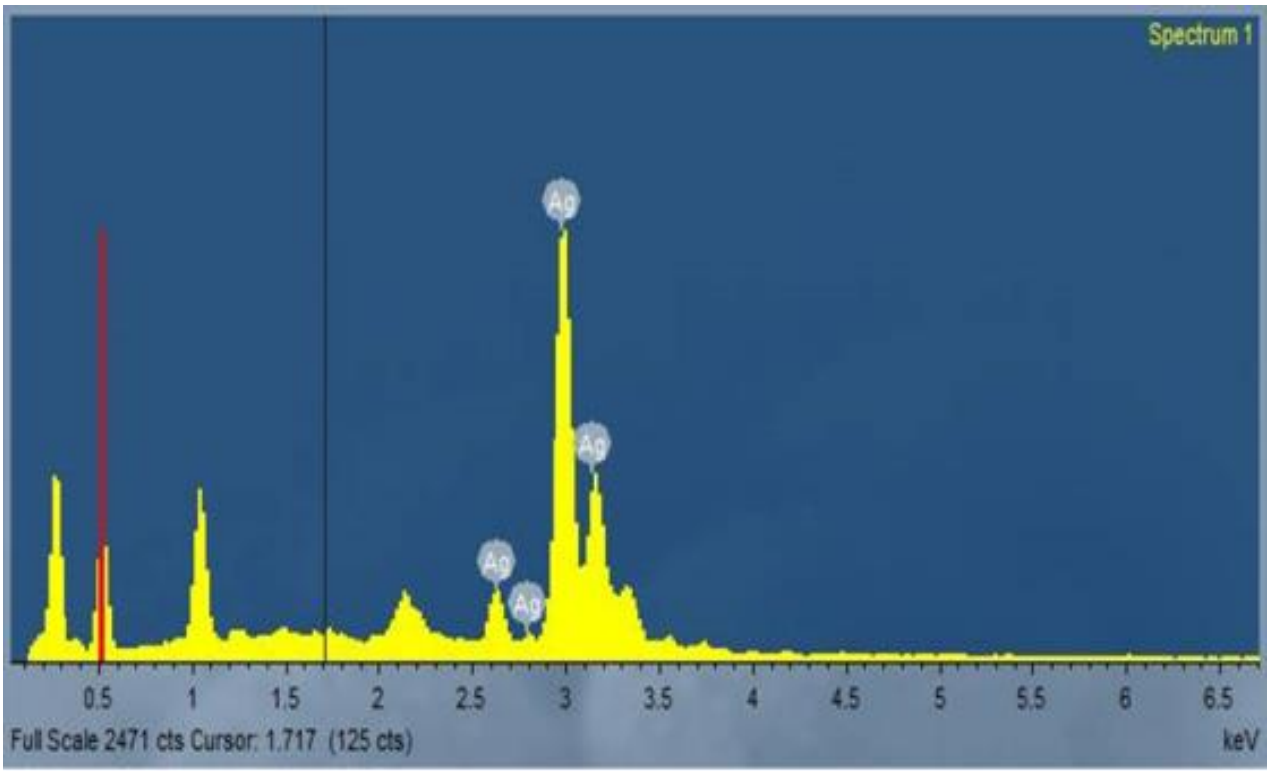

Figure 32: EDX-image of AgNP

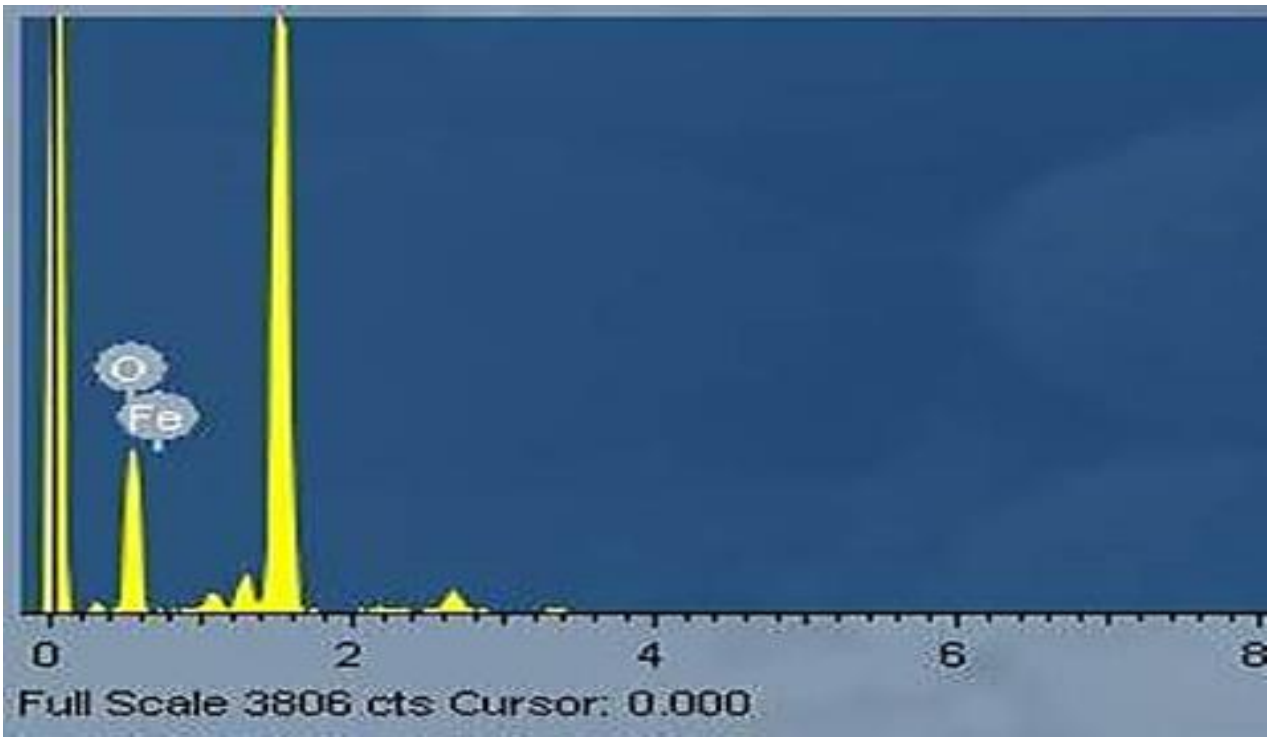

Figure 33: EDX-image of Fe_2O_3

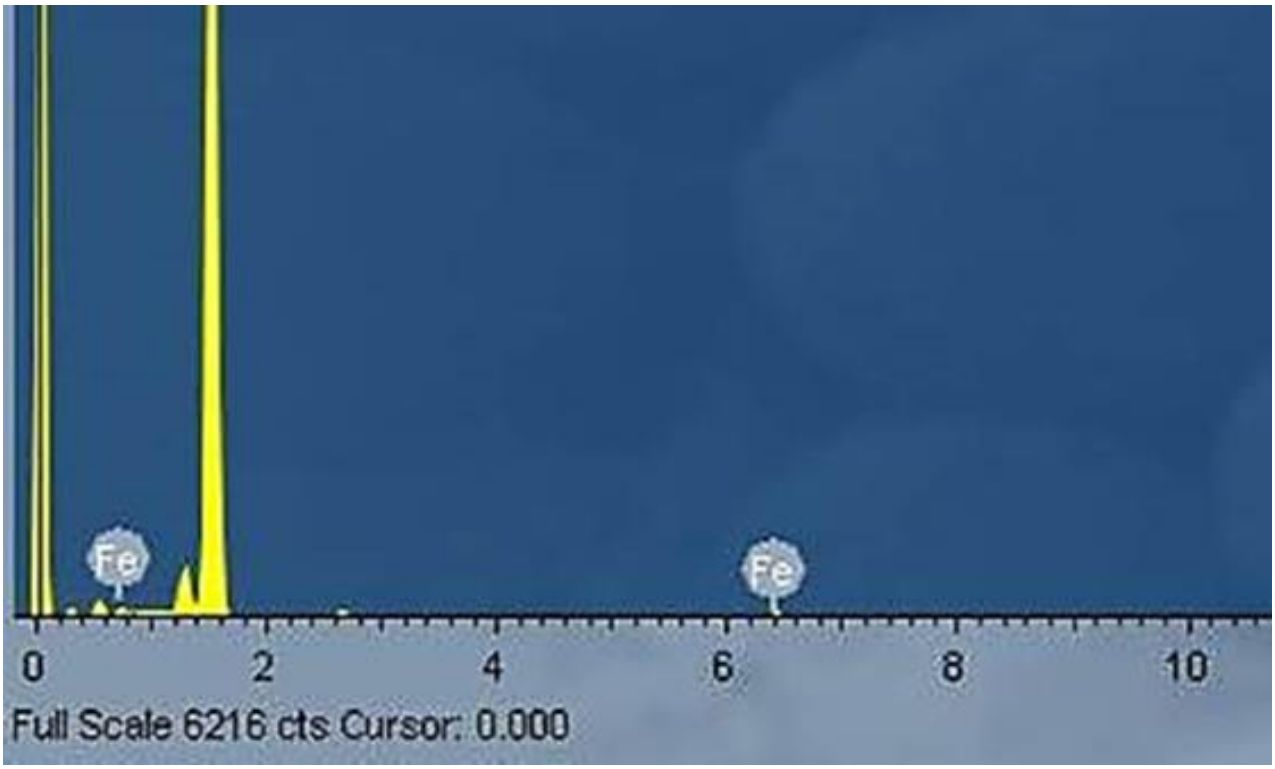

Figure 34: EDX-image of nZVI

4.3.3 Brunauer-Emmett-Teller (BET) surface area analysis and porosity analysis

The specific surface area and pore volume of the biosynthesized nanoparticles obtained by adsorption/desorption of nitrogen at -196°C is shown in Table 4.3.

Fe_2O_3 has a specific surface area of 14.76 m^2/g and a pore volume of 0.02 cm^3/g. The specific surface area and pore volume of nZVI are 15.17 m^2/g and 0.06 cm^3/g respectively. While similar result was obtained by Saware et al., (2014) for synthetic nZVI, it was attributed to the aggregation of the nanoparticles. Other researches (Watts et al., 2015) also reported that the specific surface area of Fe_2O_3 decreases with an increase in the size of the nanoparticles. At a particle size of 72 nm, they recorded a specific surface area of 21 $m^2 g^{-1}$. Biosynthesized AgNP also recorded a surface area of 14.03 m^2/g and a pore volume of 0.02 cm^3/g.

Table 4.3 showing the BET surface area and porosity of biosynthesized nanoparticles

Adsorbents	BET surface area (m^2/g)	Pore volume (cm^3/g)
AgNP	14.03	0.02
NZVI	15.17	0.055812
Fe_2O_3	14.76	0.05

4.3.4 Thermogravimetric Analysis (TGA)

Thermogravimetric analysis of the biosynthesized nanoparticles were carried out to determine the effect of temperature on the weight and subsequent decomposition of the

nanoparticles. The TGA result shows the decomposition of the nanoparticles with respect to temperature change. It can be observed from Figure 35, 36 and 37 that the weight of nZVI decreased rapidly within the first 100°C compared to Fe_2O_3. AgNP, also experience a less rapid decomposition within the first 100°C of heating (Figure 35). However, all the nanoparticles experience rapid decrease in weight after 300°C. The decomposition observed within the first 100°C may be due to the loss of water in the sample (Kanel and Manning, 2005). Subsequent decomposition between 150 and 450°C may be due to the decomposition of residues of biomolecules and organic capping agents present on the surface of the nanoparticles (Dong et al., 20011; Khalil et al., 2013).

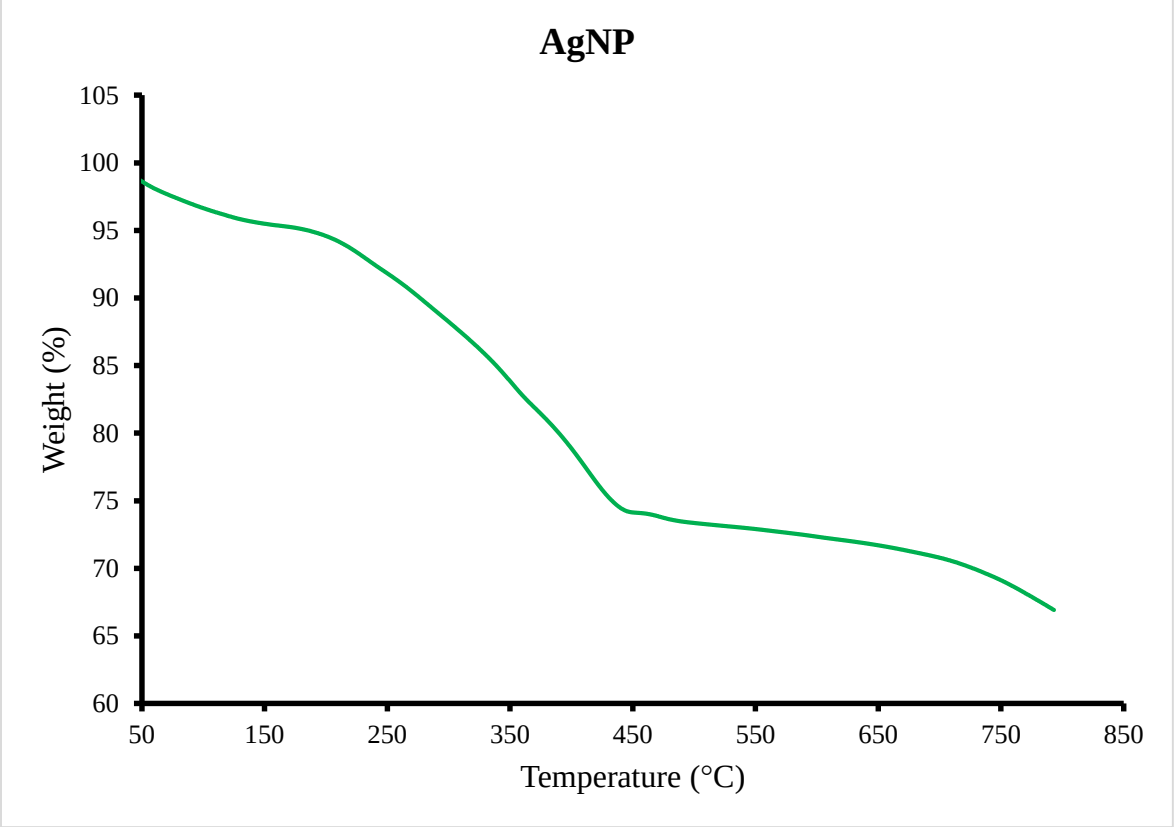

Figure 35: TGA result of AgNP

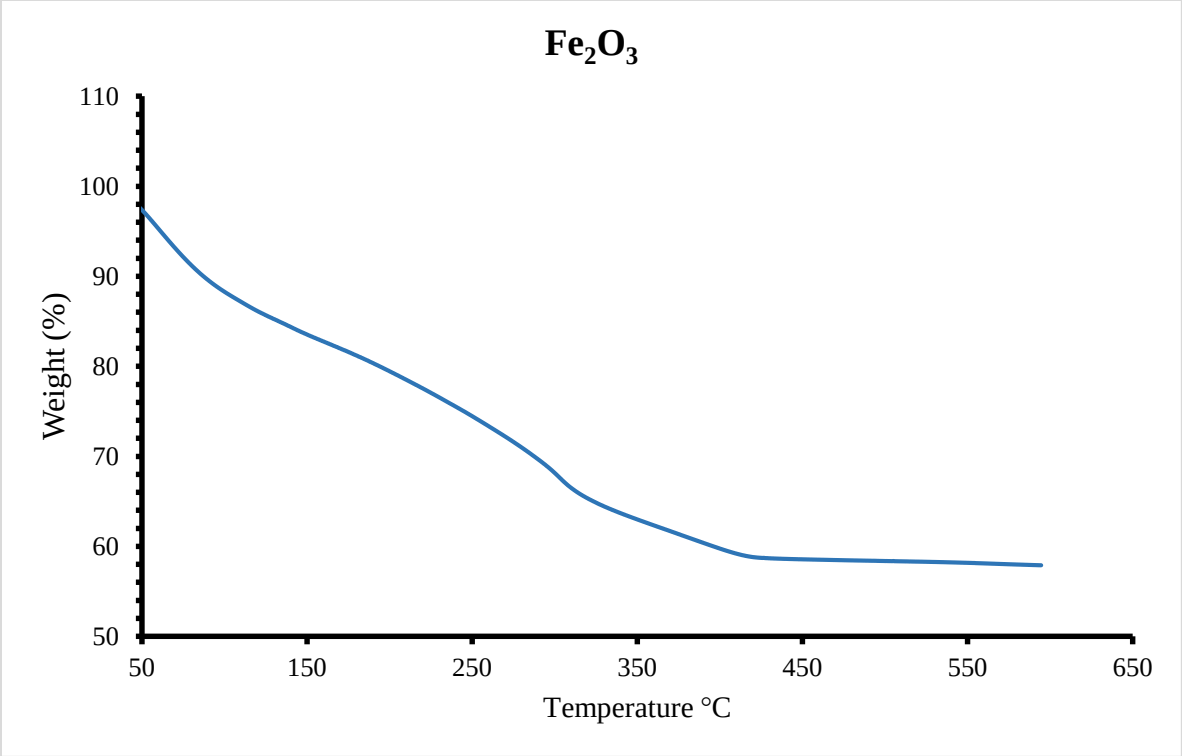

Figure 36: TGA result of Fe_2O_3

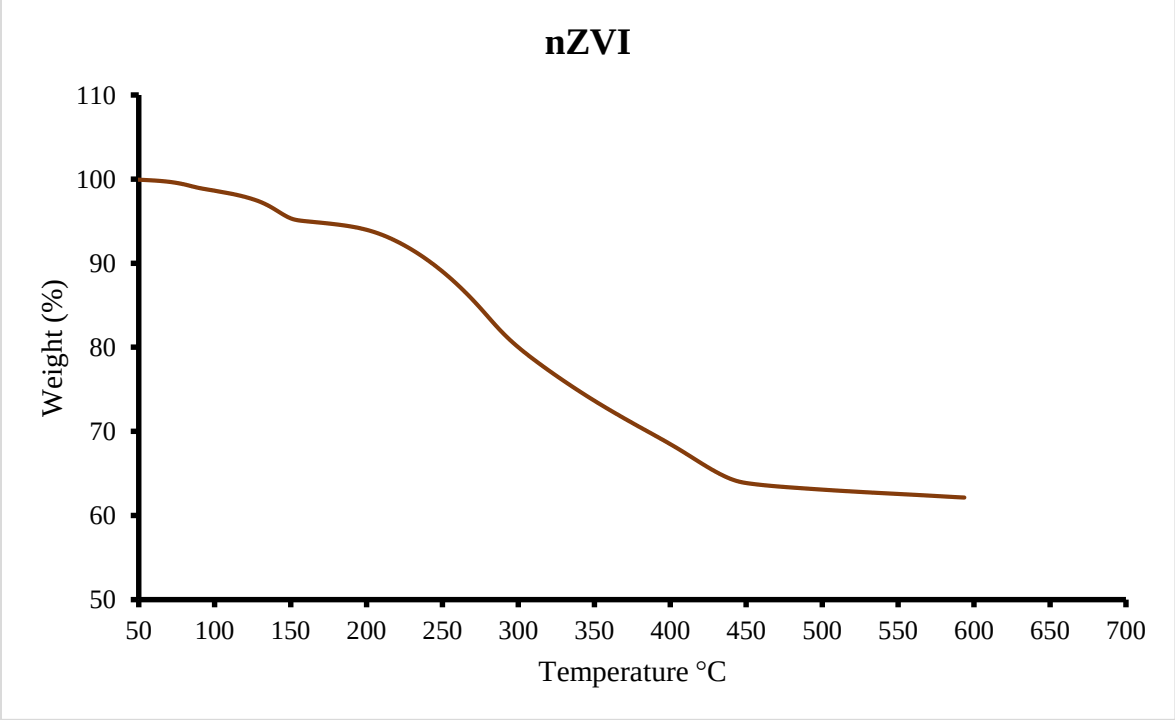

Figure 37: TGA result of nZVI

4.3.5 Fourier transform infrared spectroscopy (FT-IR)

The result of the FTIR analysis shown in Figure 38, 39 and 40 reveal different absorption bands. The peaks at approximately 3400 cm^{-1} shows either O-H stretching vibrations of hydroxyl groups (Rastogi and Arunachalam, 2011) or N-H stretching of amine and amides (Vanaja et al., 2013). The O-H stretching corresponds to fatty acids and protein structures which may be the constituents of the plant extracts. The bands at 2920 cm^{-1} and 2852 cm^{-1} may be due to C-H and C-H_2 stretching vibrations. Those at about 1,637 cm^{-1} are assigned to C=O bond stretching mode which also represent protein and fatty acid structures. The band at 1600 cm^{-1} shows alkene stretching vibration (Philip and Unni, 2011) while that at 1390 cm^{-1} is assigned to O-H bending and indicates carboxylates (Maria et al., 2005). The band at 1080 shows the absorption peak of -C-O-C- while that at 600 cm^{-1} may be due to the C-H bend of alkynes (Rastogi and Arunachalam, 2011).

The FT-IR spectrum of Fe_2O_3 (Figure 38) shows bands between 400 and 800 cm^{-1} for iron oxide. The band between 1600 cm^{-1} and 1800 cm^{-1} was assigned to carbonyl group or amine groups. Similar bands have been identified (Dubey et al., 2013; Zhou et al., 2009) in the biosynthesis of iron oxide nanoparticles using other reducing agents. For nZVI, Figure 39, the spectrum obtained shows OH stretching bands at 3, 400 cm^{-1}, CH and CH_2 bands at 2880 and 2800 CM^{-1} respectively. Signal at 2350 cm^{-1} are due to the presence of CO_2 in the air while that at 1600 cm^{-1} is attributed to C=O group binded to the nanoparticles (sundaram et al., 2012). The band observed at 1378 cm-1 is assigned to NO_3^-. The bands at 798 and 895 cm^{-1} are assigned to Fe-OH bending vibrations while 624 cm^{-1} is assigned to Fe-O stretching vibrations.

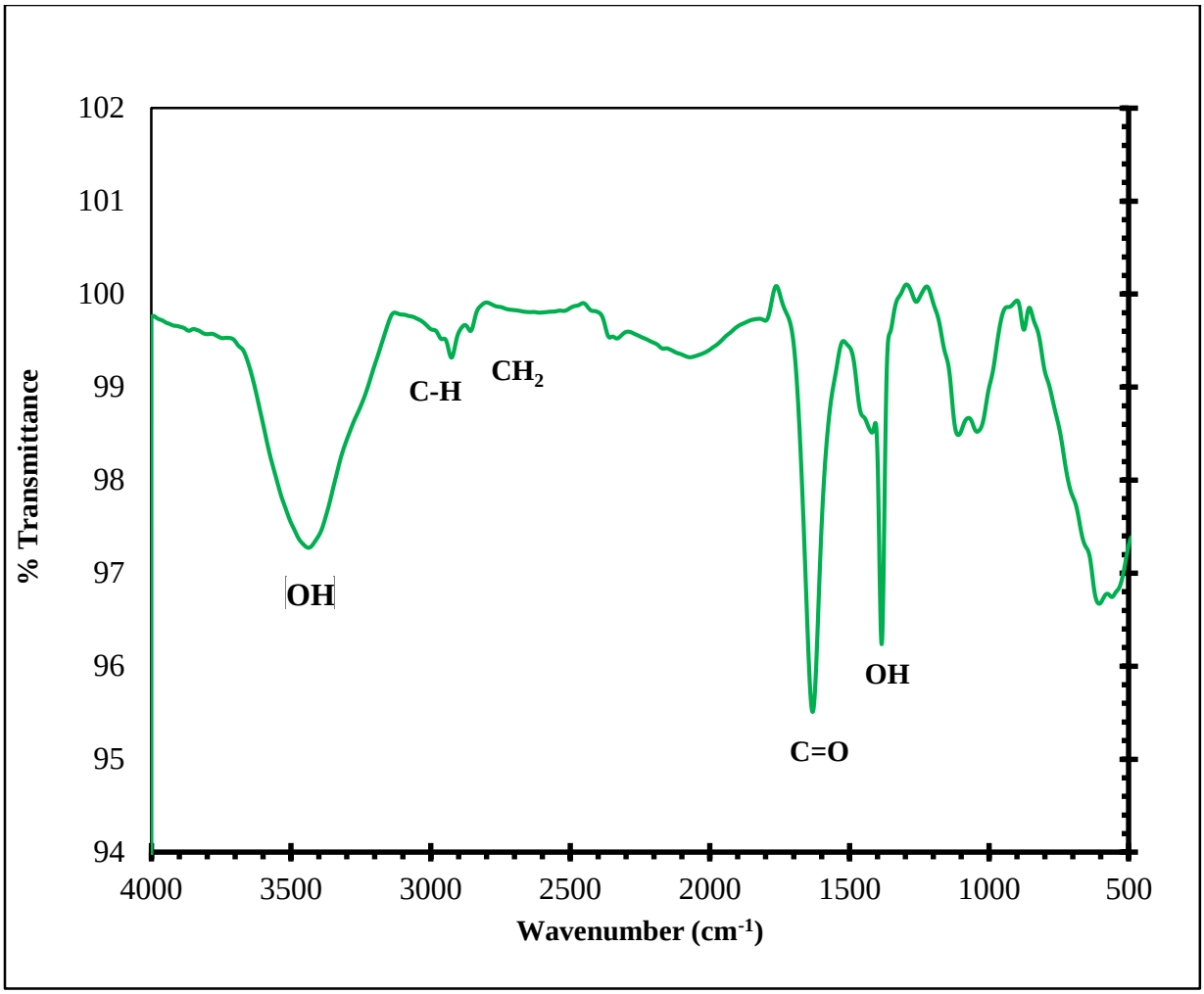

Figure 38: FT-IR spectrum of AgNP

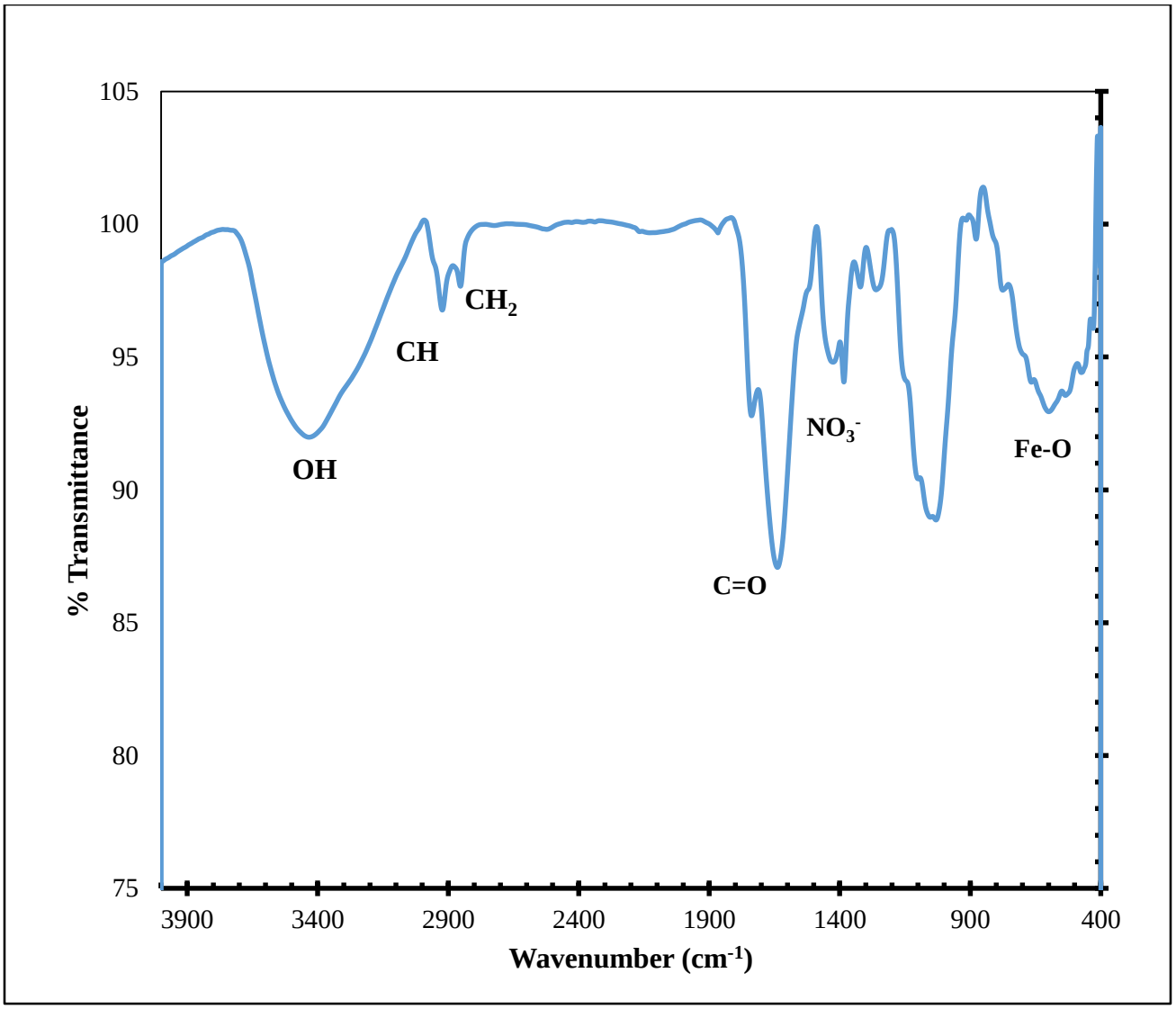

Figure 39: FT-IR of Fe_2O_3

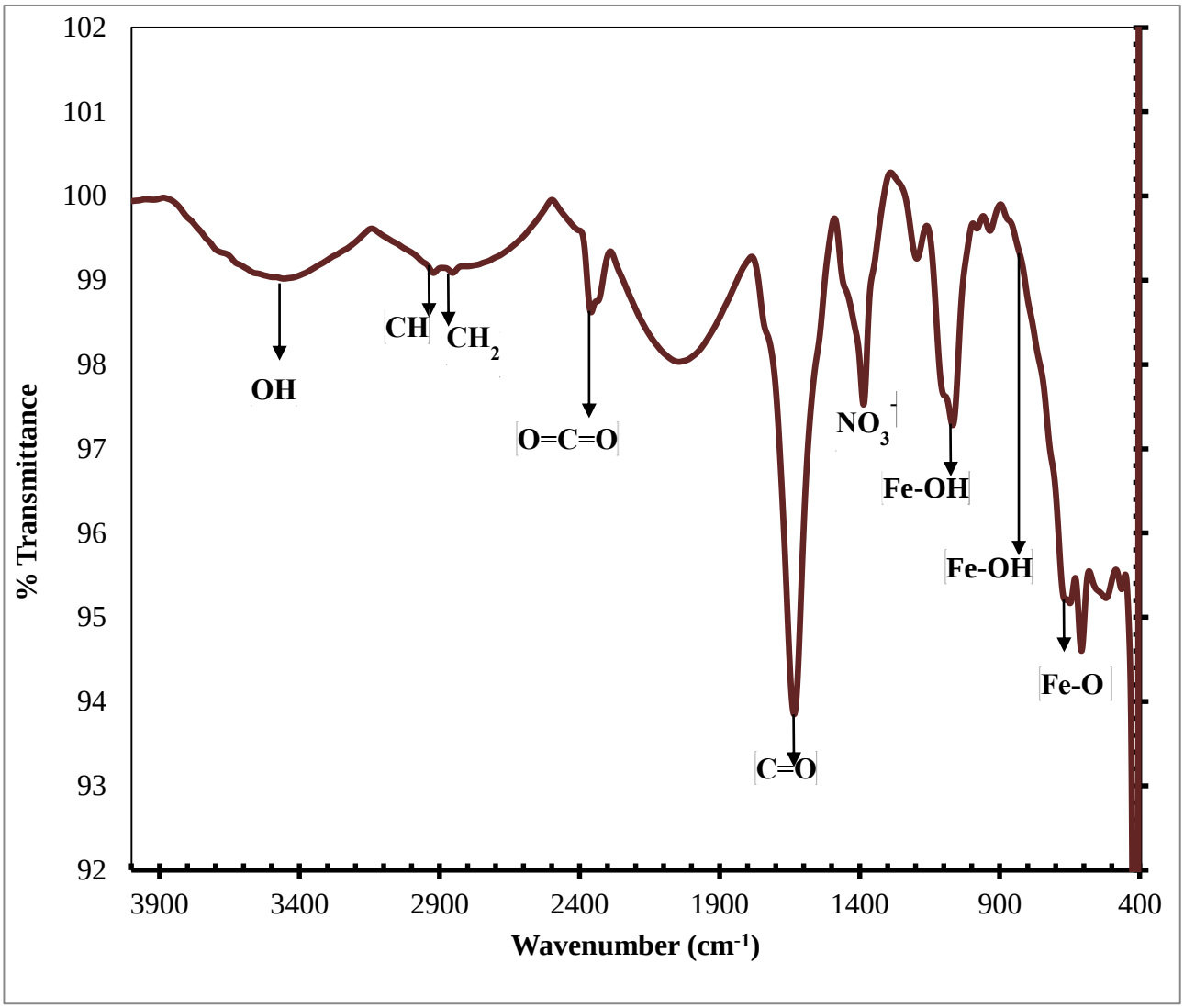

Figure 40: FT-IR of nZVI

4.3.6 X-ray diffraction (XRD) analysis

The XRD analysis is used to determine the composition, crystallinity and average particle size of the biosynthesized nanoparticles. The XRD result of the biosynthesized nanoparticles is shown in Figures below. The XRD pattern of the biosynthesized AgNPs is shown in Figure 41. The peaks are indexed as 111, 200, 220 and 311 planes of face-centered

cubic (fcc) structure of silver according to JCPDS file No. 00-004-0783. The peaks in Figure 42 are indexed as 111, 220, 311, 400, 422, 511, 400, 620 and 622 according to the Joint Committee on Powder Diffraction Standards (JCPDS) file No 01-078-6916 for biosynthesized Fe_2O_3. Similar peaks were observed by other researchers (Das et al., 2007; Sahoo et al., 2010). The scan for nZVI (Figure 43) shows peaks indexed as 110 and 200 which is in accordance with the JCPDS file No 01-085-1410. Similar results have also been reported by Yu et al., and Taha and Ibrahim, (Yu et al., 2008; Taha and Ibrahim, 2014). The low intensity of the peaks were attributed to the amorphous nature of the iron phase (Giasuddin et al., 2007). It is important to note that the JCPDS is a database of powder diffraction patterns.

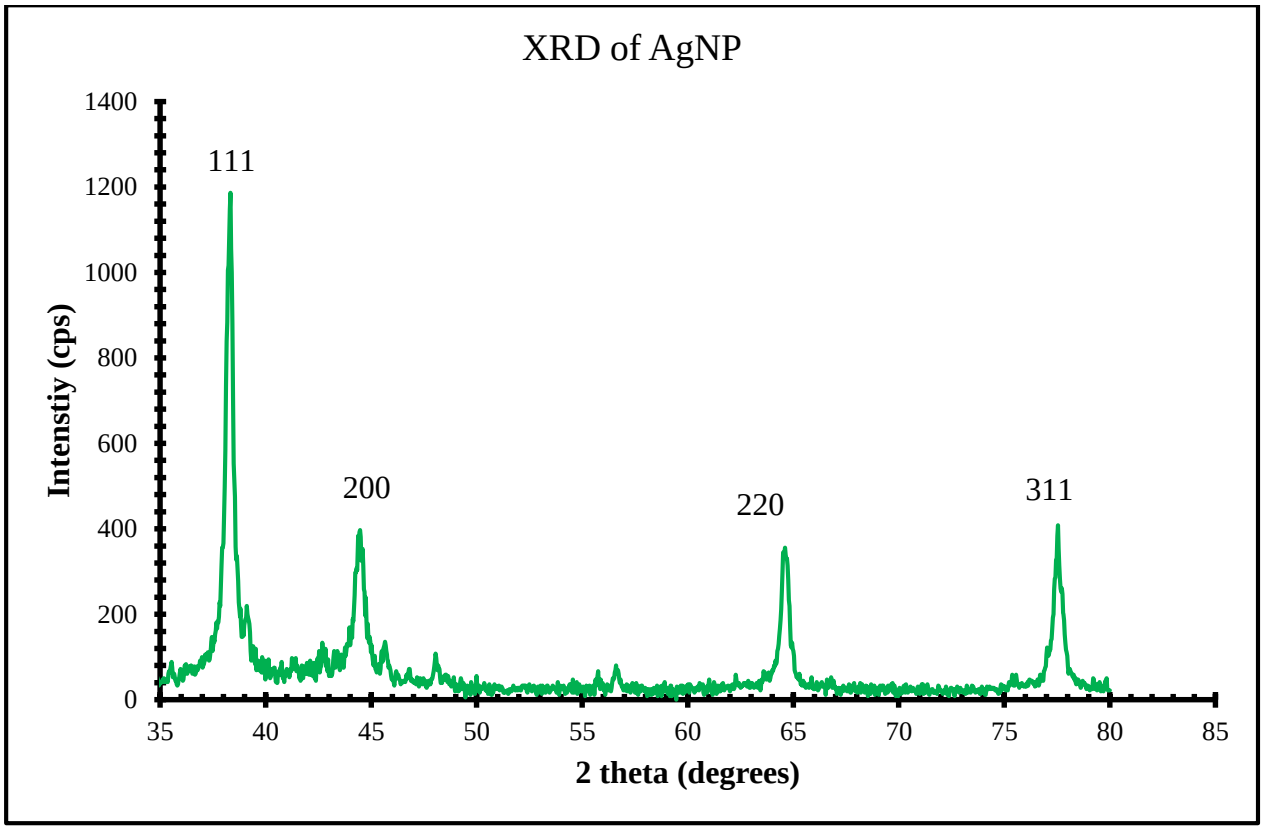

Figure 41: XRD of AgNP

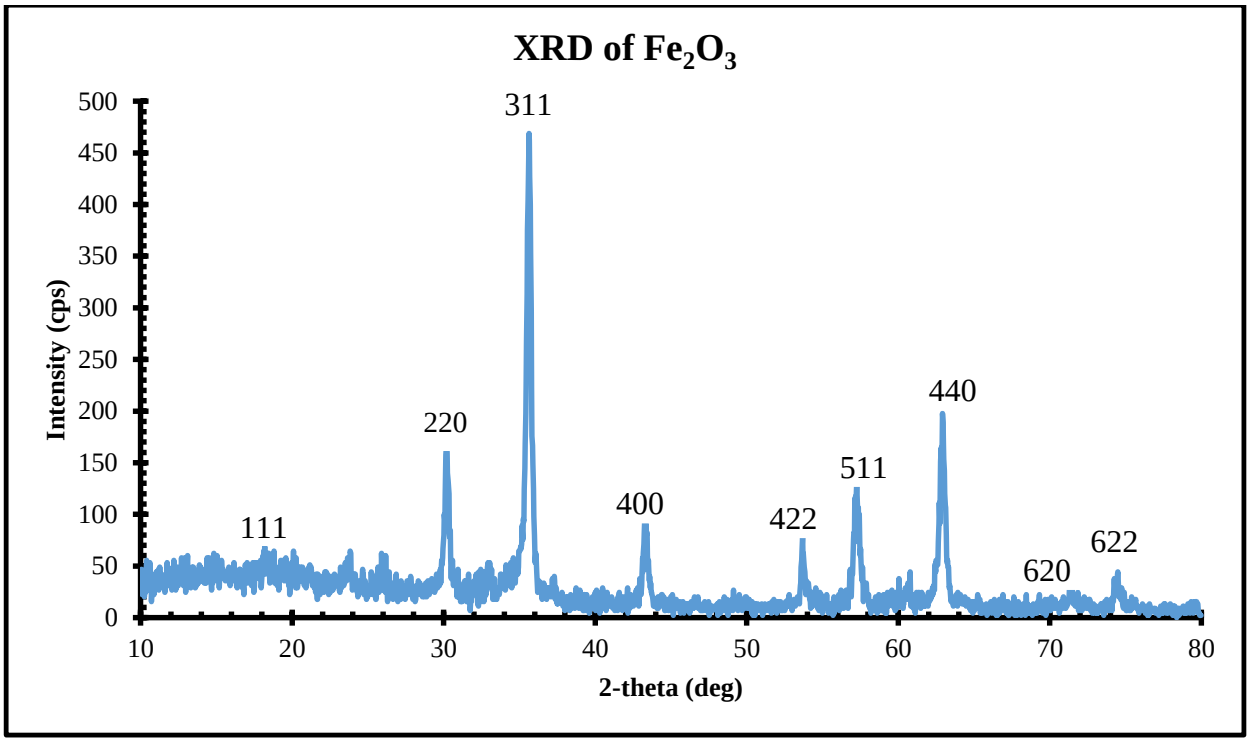

Figure 42 XRD of Fe_2O_3

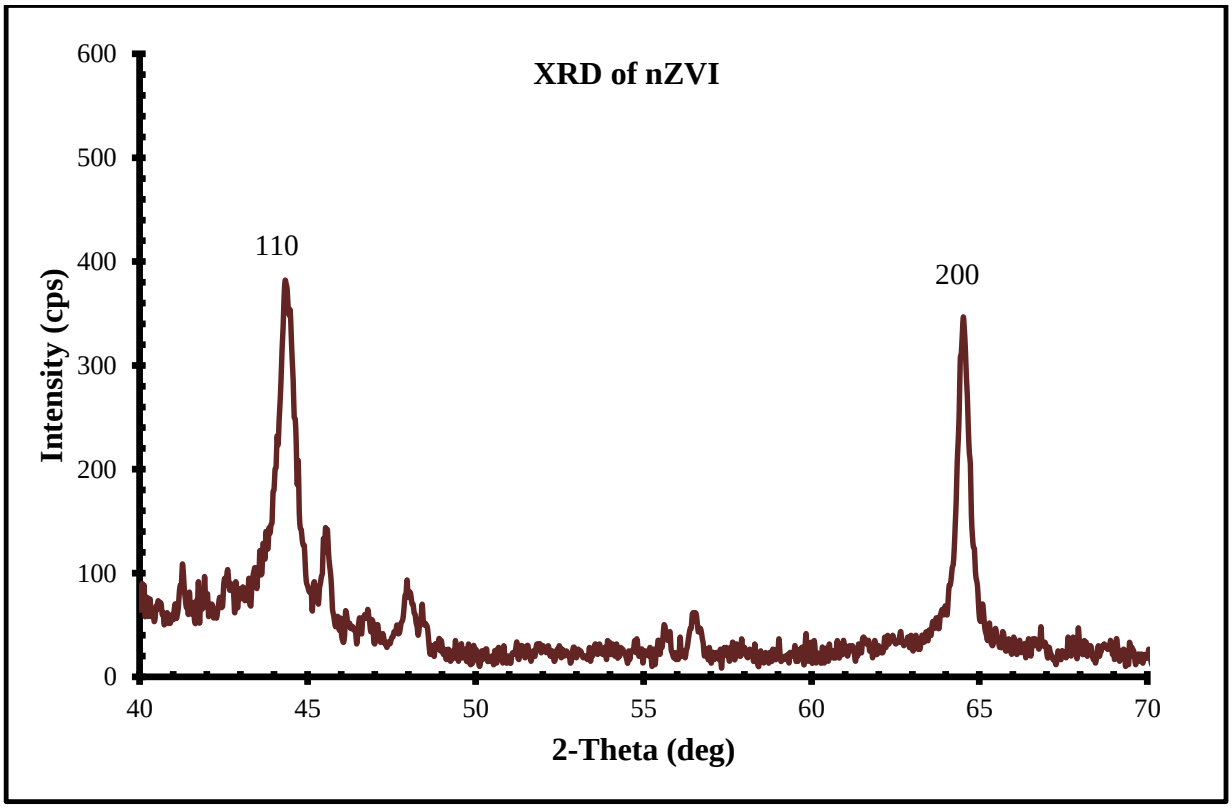

Figure 43: XRD of nZVI

4.4 Colorimetric analysis of the detection of Hg (II) in water using silver nanoparticles

4.4.1 Sensitivity studies

The sensitivity and selectivity of as-prepared silver nanoparticle in the detection of Hg (II) in aqueous solution was determined. Immediately after the addition of 1 ml of AgNPs to 9 ml of 1mM Hg (II), the colorless Hg (II) solution changed to golden brown. However, a gradual change in color from golden brown to light brown and finally to colorless occurred within 5 minutes. The change in color of the mixture indicated that the Hg (II) has a large effect on the surface plasmon resonance vibration of the AgNPs. This, however, was not the case for the other metallic cations (Ca^{2+}, Cu^{2+}, Mn^{2+}, Ni^{2+}, Na^{+}, Zn^{2+}, Ba^{2+}, K^{+}) investigated. None of the other metal salts, when subjected to the same treatments, showed any color change, even after 15 minutes. Figure 44 shows the UV-VIS of all the metal cations after the addition of volume of AgNPs. As shown in Figure 45, Hg (II) showed the highest change in absorbance of all metal cations studied. Also the absence of Hg (II) peak at 400nm (Figure 44), where all other metal cations and the blank show a broad peak, confirms that AgNPs could selectively and colorimetrically detect Hg (II) in solution. The colour change may be attributed to the aggregation of the AgNP (Bothra et al., 2013). Rastogi et al., (2014) also reported a similar de-coloration upon the addition of Hg (II) to as-synthesized silver nanoparticle. They attributed the de-coloration to the formation of Ag-Hg amalgam. As such the change in color illustrated in Figure 46 further confirms the selectively of AgNPs in mercury (II) detection. This selectivity occurs because the AgNPs and the Hg (II) form silver-mercury amalgam, where the mercury II ion is reduced to metallic mercury.

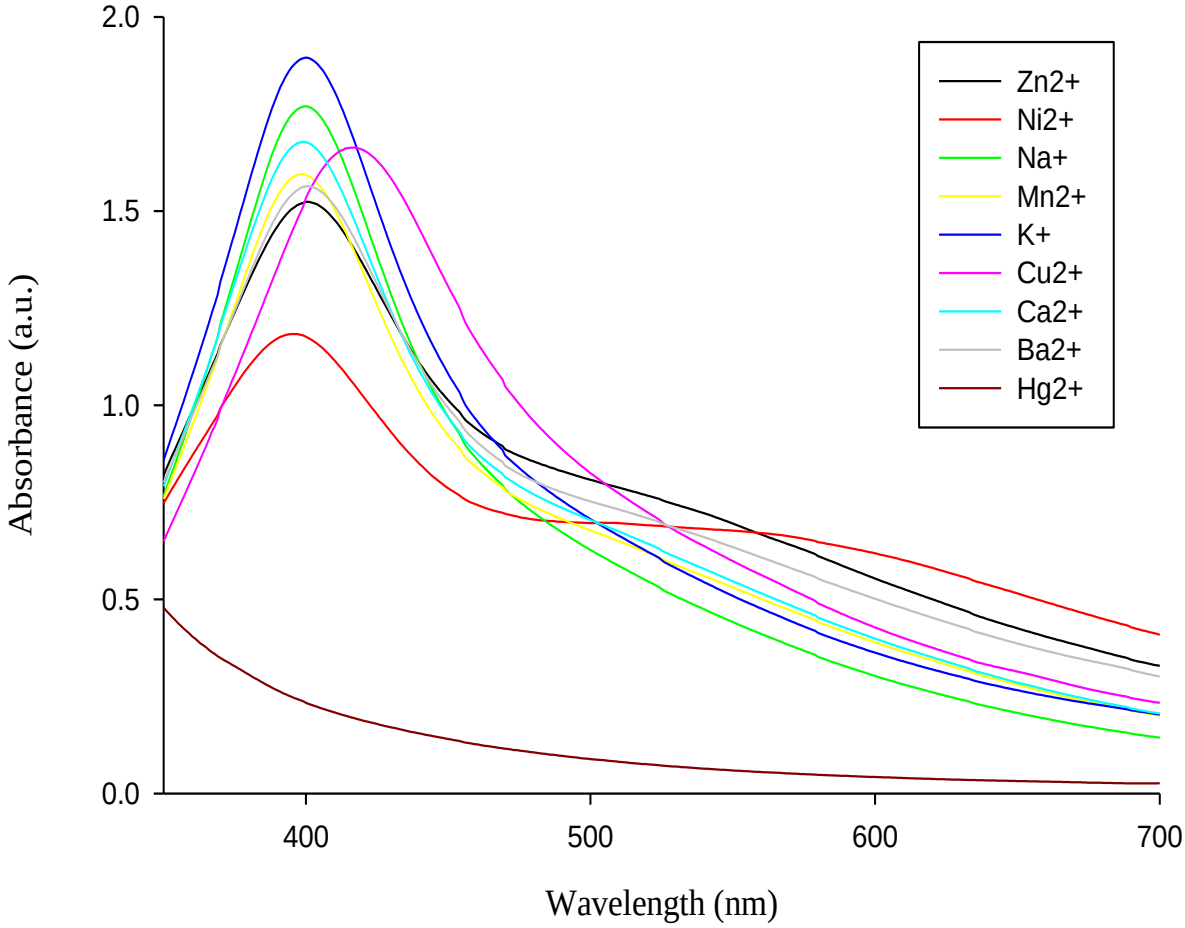

Figure 44: UV-Vis spectra of a 1 ml AgNPs solution after adding 9 ml of a different metal salt

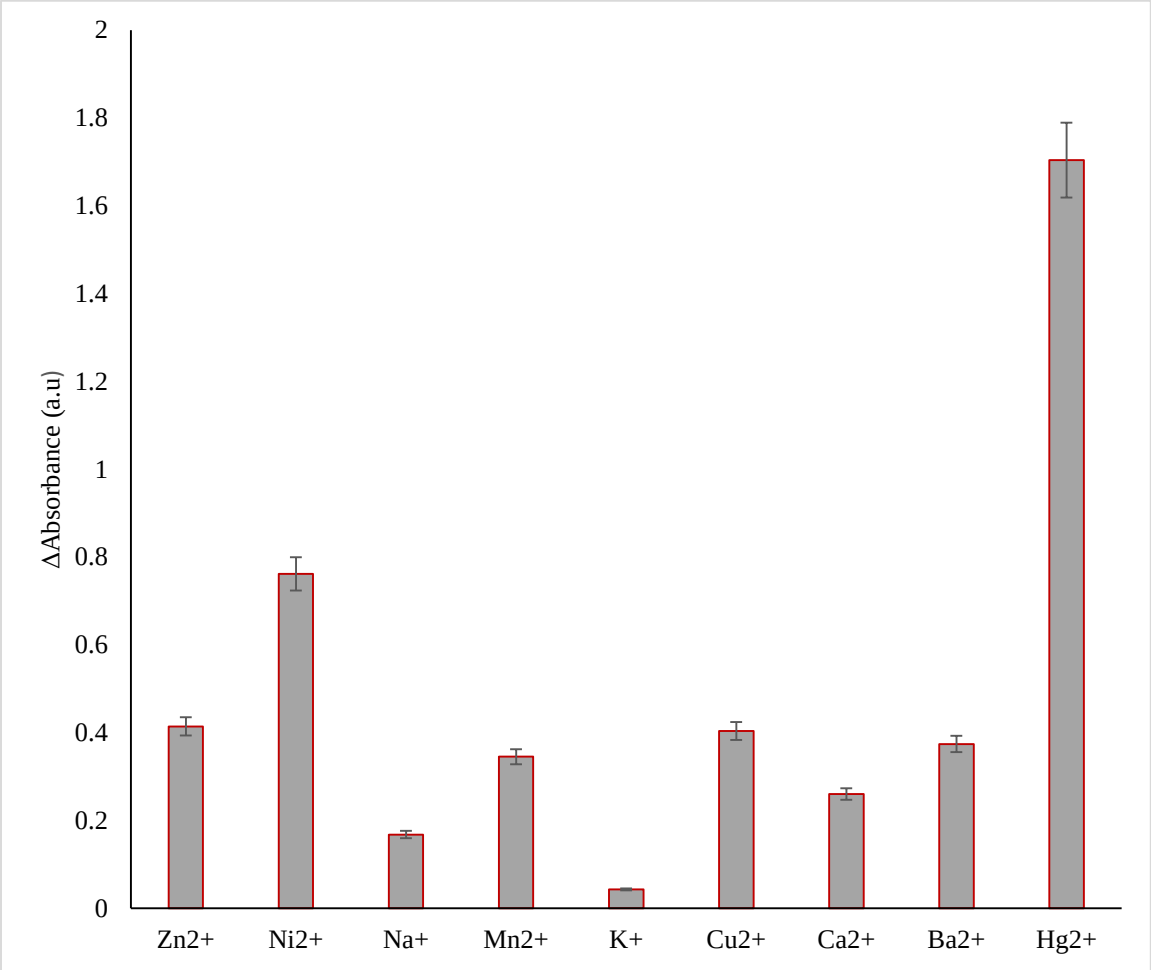

Figure 45: Change in the visible absorbance of all metallic cations, reflecting their colorimetric response upon exposure to AgNPs

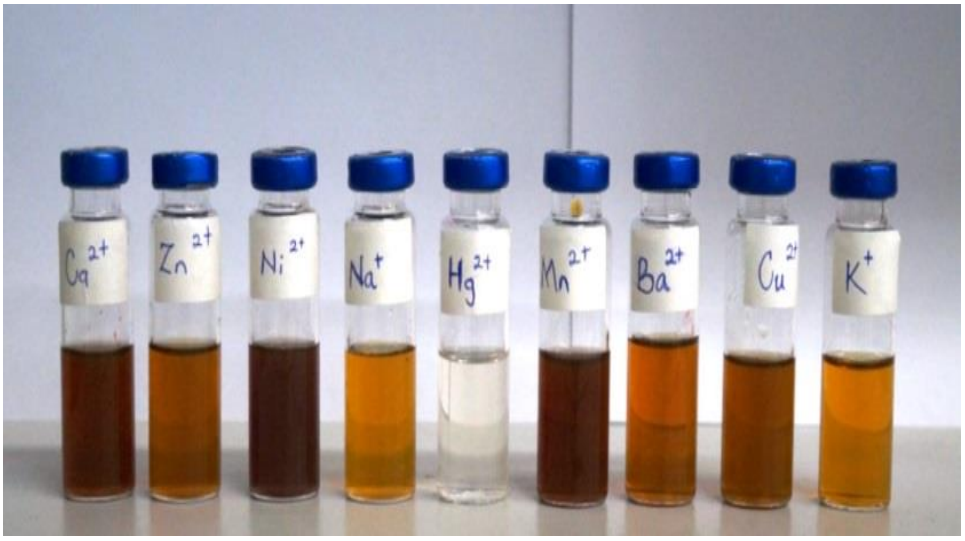

Figure 46: Image reveals the color of each metal immediately after addition of AgNPs

In order to determine the sensitivity of as-prepared AgNPs to Hg (II) and hence the detection limit of Hg (II) in the mixture of Hg (II) and AgNPs, the concentration of Hg (II) was reduced from 90µM to 62.5 nM. This caused the color change in the aqueous solution to gradually lessen. As the concentration of Hg (II) drops, the intensity of the color change diminished; however the UV-vis analysis continues to reveal absorbance differences for each of the Hg (II) concentrations examined in Figure 47. Thus the UV-vis analysis showed that as the concentration of Hg (II) has increased. The change in absorbance is linear from 1 µM to 90 µM, with a regression value of 0.98, Figure 48. At nano-scale (inset of Figure 48) the regression value obtained was also 0.98. Calculation of the limit of detection was done according to the guidelines of American Chemical Society's Committee on Environmental Analytical Chemistry and IUPAC using the relation; $S_{LOD} = S_{RB} + 3\sigma_{RB}$, where S_{LOD}, and S_{RB} are the signal at the limit of detection and of the reagent blank respectively, while σ_{RB} is the reagent blank's standard deviation. A comparison of the limit of detection obtained in this word with other similar previous study is shown in table 4.4. Thus the low detection limit obtained in this study may be attributed to the basil extracts

in reducing $AgNO_3$. Previously, Ahmed et al. (2010) reported that basil leaves are suited to be used in the biosynthesis of silver nanoparticles and described their ability to ensure an effective coating on silver nanoparticles enhancing their stability and reducing agglomeration. The stability of silver nanoparticles synthesized using basil leaves has been reported by Ahmed et al., in (2010) and Daizy Philip and C. Unni in (2011). The stability is reported to be due to the formation of a thin layer of silver electride; which aids in the conversion of the silver ion to nanosilver. Huang et al., (2005) also reported that the stability of as-synthesized is enhanced as a result of the strong interaction between biomolecules and the nanoparticles. Also, nanoparticles with very small particle sizes are expected to provide a high surface area for the amalgamation of more Hg (II). As such, forming very small particles that show less agglomeration may have enhanced the colorimetric detection of Hg (II) in our study.

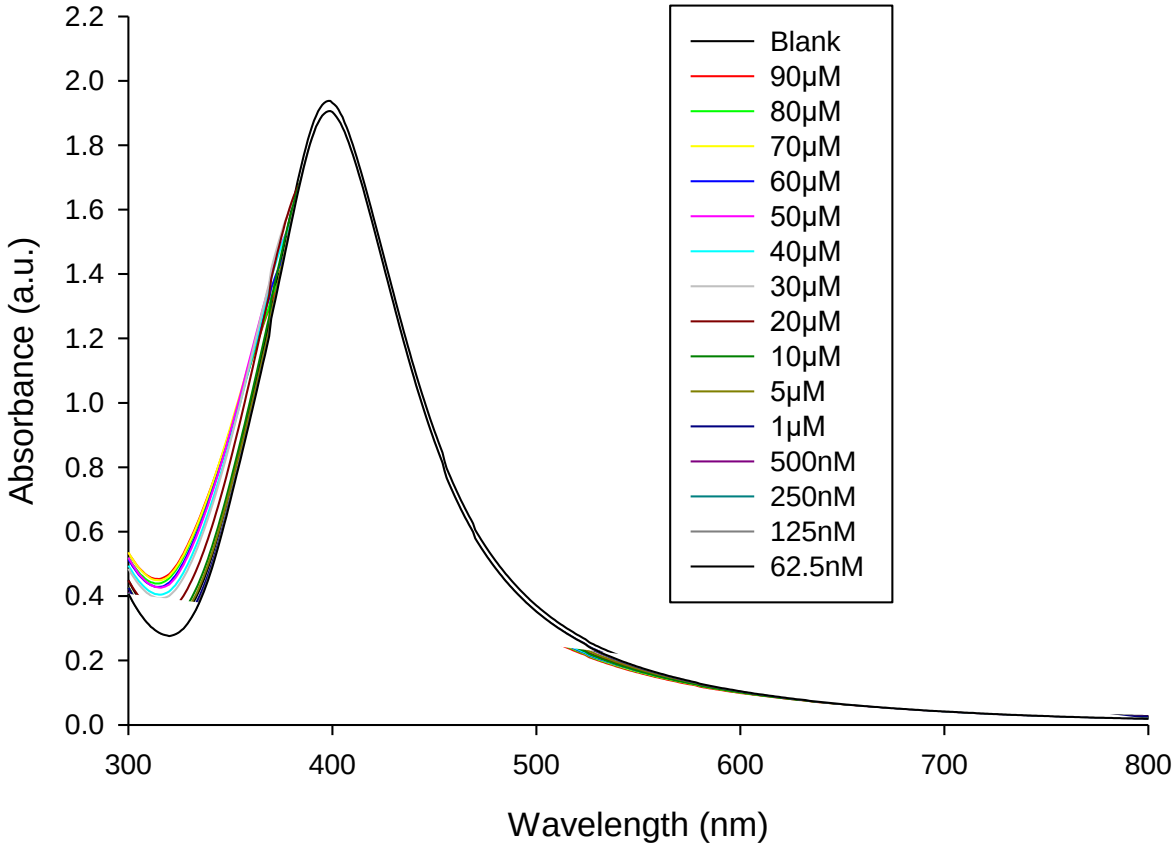

Figure 47: UV-Vis spectra of a 1 ml AgNPs solution after adding various concentrations of Hg (II) ions

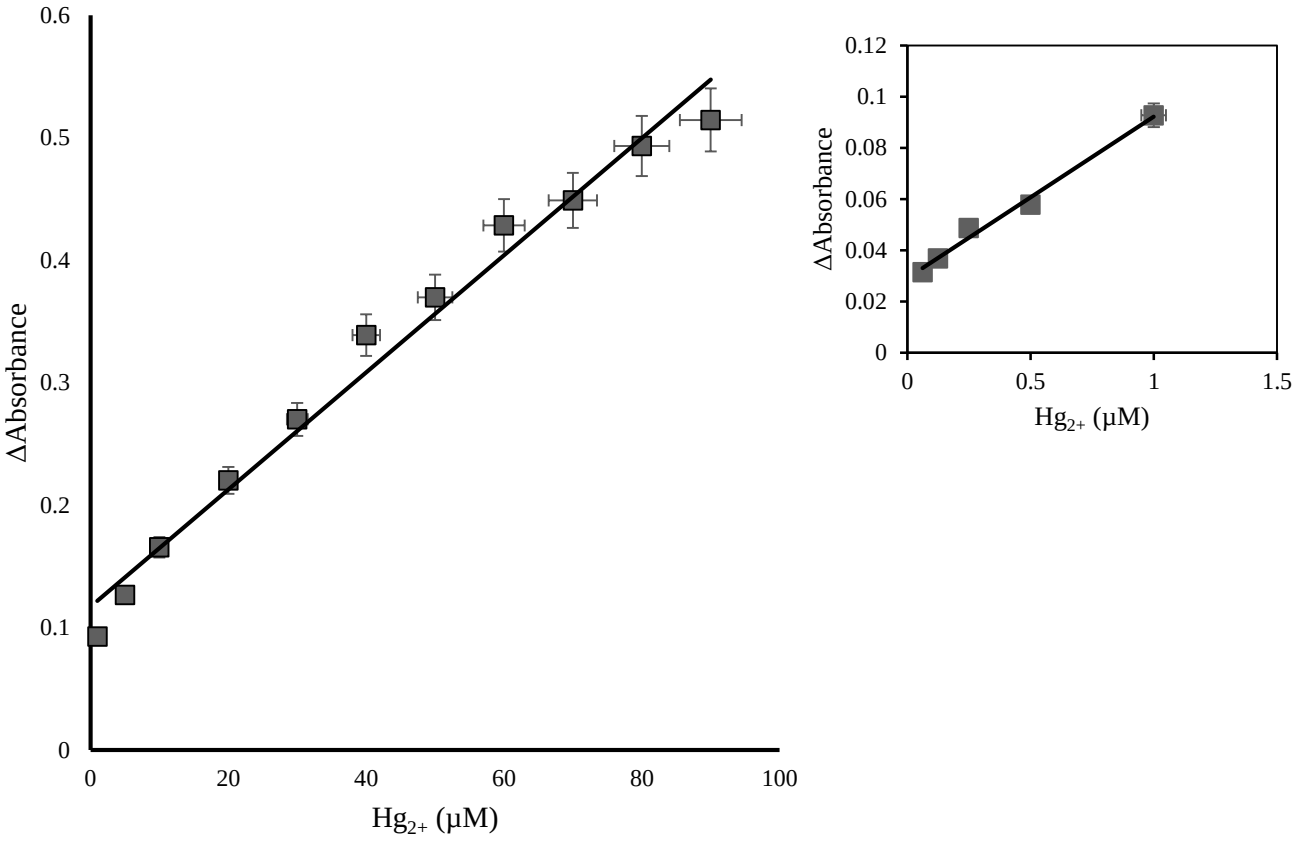

Figure 48: A plot showing the change in absorbance at 400 nm as the concentration of Hg (II) used in the colorimetric study is increased. Inset shows the change in absorbance at very low concentration.

Figure 46 confirms the selectivity of AgNPs to detect mercury in aqueous solution. Also, to determine the efficiency of this method to a real life situation, a complex matrix was formed to simulate a situation where different metals are mixed together. An equal volume (10mL) of a 1 mM solution of Ca^{2+}, Cu^{2+}, Mn^{2+}, Ni^{2+}, Na^{+}, Zn^{2+}, Ba^{2+}, K^{+}, and Hg^{2+} were mixed together, and 1 mL of AgNPs added to 9 mL of the complex matrix, making a 10× diluted solution. This was repeated for a matrix without Hg (II), for a solution containing only Hg (II) and a blank to serve as controls. Figure 49 shows the color change that occurred during this experiment, while Figure 50 shows the corresponding UV. From the figures, it can be deduced that the presence of other metals poses very little interference to

the detection of Hg in the aqueous medium. While a solution containing mercury alone appears to be the clearest, the complex matrix without Hg (II) is almost the same as the blank containing de-ionized water and AgNPs only.

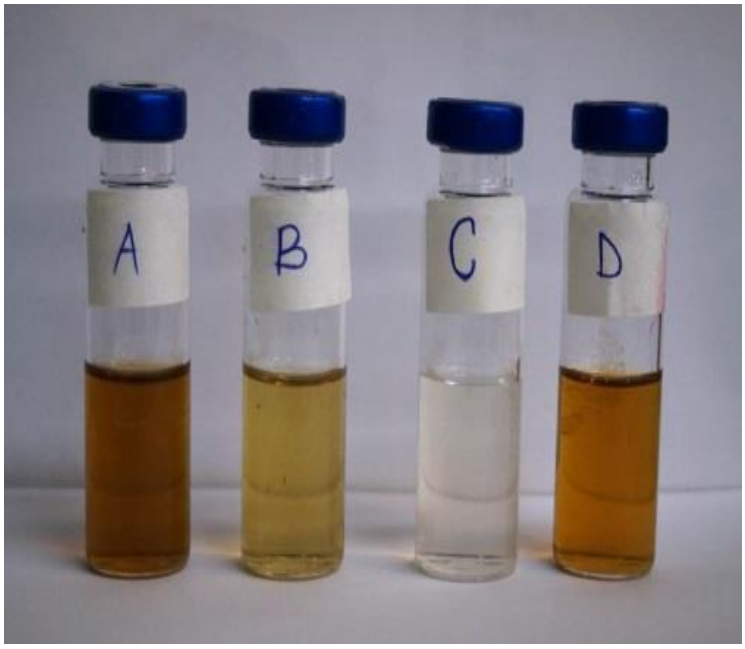

Figure 49: Image as labeled shows A: AgNPs + all metals except Hg; B: AgNPs + all metals including Hg; C: AgNPs + Hg alone; D: AgNPs + deionized water.

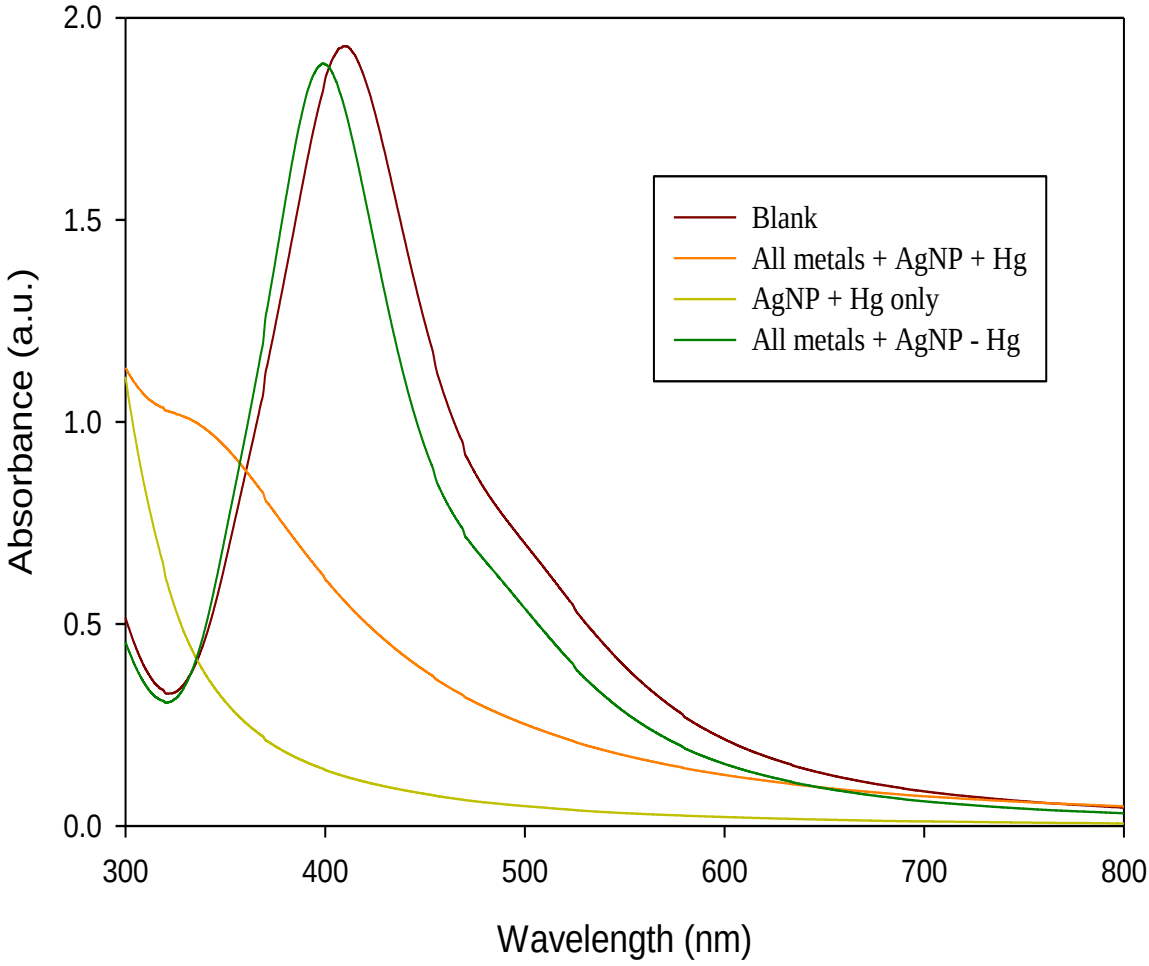

Figure 50: UV – Vis showing how the method responds to interference

Field emission scanning electron microscopy images of AgNPs after the addition of mercury (II) is shown in Figure 51. The SEM image before the addition of mercury (II) shows an agglomeration of spherical-shaped AgNPs (Figure 29). Figure 51 shows changes in the surface morphology of the AgNPs and a reduction in the amount of nanoparticles noticed in the first image. The presence of mercury in the solution was confirmed in the FE-SEM and EDX images in Figure 51.

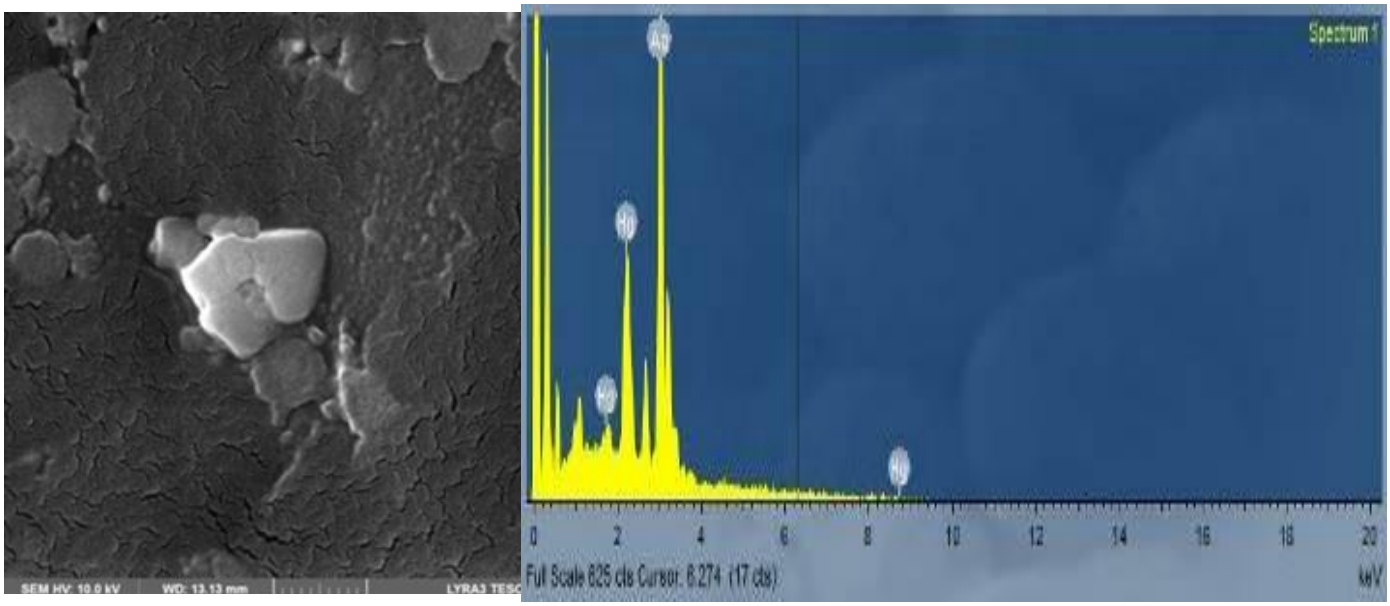

Figure 51: FE-SEM and EDX images of AgNP after the addition of Hg (II)

Table 4.4 Comparison of detection limits of different colorimetric approaches in detection of Hg (II)

Work	**Colorimetric detector used**	**Limit of detection**
Huang et al., (2015)	(Z)-2-(4-amino-phenyl)-3-(pyridine-4-yl)acrylonitrile (I) and (Z)-2-phenyl-3-(pyridin-4-yl)acrylonitrile (II)	1.74×10^{-10} M
Pan et al., (2015)	Silver and graphene oxide nanocomposite	3.38×10^{-7} M
Bothra et al., (2013)	surface functionalization of silver nanoparticles (AgNPs) with β-alanine dithiocarbamate (ADTC)	4.89×10^{-6} M
This work	Biogenic synthesized silver nanoparticles	6.25×10^{-8}M

4.5 Adsorption studies

Adsorption studies were carried out using the various adsorbents and the effect of different treatment conditions fully investigated. The effects of pH, contact time, adsorbent dosage and agitation speed were evaluated in batch adsorption mode for the removal of Hg (II) in water

4.5.1 Effect of contact time

The effect of contact time necessary for the adsorption of Hg (II) by biosynthesized nanoparticles was obtained by running the experiment at constant values of pH and nanoparticle dosage. The adsorption of Hg (II) to the nanoparticles increased with time as shown in Figure 52. Equilibrium was attained after 120 mins for both adsorbents. A less pronounce increase in adsorption after 120 minutes may be attributed to the saturation of the active sites of the adsorbents. Yardim et al., (2003) reported the removal of Hg (II) using activated carbon obtained from furfural at a shorter time (60 mins). They also reported a similar trend in the removal of Hg (II) as equilibrium is attained. The trend was attributed to the saturation of less available adsorption sites.

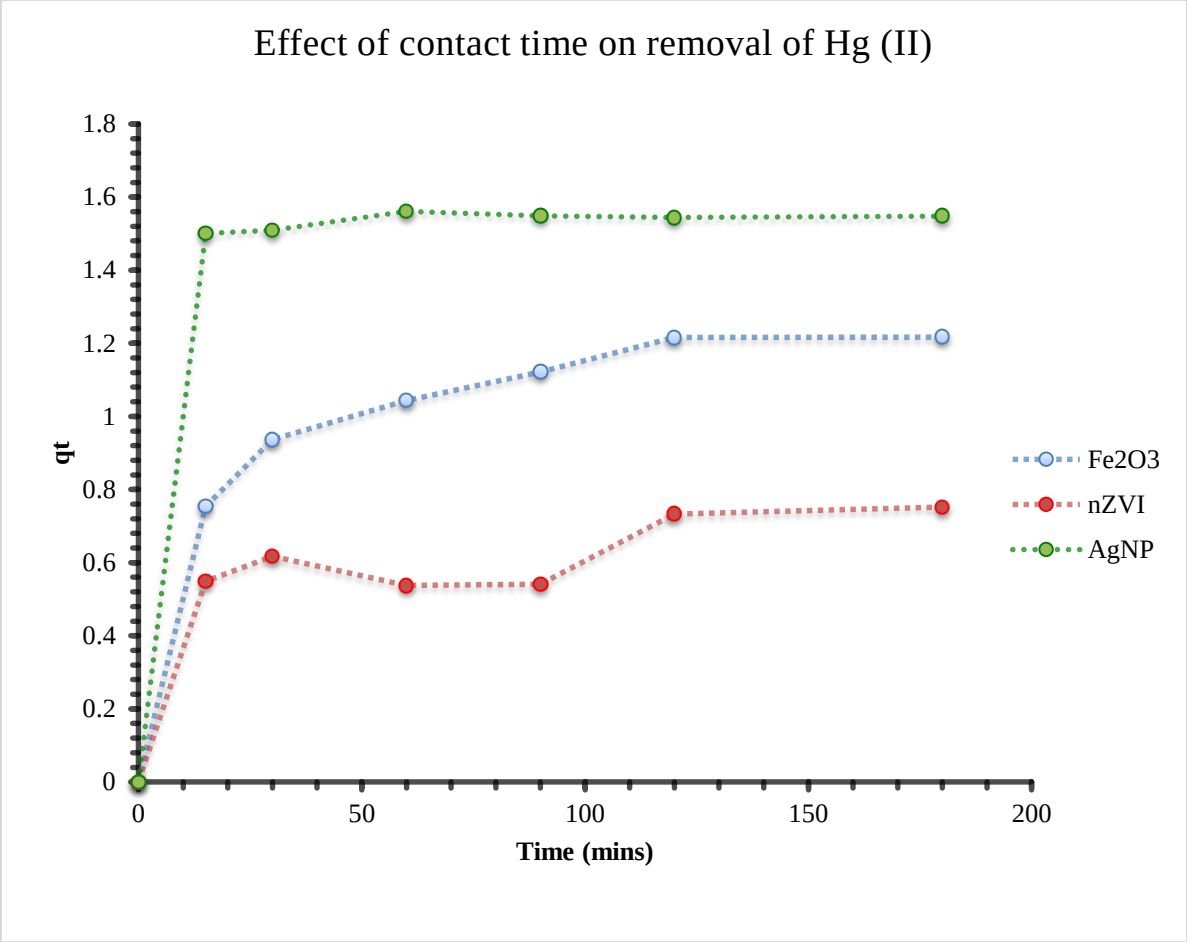

Figure 52: Effect of contact time on the removal of Hg (II) from water

4.5.2 Effect of adsorbent dosage

Nanoparticle dosages (15, 20, 30 and 40mg) were varied to determine its effect on the removal of the contaminant from water. All other parameters were kept constant. The result obtained shows that as the dosage increased, there was an increase in the removal of Hg (II) from water using nZVI and Fe_2O_3 (Figure 53). The increase may be due to the fact that more active sites, for binding Hg (II), becomes available as the dosage is increased. Similar result has been reported by (Dehner and Barton, 2010) in the removal of Hg (II).

Namasivayam and Kadirvelu (1999) also observed increasing removal efficiency of Hg (II) with an increase in the dose of activated carbon.

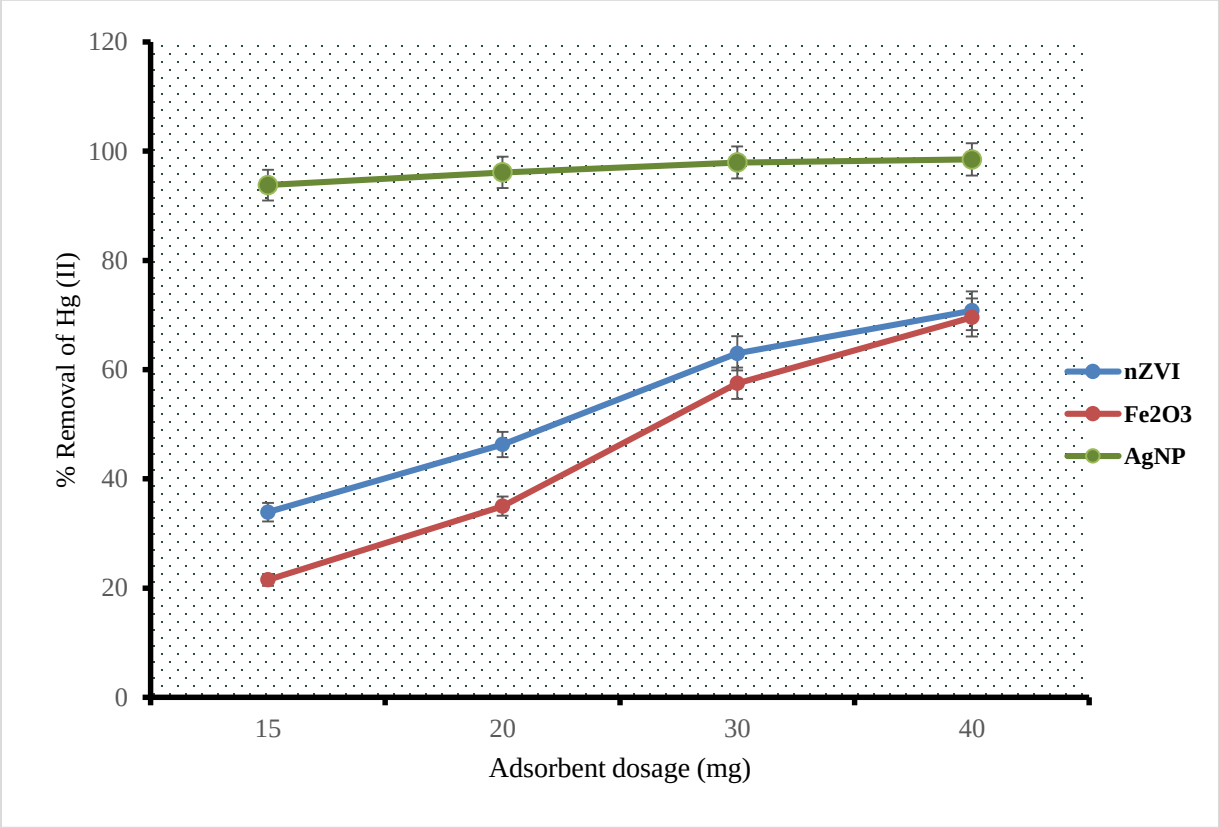

Figure 53: Effect of dosage on the removal of Hg (II) from water

4.5.3 Effect of pH

Adsorption characteristics at varying pH of the aqueous solution were investigated within pH range 4-9. Adsorption of Hg (II) to both adsorbent increased as the aqueous solution is changed from acidic to basic as shown in Figure 54 with the optimum removal of Hg (II) recorded at pH 7. It can be deduced that the adsorption of Hg (II) to the biosynthesized nanoparticles is lowest in acidic medium and highest in a neutral medium. However a

continuous reduction is noticed as the solution becomes more basic at pH 9. This is in accordance with result reported by (Dubey et al., 2013). The low adsorption at acidic medium may be due to the fact that the competition for adsorption between Hg (II) and H^+ is supported at acidic medium. Thus, as pH increases the amount of H^+ available in the solution decreases making it easier for Hg^+ to be adsorbed from solution. However, as the pH of the solution becomes basic, the reduction in the adsorption of Hg (II) may be due to formation of soluble hydroxide of the contaminant.

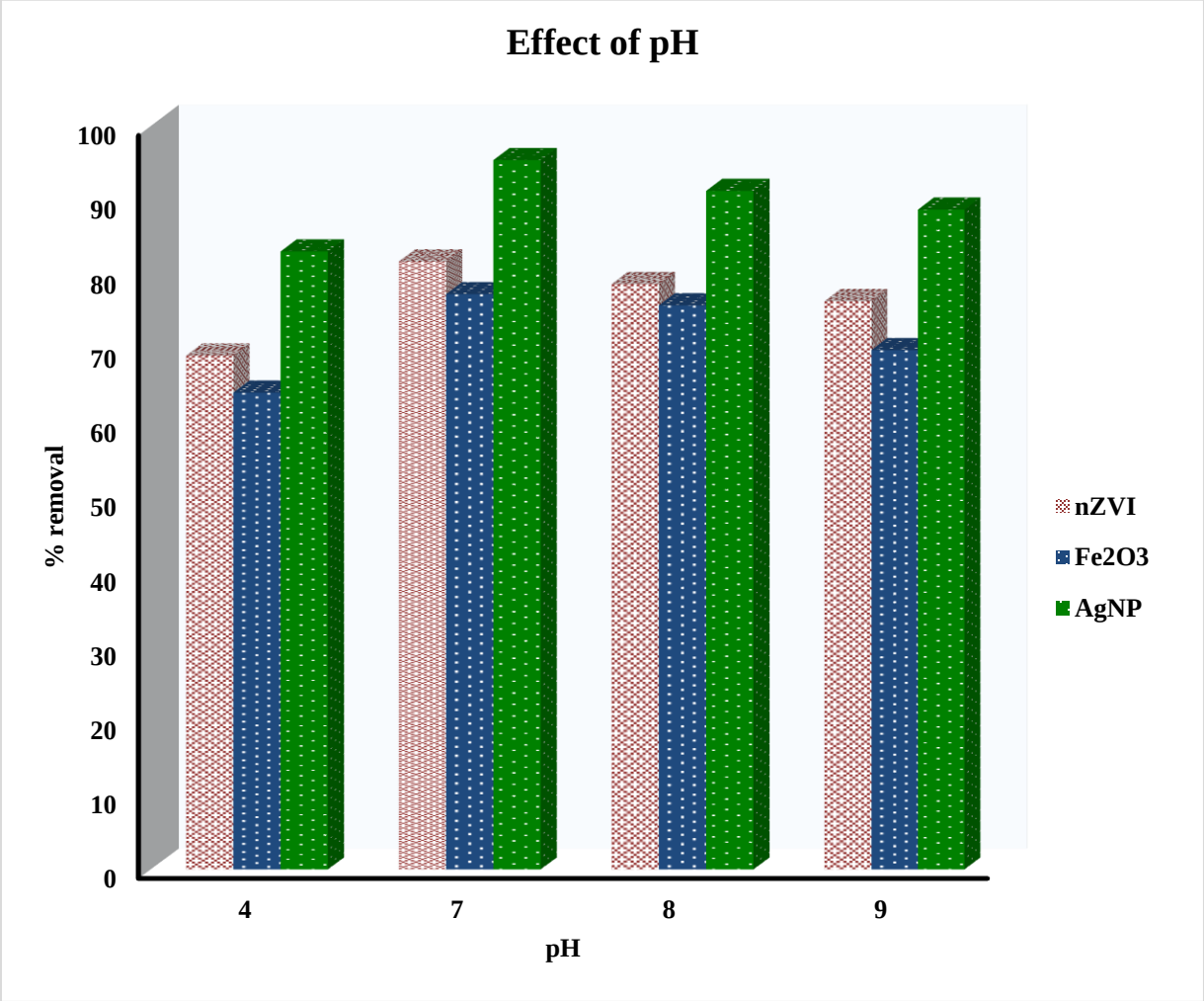

Figure 54: Effect of dosage on the removal of Hg (II) from water

4.5.4 Effect of agitation speed

A shaker produced agitation of the batch adsorption experiment to determine the effect of agitation speed on the adsorption of Hg (II) to the nanoparticles. The speed of the shaker was varied from 50 to 200 rpm while other parameters were kept constant at pH = 7, 25 mg dosage, 20 mL solution and 2 hours. As illustrated in Figure 55 below, the percentage of Hg (II) removed increased as the agitation speed increased. The increase in adsorption of Hg (II) as the agitation speed increases can be attributed to increase in the effective contact of mercury ion as the speed of the shaker increases. Tawabini et al., (2010) recorded up to 98% removal of Hg (II) at 150 rpm agitation speed.

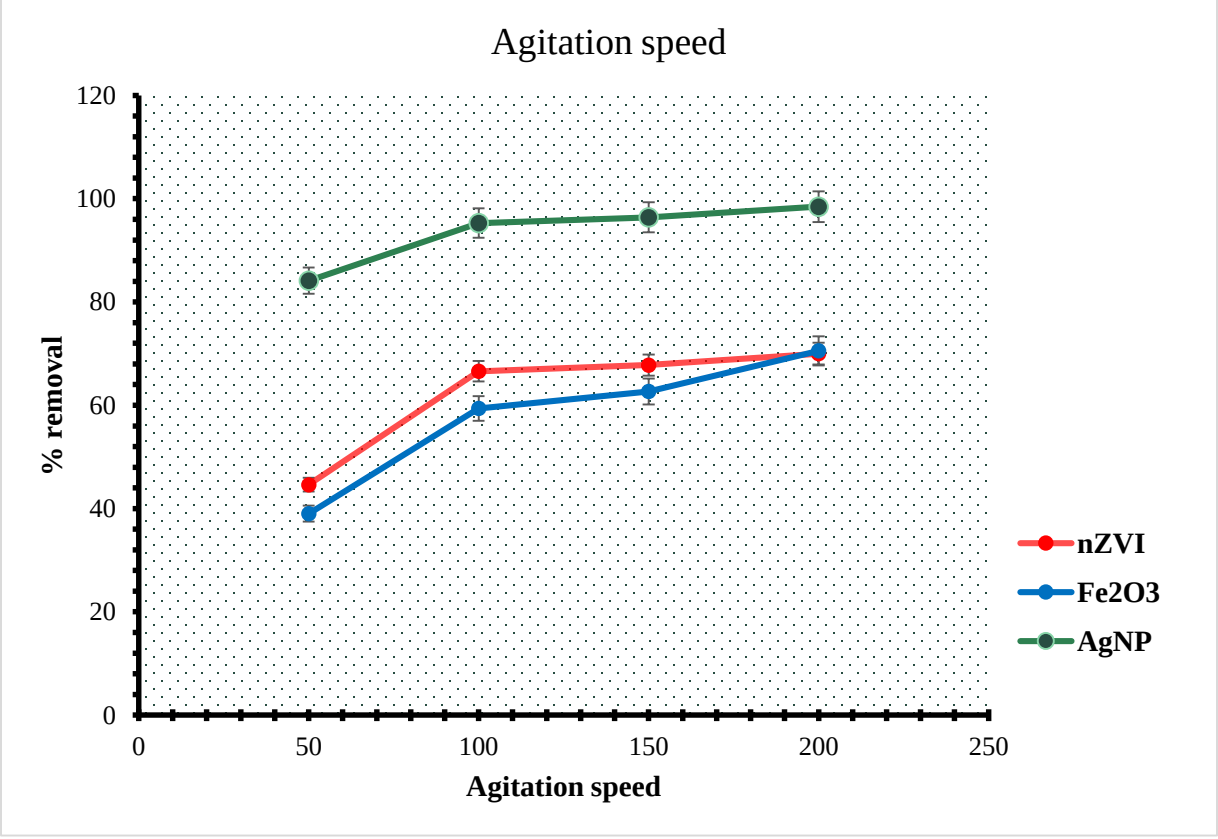

Figure 55: Effect of dosage on the removal of Hg (II) from water (pH = 7, 25 mg dosage, 20 mL solution and 2 hours.)

4.5.5 Influence of Hg (II) adsorption on the functional group contained in the adsorbent

After the treatment process, the adsorbents were collected and analyzed using FT-IR to show the loading of Hg (II). A comparison of the pure adsorbent and Hg (II) loaded adsorbent shown in Figure 56, Figure 57 and Figure 58 reveals shift, disappearance and increase in the intensity of some bands. Bands at ~3400 cm^{-1}, ~1600 cm^{-1} and 1400 cm^{-1} shifted slightly in the case of Fe_2O_3 (Figure 57). While these bands and other bands at 2900 cm^{-1} and 600cm^{-1} experienced an increase in intensity. New bands appeared in 2400 cm^{-1} and between 990 and 1100cm^{-1} (double band). Also a broadening of the bands around 3400 cm-1 was noticed for nZVI (Figure 58). Bands at 1621cm-1 and 1384cm-1 increased in intensity. Similar trends were also noticed in the case of Hg adsorption to AgNP (Figure 56). The appearance, disappearance, shift and increase in the intensity of these bands show that there is a reaction between the functional group contained in the adsorbent and Hg (II) (Zohdi et al., 2014). These reactions may be ionic or covalent (Zohdi et al., 2014).

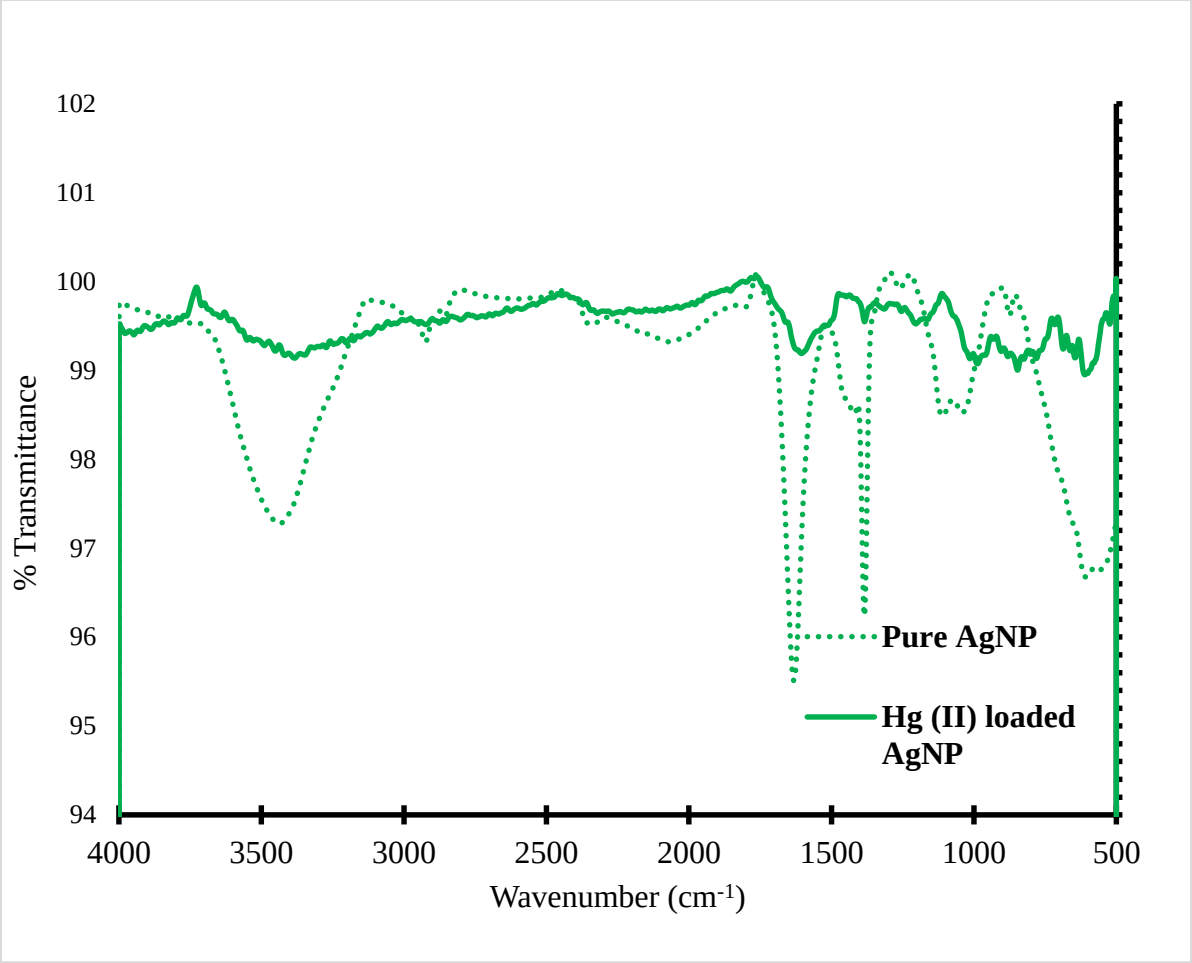

Figure 56: FTIR of Hg (II) loaded AgNP

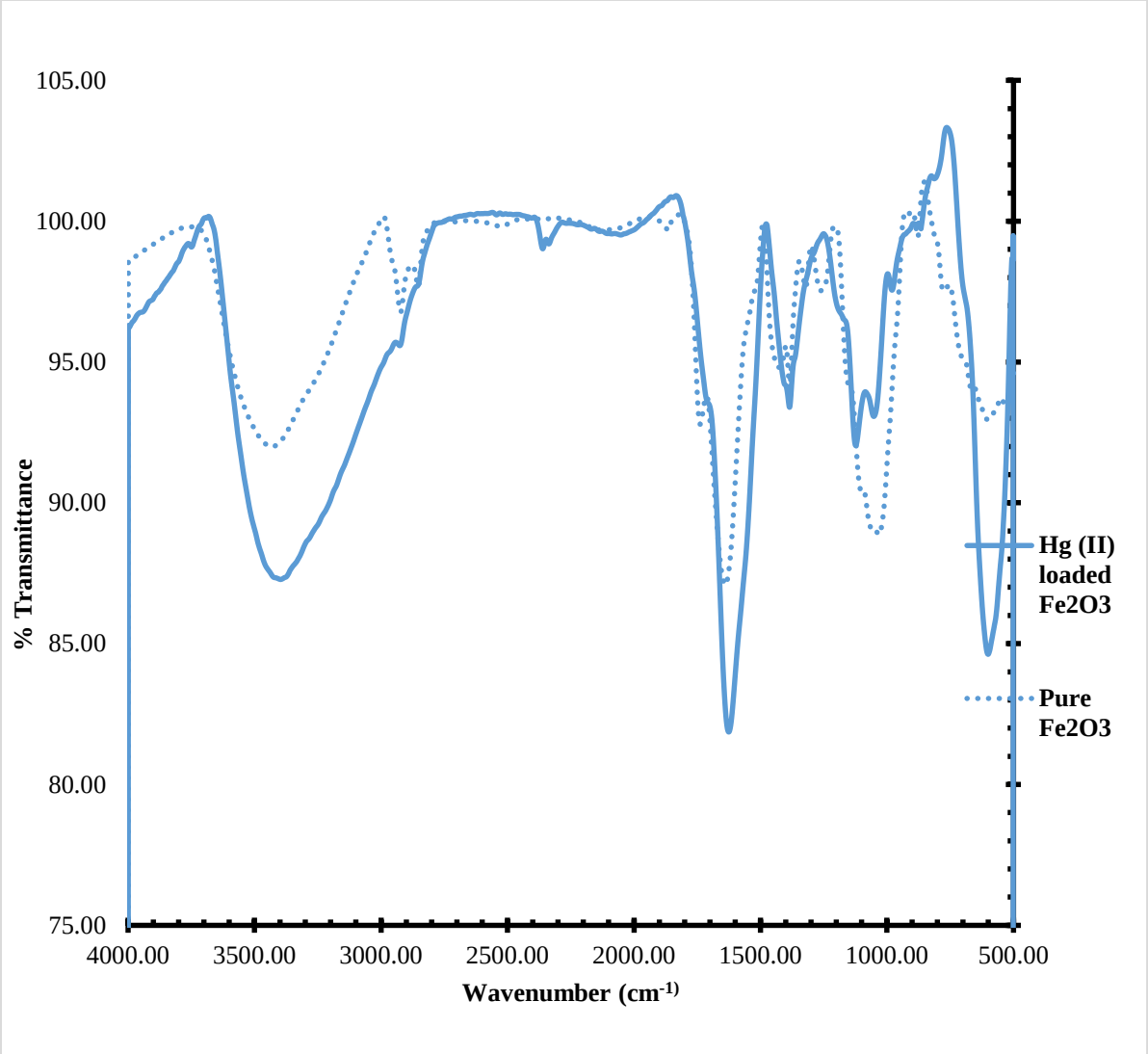

Figure 57: FTIR of Hg (II) loaded Fe_2O_3

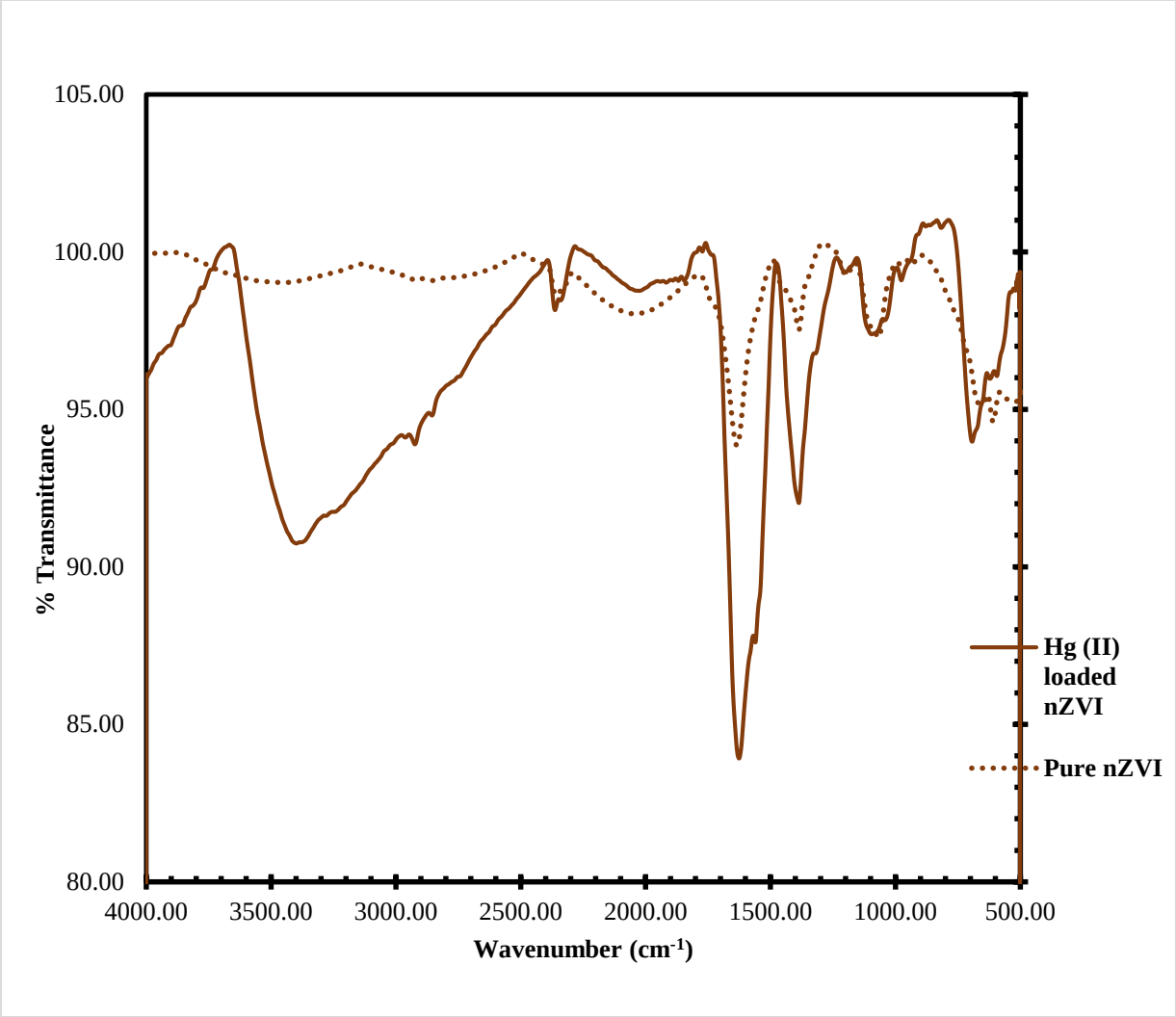

Figure 58: FTIR of Hg (II) loaded nZVI

4.6 Adsorption Isotherm study

Adsorption isotherms are mathematical models that describe the phenomenon governing the retention or distribution of a substance, the adsorbate, from a liquid to a solid phase, the adsorbent at constant conditions of temperature and pH. They show the affinity between an adsorbent and an adsorbate and can be used to compare the adsorptive capacities of different adsorbents. Different mathematical relations have been used to describe the process of adsorption; the isotherms of Freundlich and Langmuir are two of the widely

accepted models (Nwabanne and Igbokwe, 2008). As such, this study has been limited to these two models.

Langmuir adsorption isotherm assumes that adsorption can only take place at a finite number of definite localized sites without lateral interaction between the adsorbed molecules. It also assumes monolayer and homogeneous adsorption (Kumar, 2007). The model is applied in its linear form given as;

$$\frac{C_e}{q_e} = \frac{1}{K_L q_m} + \frac{C_e}{q_m}$$

Where $\frac{C_e}{q_e}$ is the ratio of the equilibrium concentration (µg/L) to the amount of contaminant adsorbed at equilibrium (µg/mg). q_m represents the Langmuir adsorption constant which describes maximum monolayer capacity (µg/mg). K_L is a Langmuir constant of adsorption energy. The slope and intercept of a plot of $\frac{C_e}{q_e}$ versus C_e (Figure 59, 60 and 61) provides the value of q_m and K_L.

Freundlich adsorption isotherm assume heterogeneous and multilayer adsorption. It is applied as presented below;

$$\ln q_e = lnK_F + \frac{1}{n} lnC_e$$

Where q_e and C_e represents the amount of analyte adsorbed and the equilibrium concentration in (µg/mg) and (µg/L) respectively. K_F (mg/g) and n are Freundlich adsorption constants and can be obtained from the slope and intercept of a plot of ln q_e versus ln C_e (Figures 62, 63 and 64).

As shown in Table 4.5, the adsorption of Hg (II) to both Fe_2O_3 and nZVI fits better to Langmuir adsorption isotherm because it has the higher R^2 value (0.992-Fe_2O_3, 0.9729-

nZVI) compared to Freundlich (0.9681-Fe_2O_3, 0.8028-nZVI). This assumes that the adsorption of the contaminant to both adsorbent is monolayer and homogeneous. This assumption was also supported by Parham in the removal of mercury from water using similar adsorbent (Sahoo et al., 2010). From the Q_m obtained, it can be concluded that biosynthesized nZVI is more efficient in the removal of hg (II) compared to Fe_2O_3. A comparison of the Q_m obtained in this study to those obtained in other studies is presented in Table 4.5.

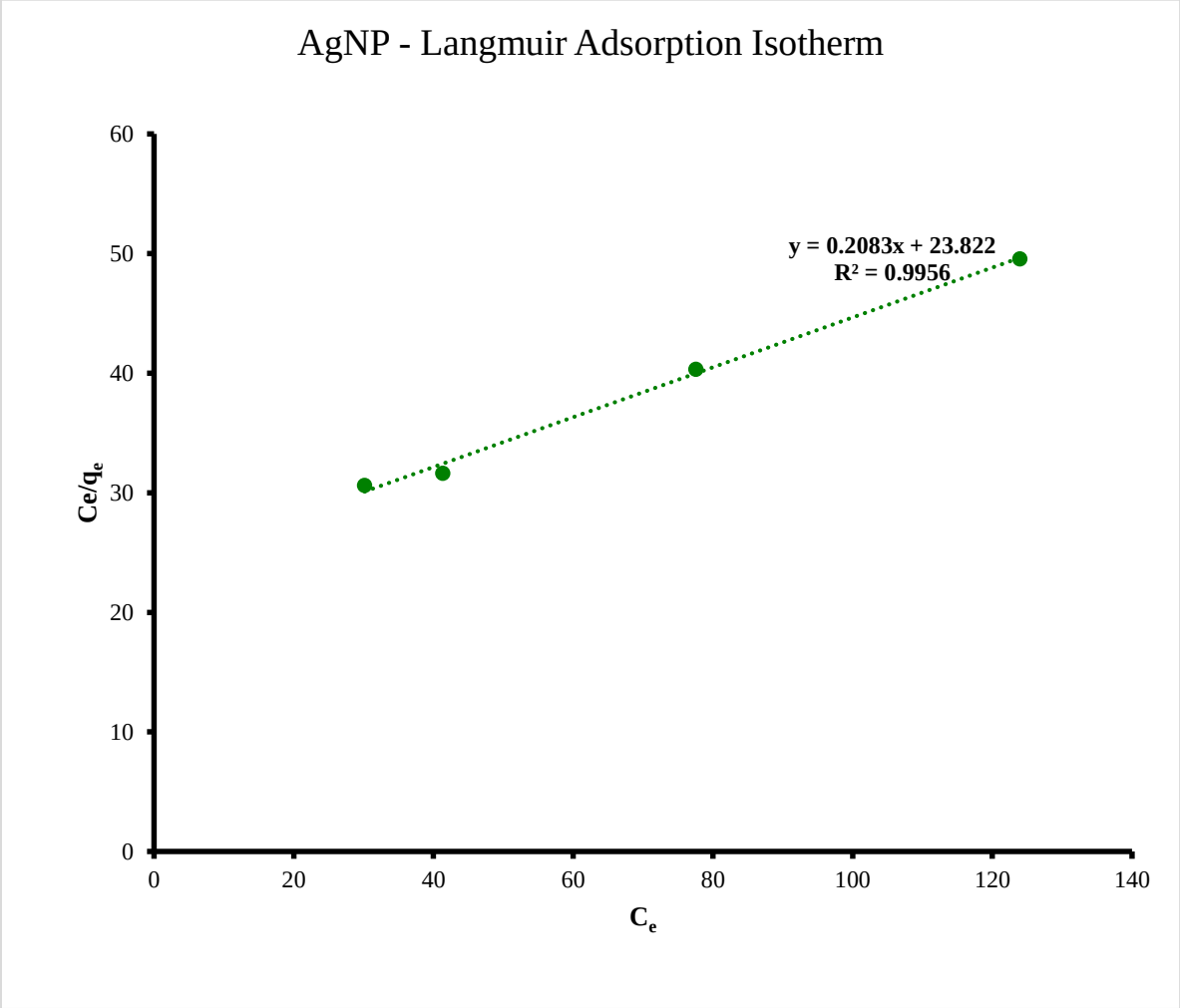

Figure 59: AgNP Langmmuir adsorption isotherm

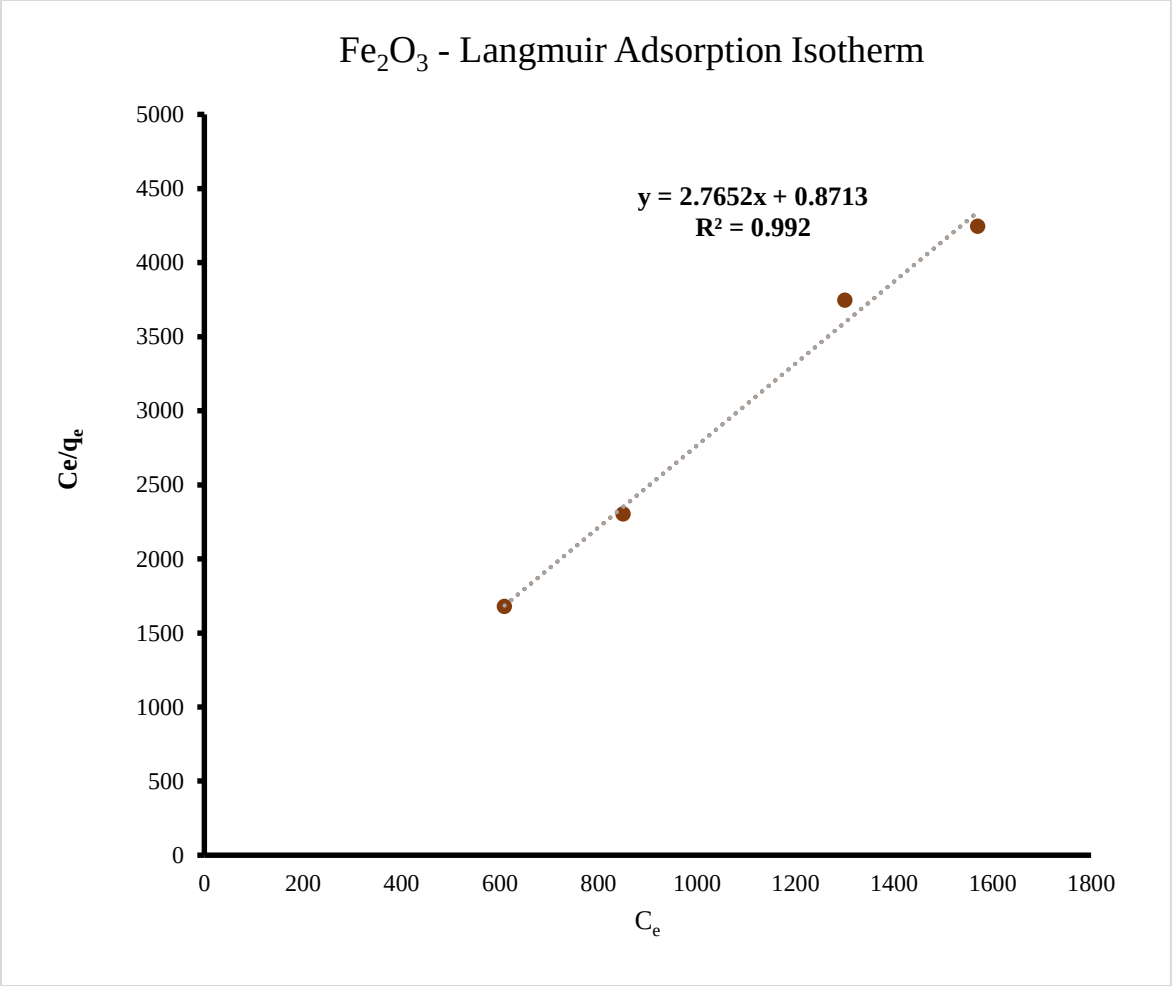

Figure 60: Fe_2O_3 Langmmuir adsorption isotherm

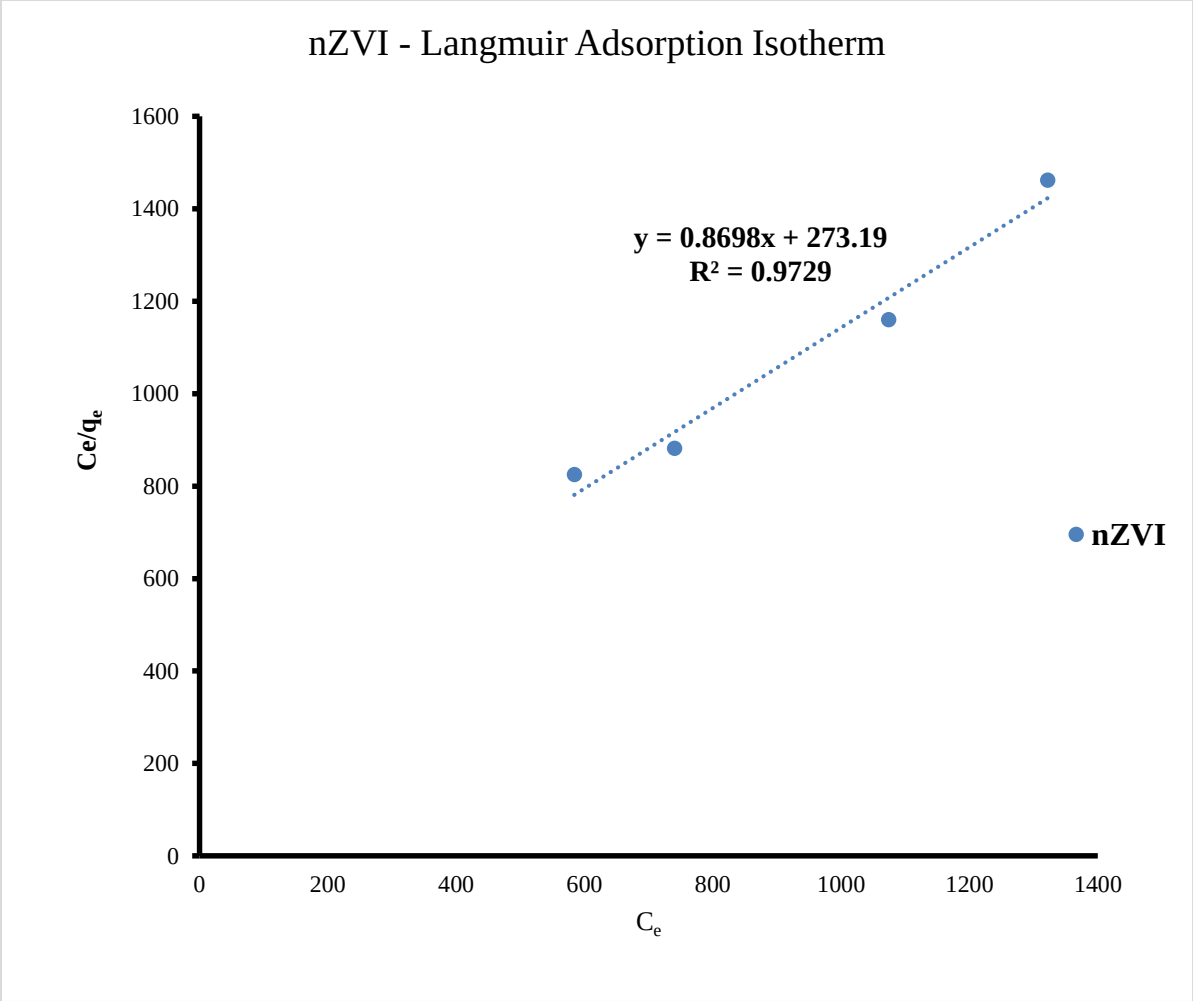

Figure 61: nZVI Langmmuir adsorption isotherm

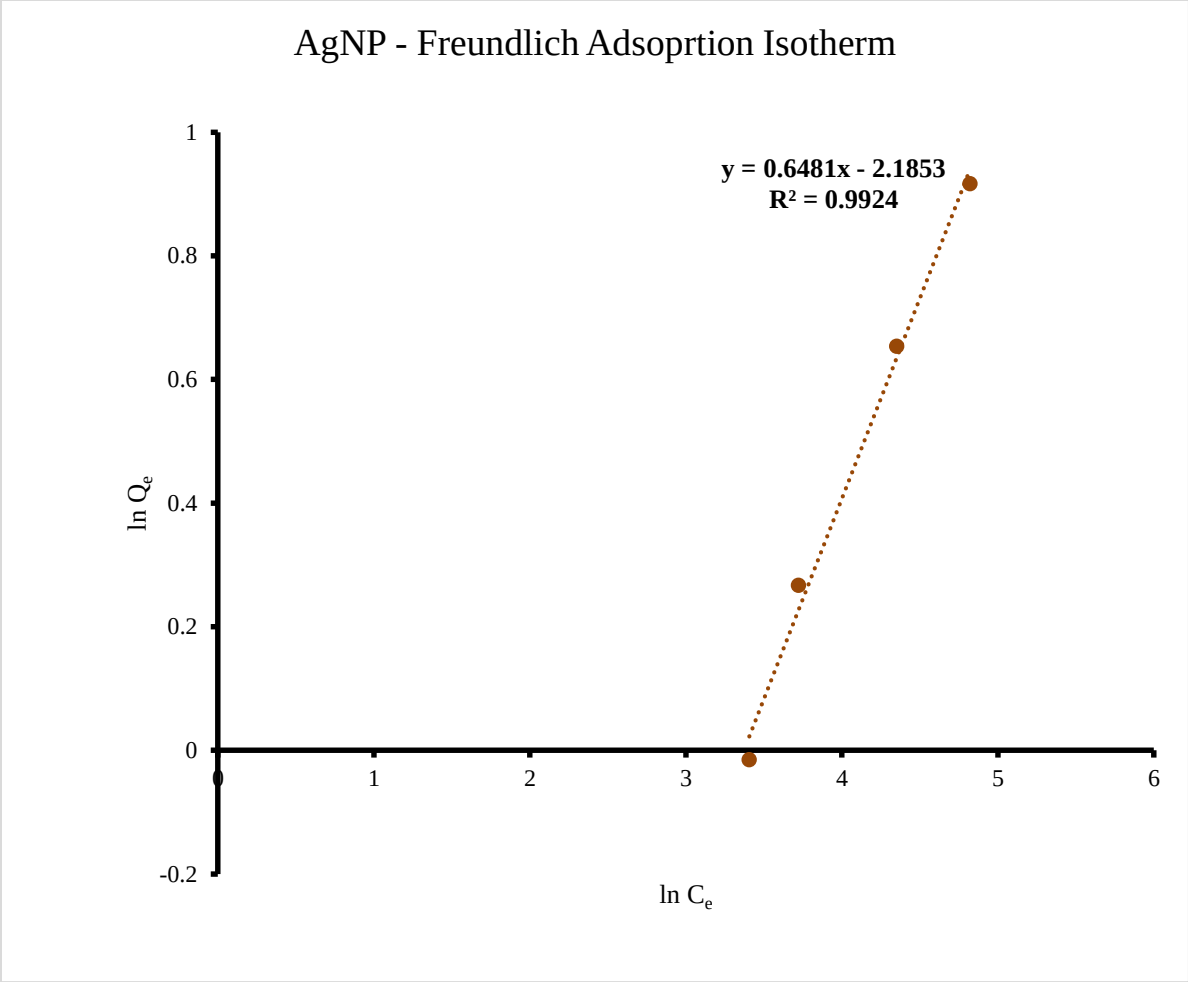

Figure 62: AgNP Freundlich adsorption isotherm

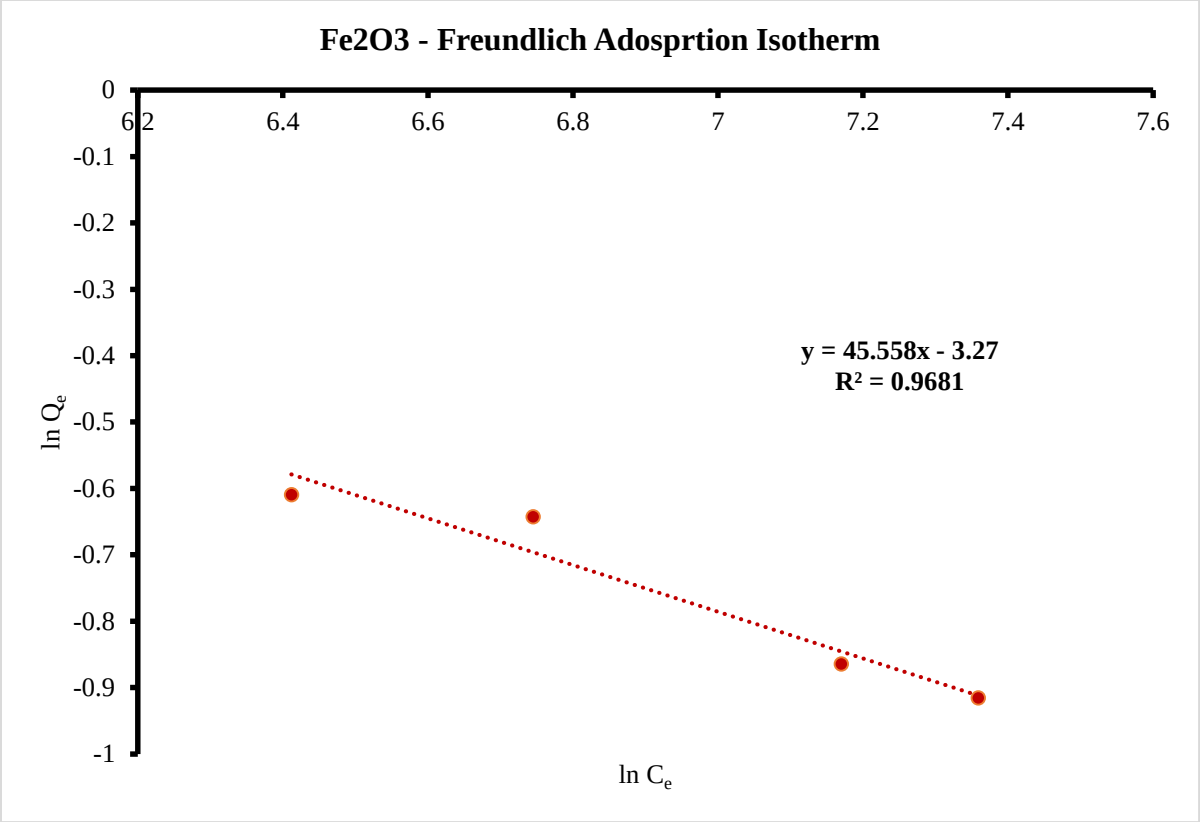

Figure 63: Fe_2O_3 Freundlich adsorption isotherm

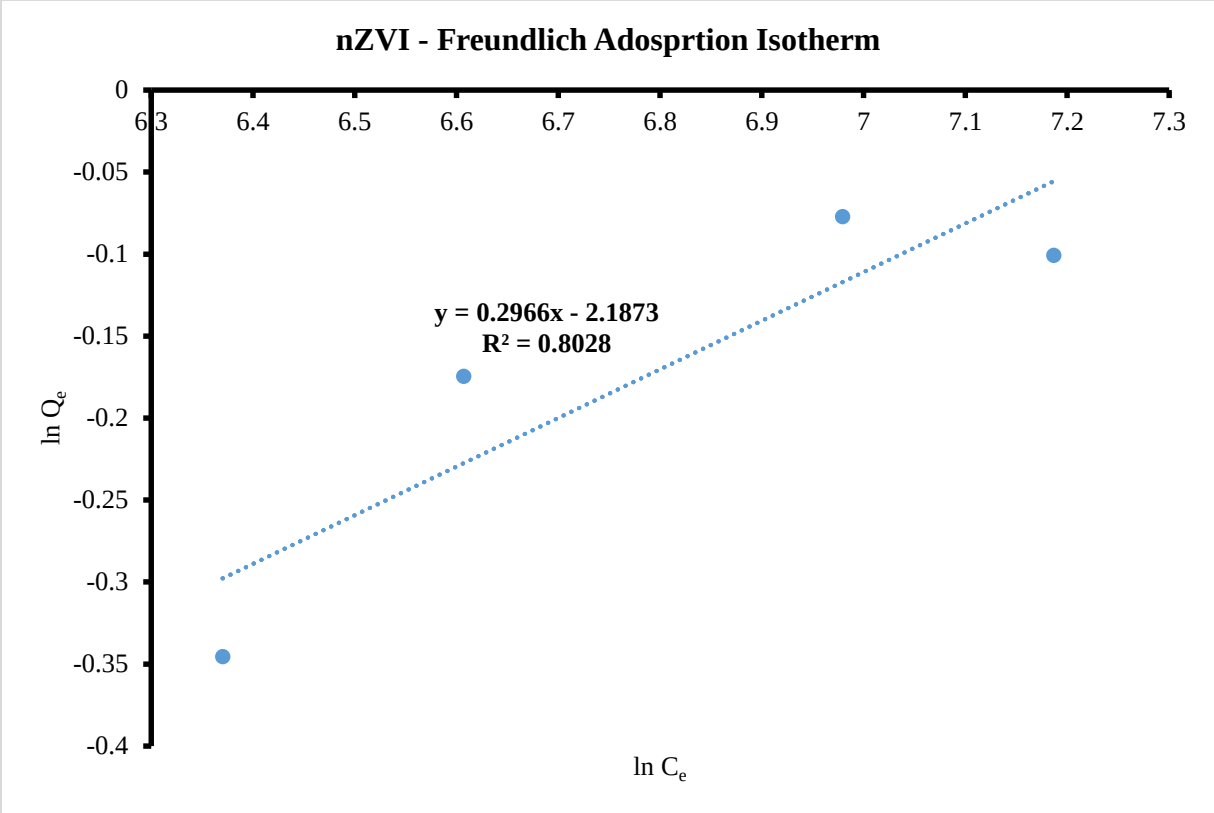

Figure 64: nZVI Freundlich adsorption isotherm

4.7 Adsorption Kinetics

Adsorption kinetics describes the adsorption pathways, mechanisms and interaction in an adsorption process. In this study, the adsorption kinetics was evaluated by applying the pseudo first and second order models and the intraparticle diffusion model. The level of compliance between the experimental value and the calculated value were ascertained from the R-square value of the plotted graphs.

The pseudo first order model described by (Vijayaraghavan and Padmeshi, 2006) is expressed as;

$$\ln(q_e - q_t) = ln\, q_e - k_1 t$$

Where q_e (µg/mg) and q_t (µg/mg) are the amount of Hg (II) adsorbed at equilibrium and contact time, t (mins) respectively. K_1 is the adsorption rate constant. The values of ln (q_e

– q_t) was plotted on the y-axis against the values of t. K_1 and q_e was also obtained from the slope and intercept (Figure 65).

Pseudo second order kinetics model described by Ho *et al.*, 1998 is give as;

$$\frac{t}{q_t} = \frac{t}{q_e} + \frac{1}{k_2 q_e^2}$$

Where q_e (µg/mg) and q_t (µg/mg) are the amount of Hg (II) adsorbed at equilibrium and contact time, t (mins) respectively and k_2 is the pseudo-second order kinetics rate constant. A plot of $\frac{t}{q_t}$ versus t of Hg (II) at fixed concentration gives slope and intercept which was used to calculate the value of q_e and k_2. The plot is shown in Figure 66. While the constants obtained from the plot is summarized in Table 4.6. The result obtained reveals that the adsorption process using nZVI is based on the chemical sorption.

The Weber's intraparticle diffusion model is given as;

$$q_t = k_{i.d} t^{1/2} + C$$

Where q_t is the amount of Hg (II) adsorbed at time *t*. $t_{1/2}$ is the square root of the contact time, K_{id} is the slope and it is taken as the intraparticle diffusion rate constant. In order to obtain the constants, K_{id} and C, the values of q_t is plotted against $t_{1/2}$. K_{id} is obtained from the slope while C is the intercept of the plot. The result (Figure 67) shows that nZVI fits to Weber's interparticle diffusion model while Fe_2O_3 didn't. AgNP however fitted perfectly to the Weber's intraparticle diffusion model (Figure 68).

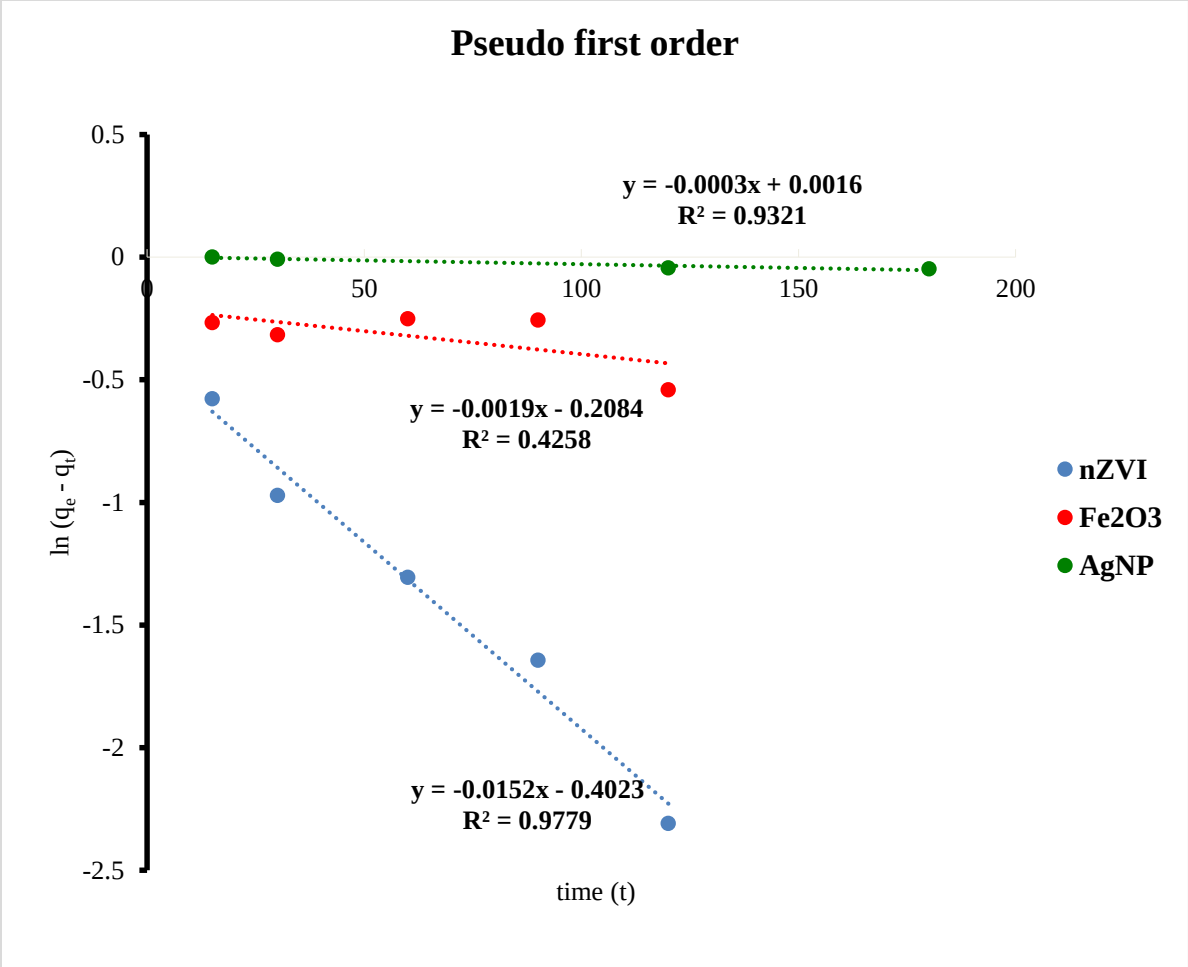

Figure 65: Pseudo first order kinetics

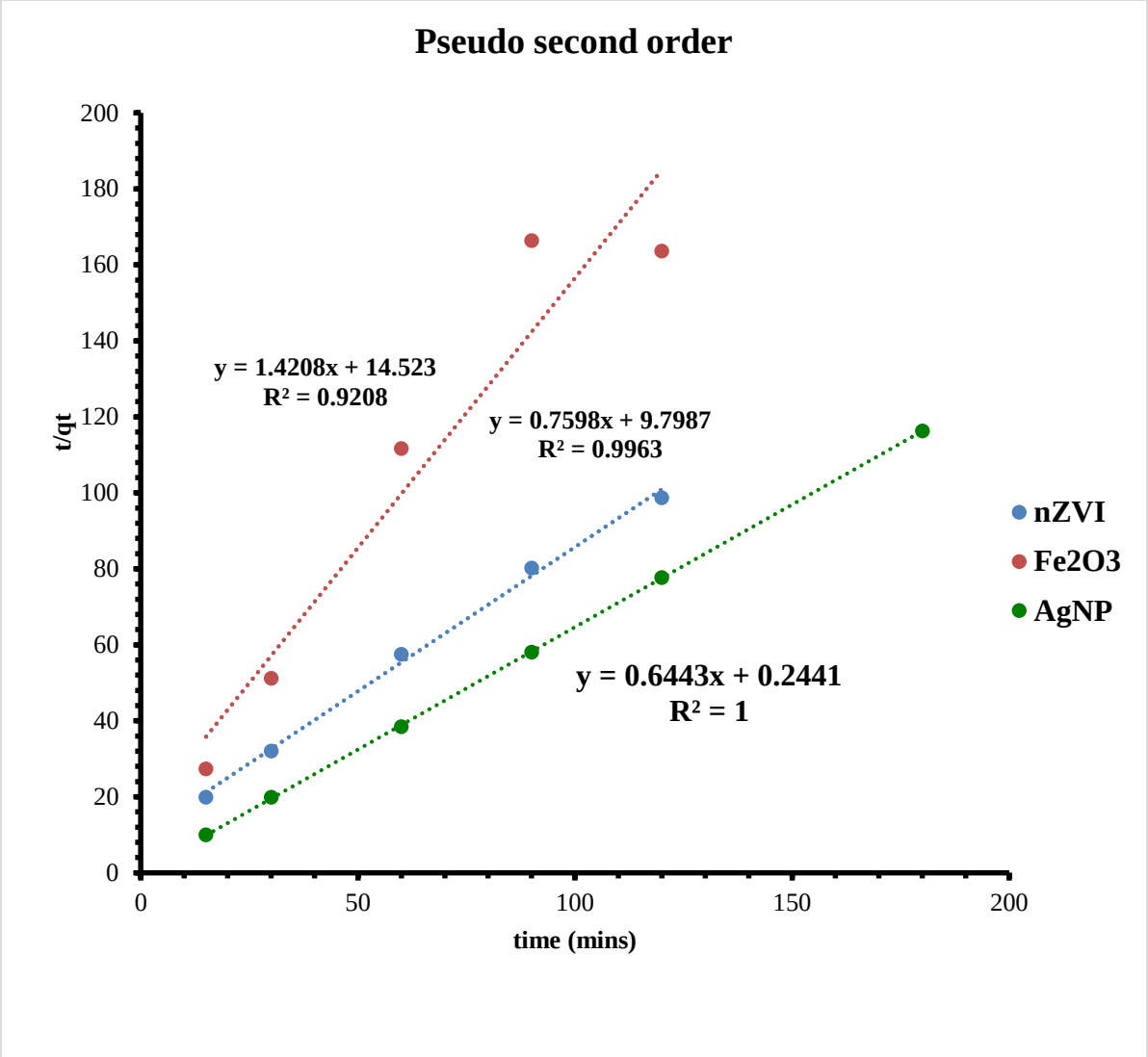

Figure 66: Pseudo second order kinetics

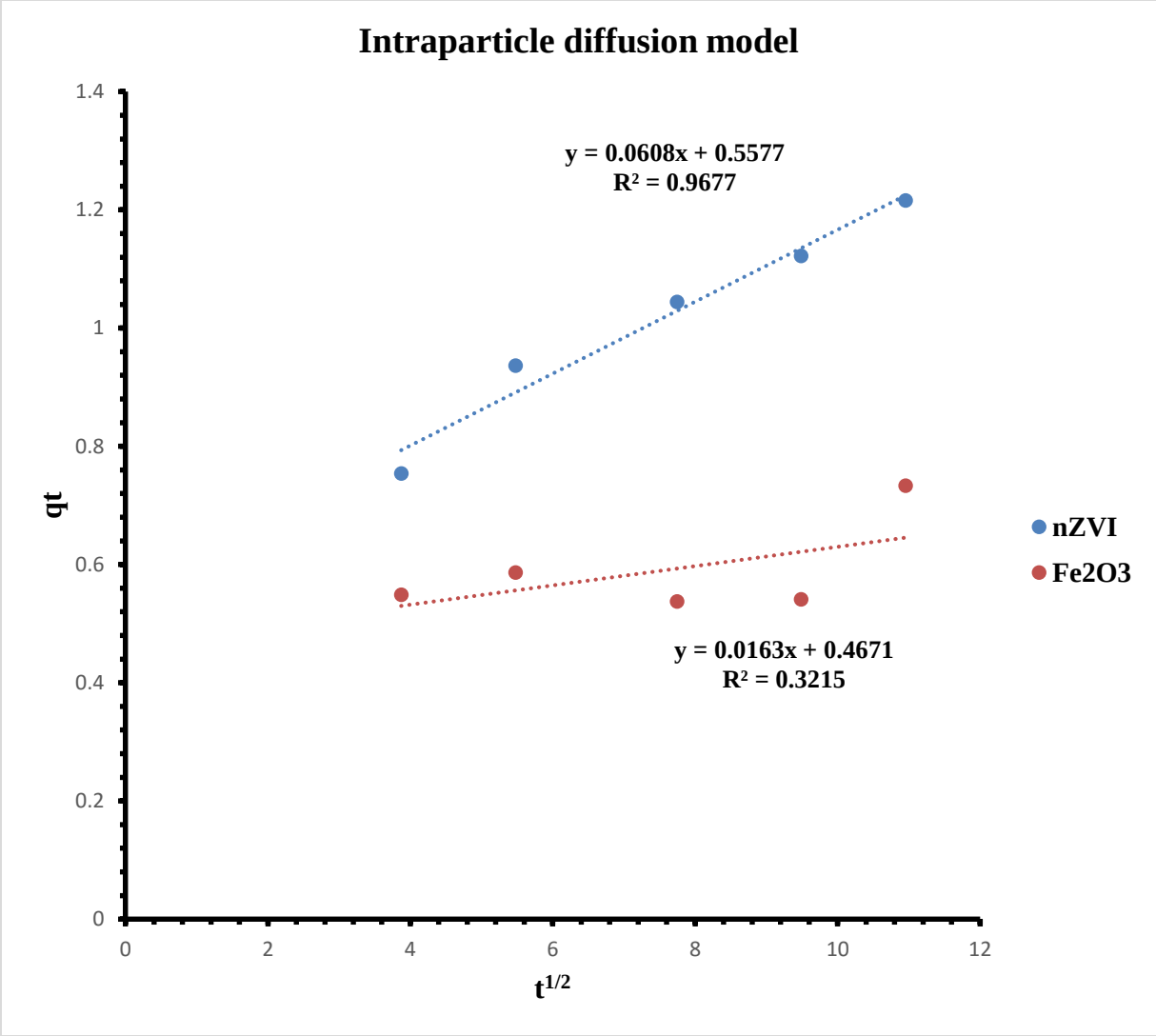

Figure 67: Intraparticle diffusion model of nZVI and Fe_2O_3

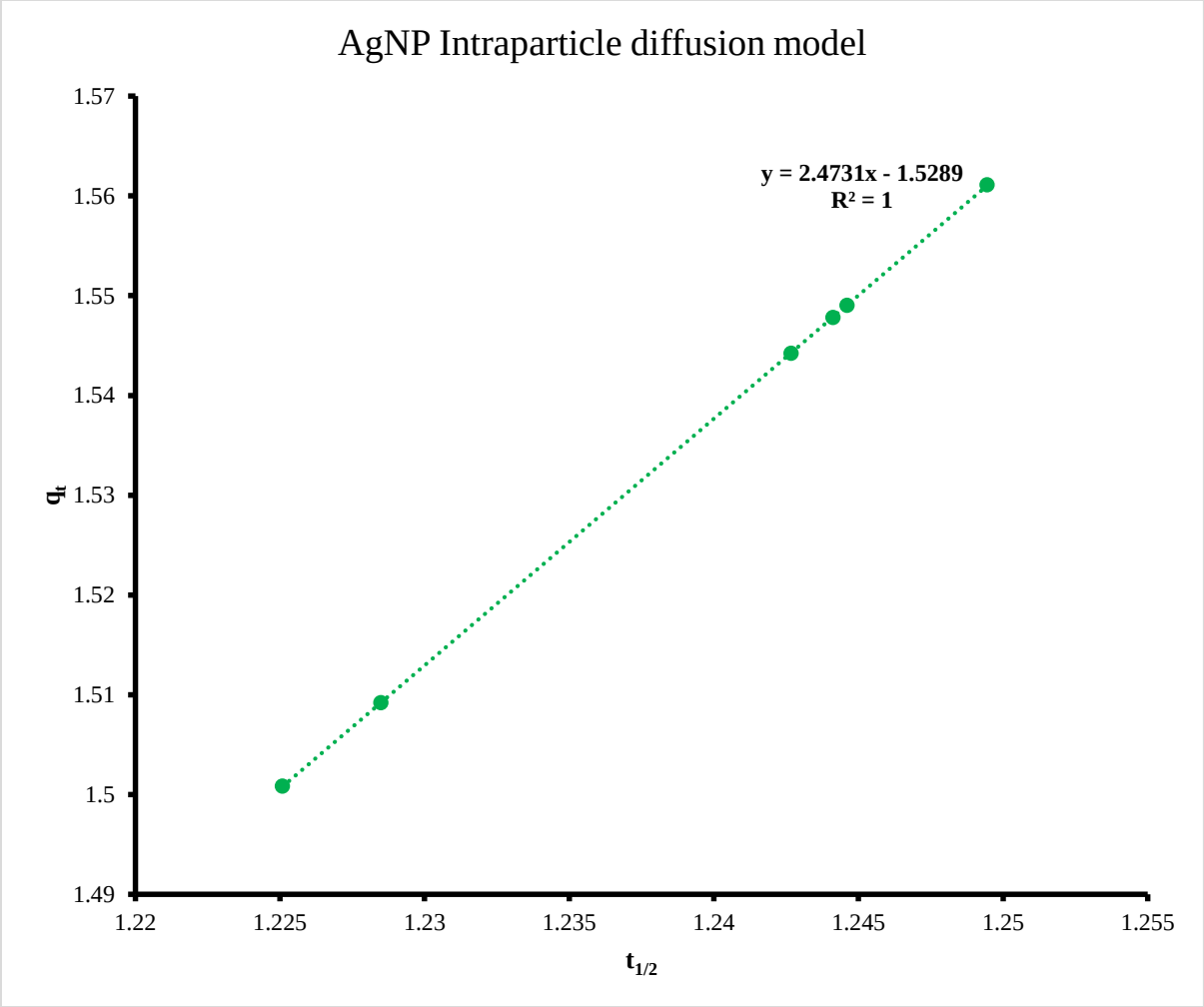

Figure 68 Intraparticle diffusion model of AgNP

Table 4.5 Langmuir and Freundlich Isotherms constant for Hg (II) removal from water

Adsorbents	Langmuir Isotherm constant			Freundlich Isotherm constant		
	q_m (mg/g)	K_L (L/mg)	R^2	K_f	n	R^2
AgNP	4.800	0.00874	0.9956	0.11244	1.5429	0.9924
Fe_2O_3	0.3616	3.17397	0.992	0.038	0.0219	0.9681
nZVI	1.14968	0.00318	0.9729	0.1122	3.37	0.8028

Table 4.6 Pseudo first order, pseudo second order and intraparticle diffusion parameters for adsorption of Hg (II) from water

		Pseudo-first order			Pseudo-second order			Intraparticle diffusion		
Adsorbent	Experimental q_e (mg/g)	K_1	Calculated q_e	R^2	K_2 (g/mg min)	Calculated q_e	R^2	$K_{i.d}$	C	R^2
AgNP	2.5015				1.70063	1.552072	1.00	2.4731	1.5289	1.00
Fe2O3	1.31528				0.05891	1.3161	0.9208	0.0163	0.4671	0.9677
nZVI	0.904				0.138998	0.7038	0.9963	0.0608	0.5577	0.3215

4.8 Design and fabrication of nanoparticle embedded membrane

Having established that AgNP is the most efficient of the three adsorbent with the highest removal capacity and Qm value, the adsorbent was used in the fabrication of a filter cartridge for subsequent column studies. Unloaded electrospun polyacrylonitrile and polyacrylontitrile loaded with AgNP were characterized to ascertain the uniform distribution of the adsorbent in the polymer.

4.9 Characterization of loaded and unloaded polymer membrane

4.9.1 Field emission scanning electron microscopy and energy dispersive spectroscopy

Field emission scanning electron microscope (FE-SEM) images of electrospun unloaded nanofibre (Figure 69). PAN nanofiber of average size 370 nm was observed. The nanofibres produced are also smooth and possessed narrow size distribution. The elemental composition of the electrospun nanofiber was confirmed using EDX mapping. As shown in Figure 70, the nanofiber are mostly composed of Carbon and Nitrogen. The two elements make up the chemical compound polyacrylonitrile. However, when the polymer is loaded with AgNP and electrospun, there was a slight increase in the size of the nanofiber produced as shown in Figure 71. The presence of silver nanoparticles in the polymer membrane was confirmed by EDX mapping. The image obtained (Figure 72) shows the distribution of the metallic nanoparticles in the nanofiber. While few beads are formed, the lack of uniform beads may be due to the complete embedding of the nanoparticles in the fibre. The nanoparticles as characterized using FE-SEM have an average size of 30 – 50

nm. The average size of the loaded electrospun nanofiber is 400 nm. The increase in size may be due to the incorporation of the adsorbent in the nanofiber. In order to confirm this, an exact particle size analysis of the adsorbent was carried out.

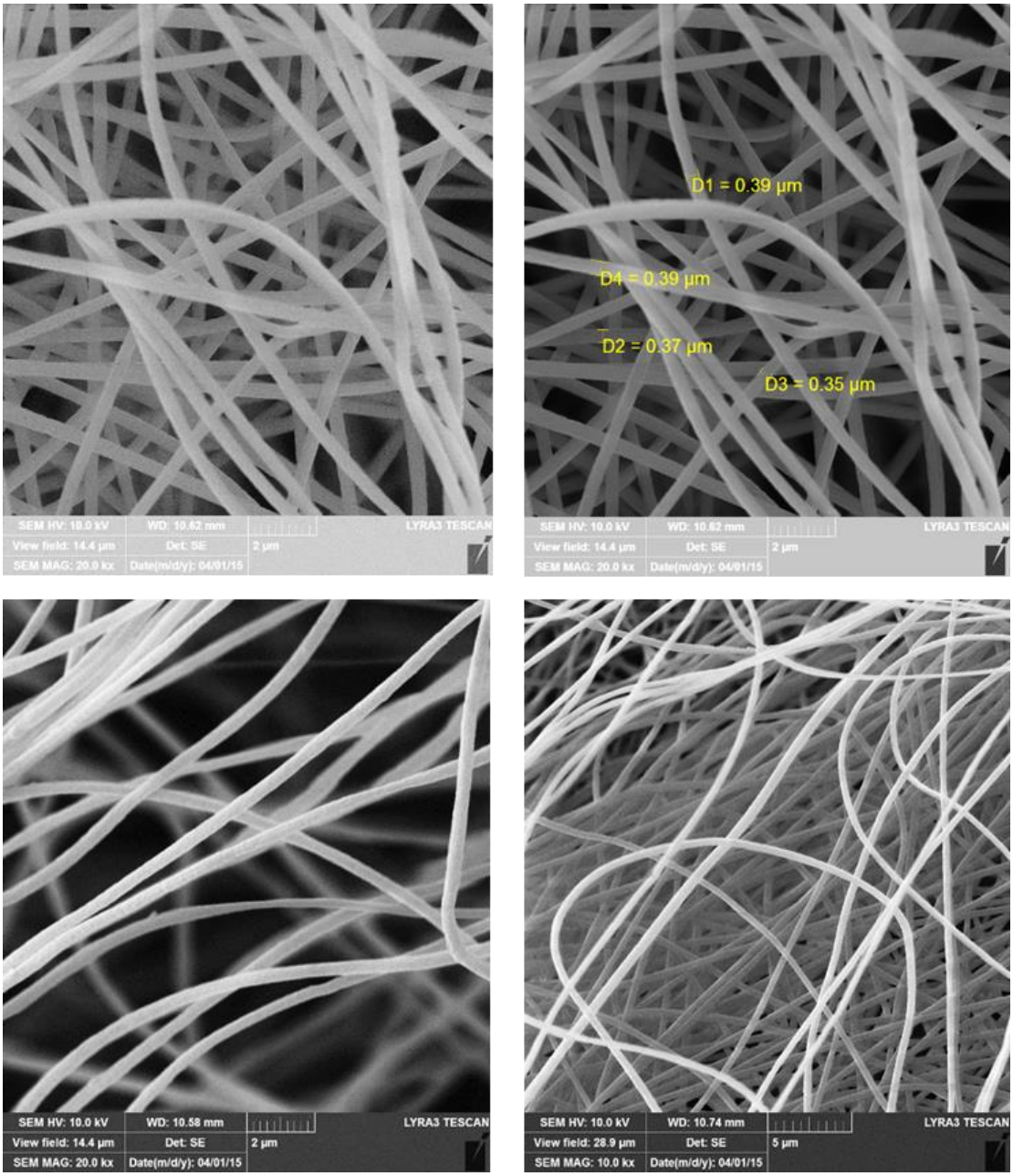

Figure 69: FE-SEM images of pure and unloaded PAN

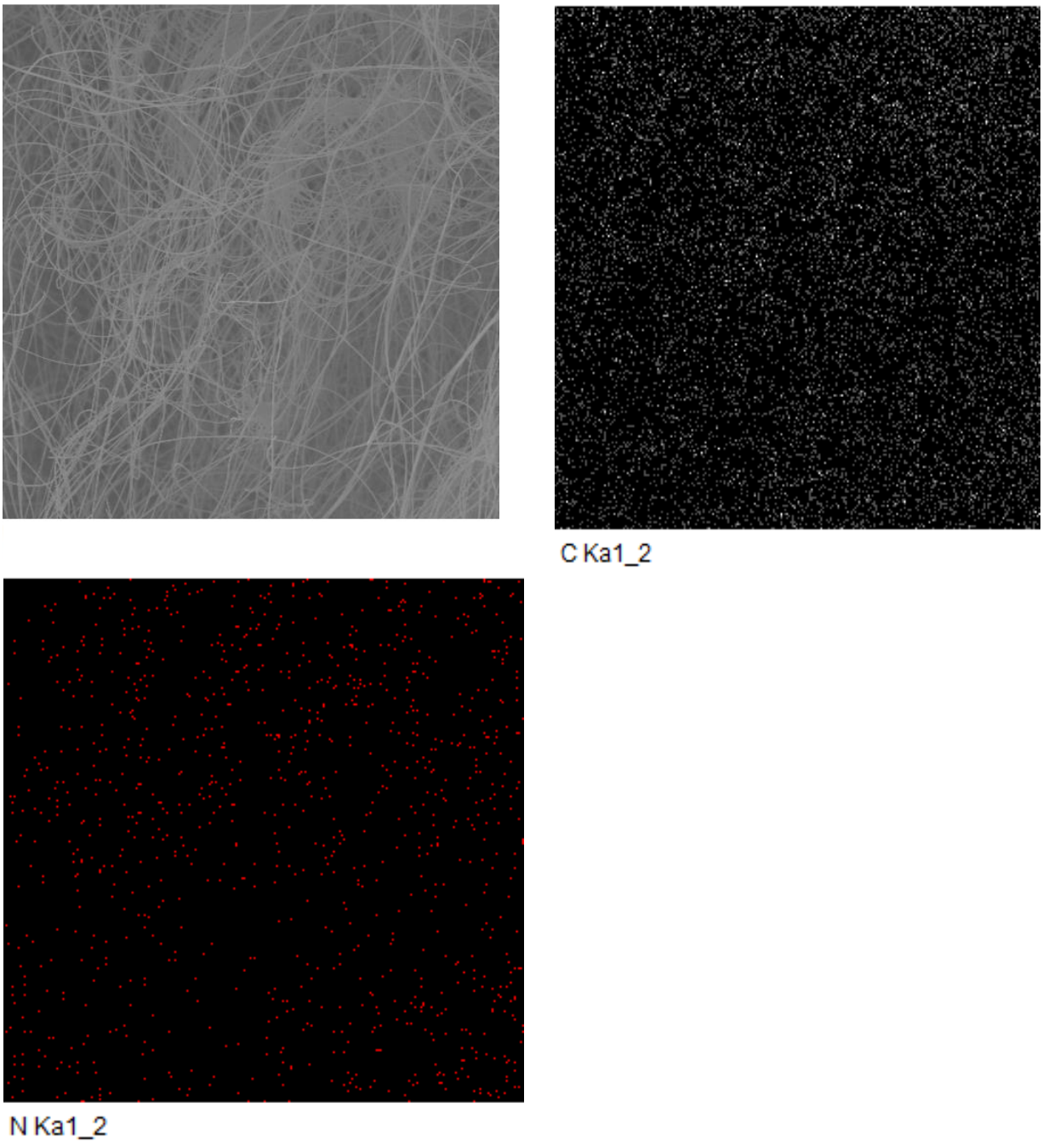

Figure 70: Mapping images of pure PAN

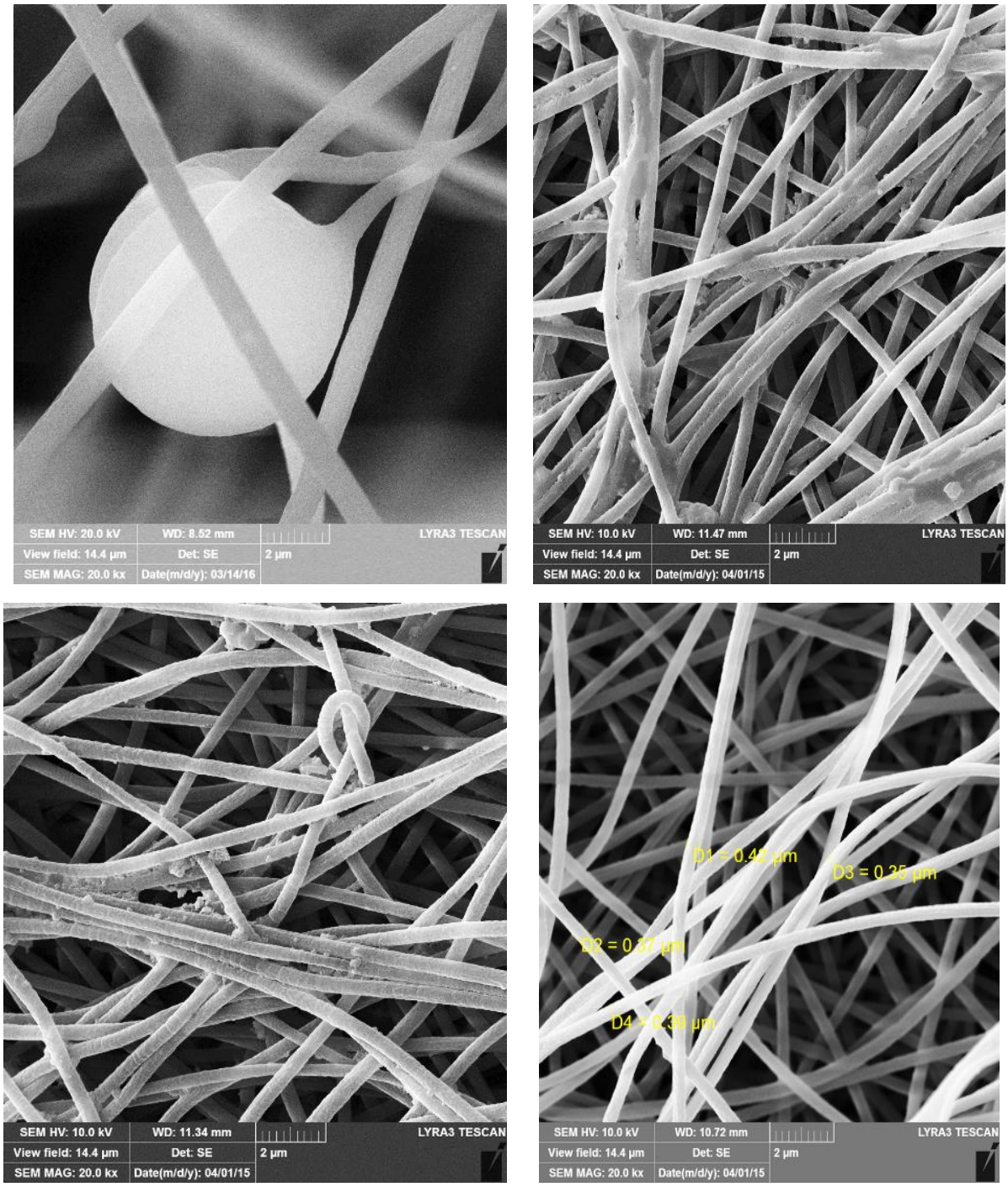

Figure 71: FE-SEM image of loaded PAN

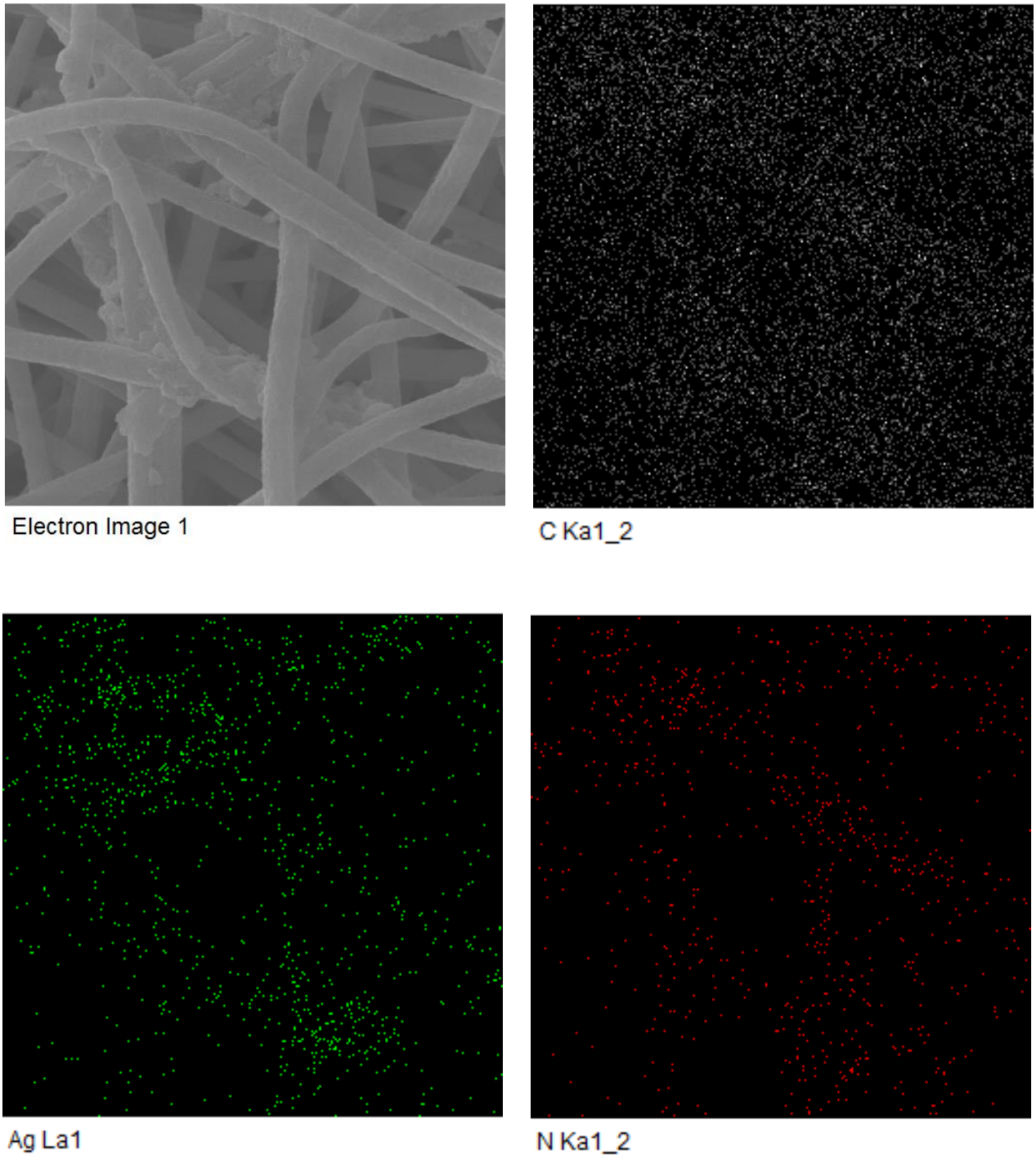

Figure 72: EDX mapping images of PAN loaded with AgNP

4.9.2 AFM particle size analysis of AgNP

AFM scans were used to confirm the exact particle size of the biosynthesized AgNP. Figure 73 shows topography and phase mode images of the nanoparticles. Figure 73 (a) shows dispersed nanoparticles of different sizes but mostly spherical shaped. Figure 73 (b) shows a 3D topography image of a single isolated nanoparticle. The characteristic size of this particle was confirmed using the line profile shown in Figure 73 (c). The image shows that the nanoparticles has a polyhedral structure with a base width of about 30 nm and height of about 1.4 nm. Figure 73 (f) and (g) also confirms nanoparticles of sizes less than 20 nm.

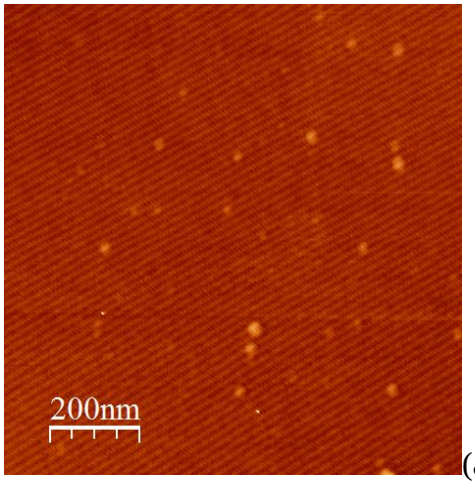

(a)

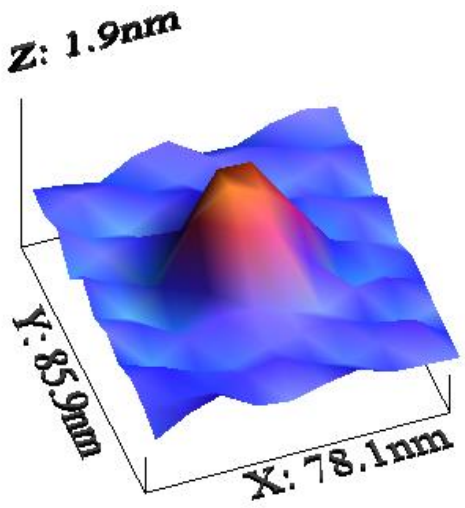

(b)

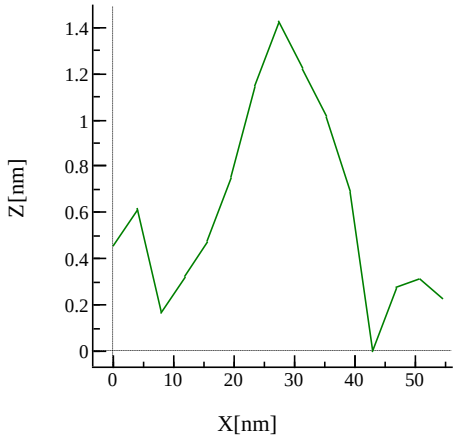

(c)

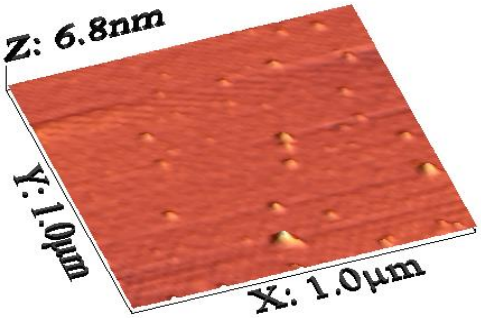

(d)

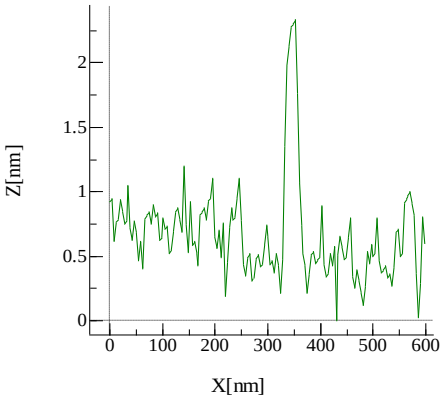

(e)

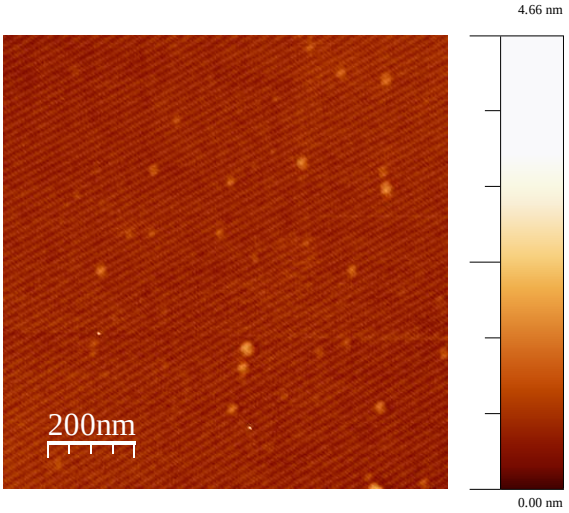

(f)

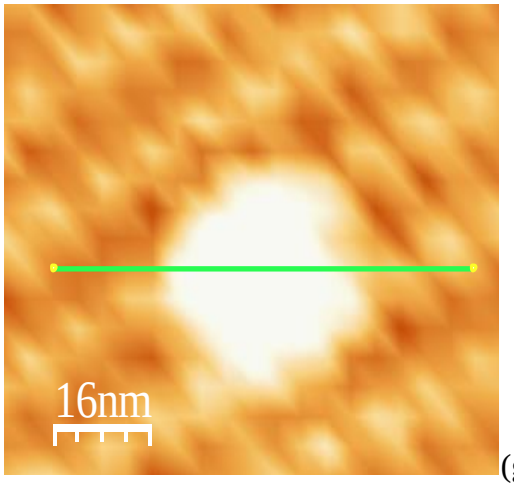

(g)

Figure 73: AFM particle size analysis of AgNP

4.10 Fixed bed adsorption studies

The fixed bed adsorption studies were performed using the adsorbent loaded PAN. The adsorbent loaded PAN was put in a filter cartridge and used as the column. Minitab 16 software used to design the experiment was also used in analyzing the response obtained. The response was used to plot the various graphs which gives an understanding of the column studies adsorption process. The experimental design and hence the result obtained from the Minitab software provides an insight into the effect of various parameters as used investigated in the experiment. It also provides an understanding of the most significant effects and the effect of interaction between the parameters in the experiment.

The main effect plot as shown in Figure 74 reveals that the initial concentration of the contaminant in water has the highest effect on its percentage removal. At high concentration, more Hg (II) was adsorbed from solution. The availability of more Hg (II) ions in water ensures that its sorption to the adsorbent is quite easy compared to when the concentration is low. Also, higher flowrate supports the adsorption process. Thus, because the experiment is recycled flow, the contaminant passes through the cartridge more times compared to a recycled flow experiment carried out at lower flowrate. This ensures that the contaminant comes in contact with the adsorbent carrying cartridge more times. The number of complete cycle of a 50 ml solution for instance at higher flowrate is higher than a similar set up but at lower flowrate. It can be assumed that for each time the contaminant passes through the cartridge more contaminant is adsorbed to the adsorbent contained within the cartridge.

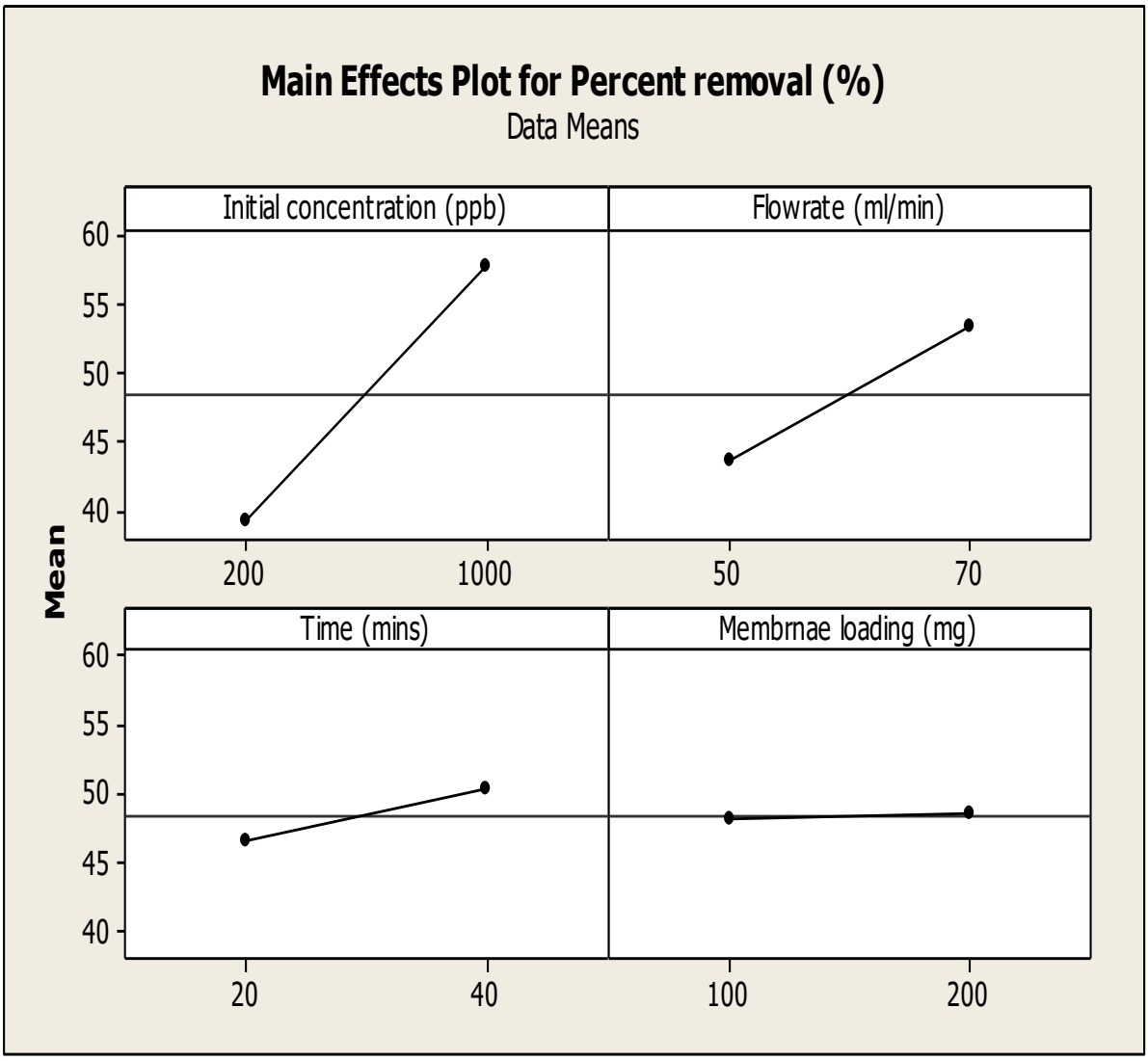

Figure 74: Main effect plot for percent removal of Hg (II) as obtained from Minitab 16 software.

Time of the experiment also has some effect on the removal efficiency of the contaminant. The longer the time allowed for the experiment, the more likely that more contaminant is adsorbed unto the surface of the adsorbent. Variation in membrane loading however has very little effect. As explained above the size of the adsorbent allows that some of the AgNP are trapped within the membrane making it slightly difficult for the removal to be influenced by a small change in the adsorbent dosage. Meanwhile, more increase in

adsorbent dosage in the polymer membrane may result in a more pronounced influence on the removal process. The cube plot shows how each parameter variation affected the removal process and also displaying the exact removal percentage Figure 75. The highest removal at about 65% was recorded at high values of flowrate and time.

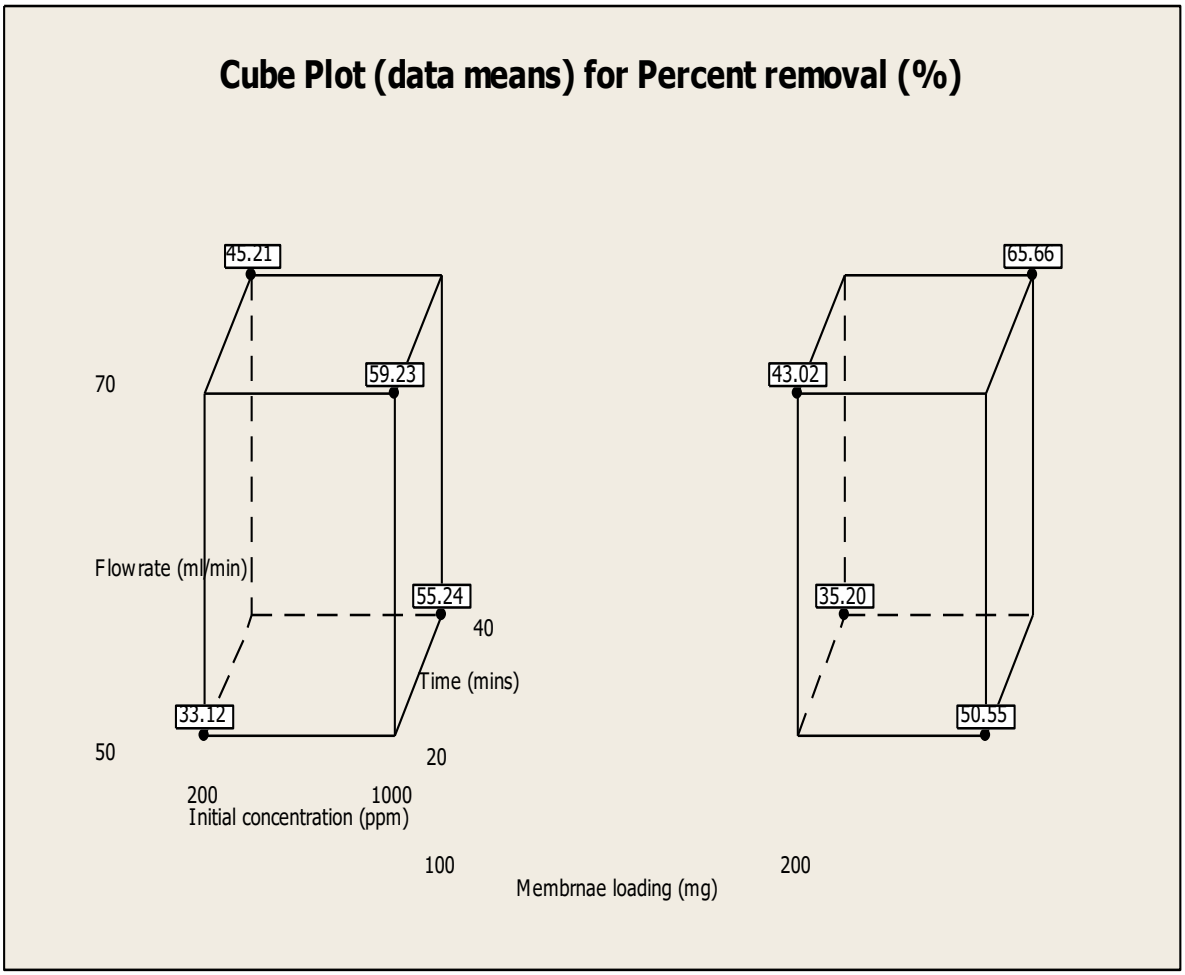

Figure 75: Main effect plot for percent removal of Hg (II) as obtained from Minitab 16 software.

The interaction between the various factors varied is shown in the interaction plot graph (Figure 76). The figure shows that an interaction between initial concentration and flowrate provides higher removal efficiency compared to low values of initial concentration and flowrate.

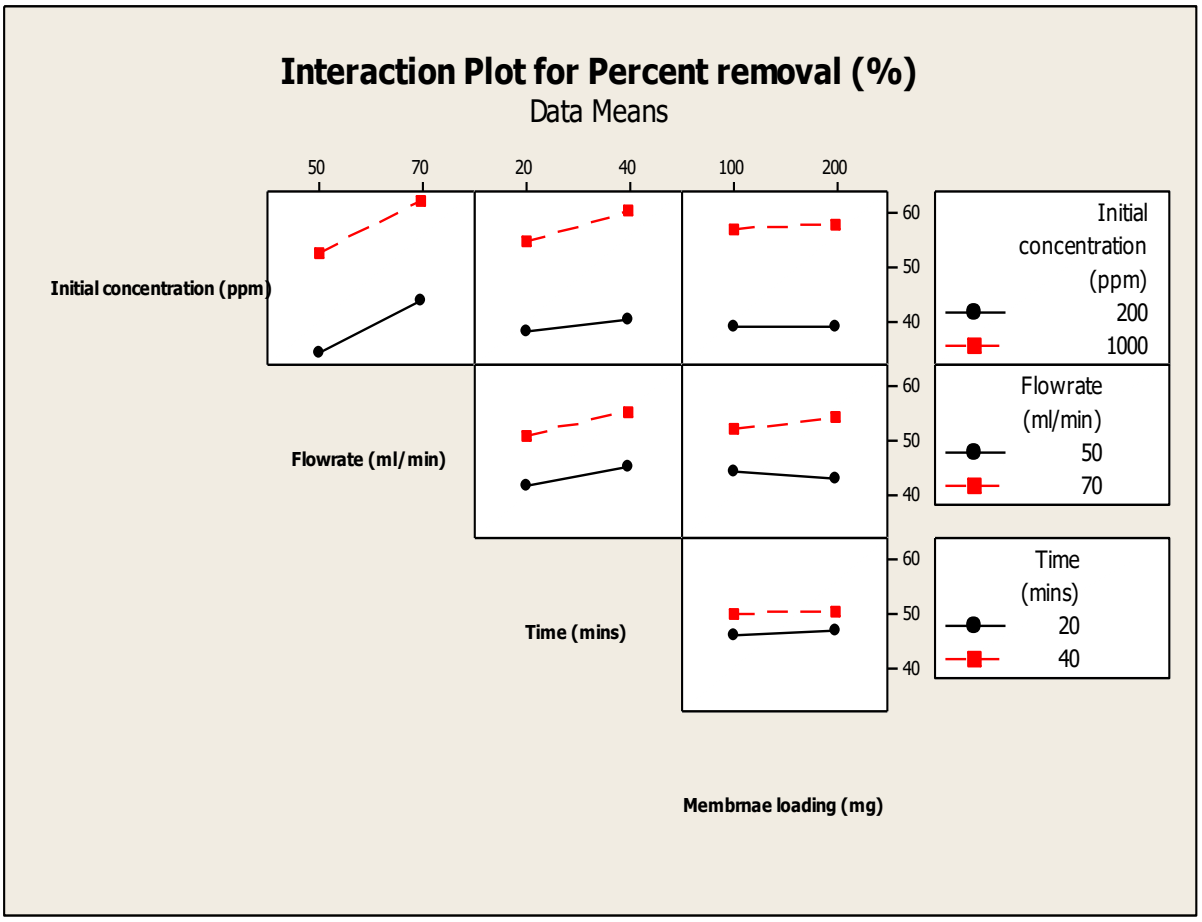

Figure 76: Interaction plot for percent removal of Hg (II) as obtained from Minitab 16

The Pareto plot (Figure 77) provides an understanding of the most significant factors in the experimental process. As shown, initial concentration, flowrate and time constitute the most important parameters in the removal of the contaminant, reasons stated above. Membrane loading and a combination of the other factors provides influences which are slightly less than significance as shown by the red line drawn from the top of the graph vertically. This result is supported by the half plot and the normal plot as shown in Figure 78 and 79 respectively. The normal and half plot figures also confirms that the effect of these factors are positive.

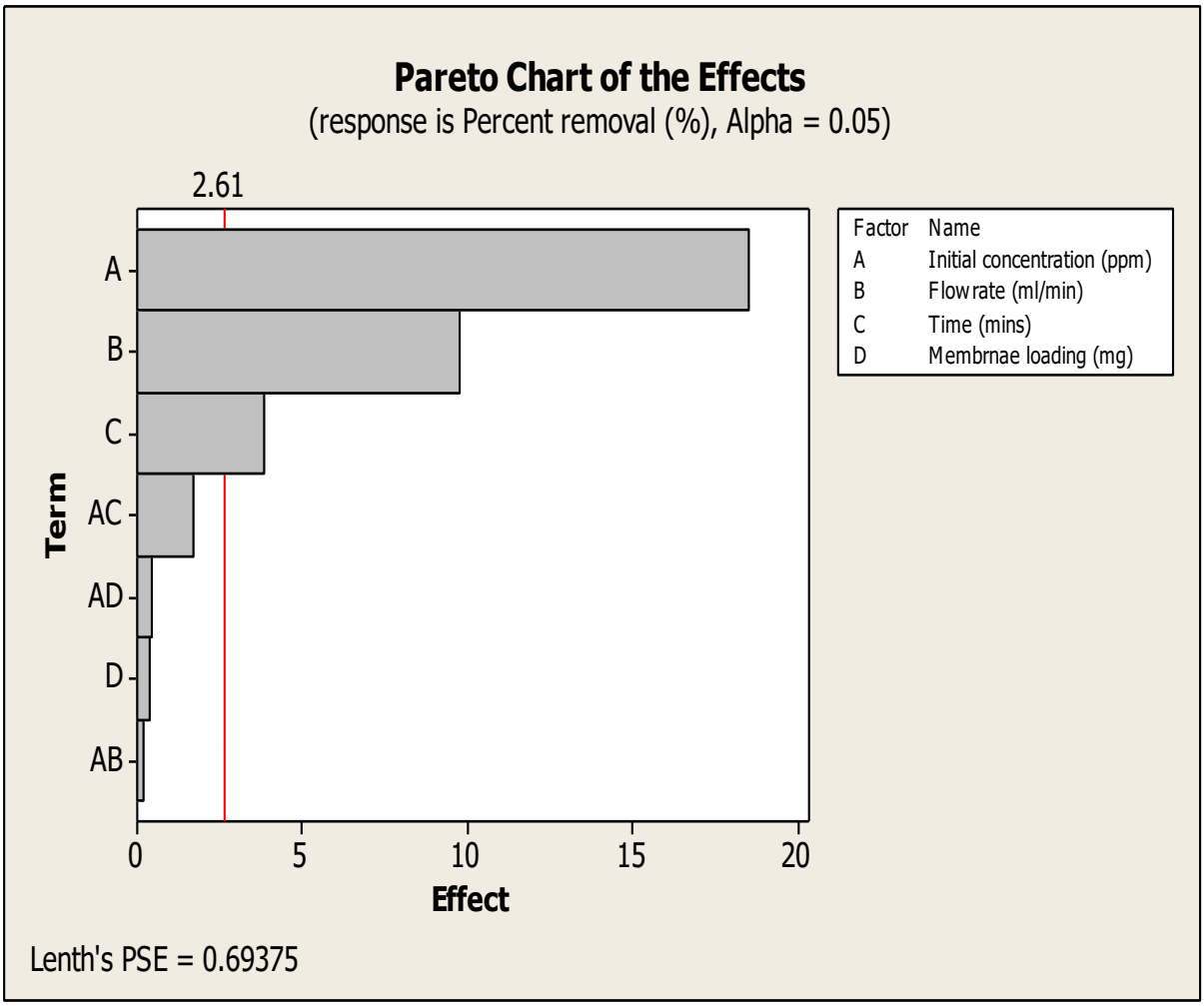

Figure 77: Main effect plot for percent removal of Hg (II) as obtained from Minitab 16

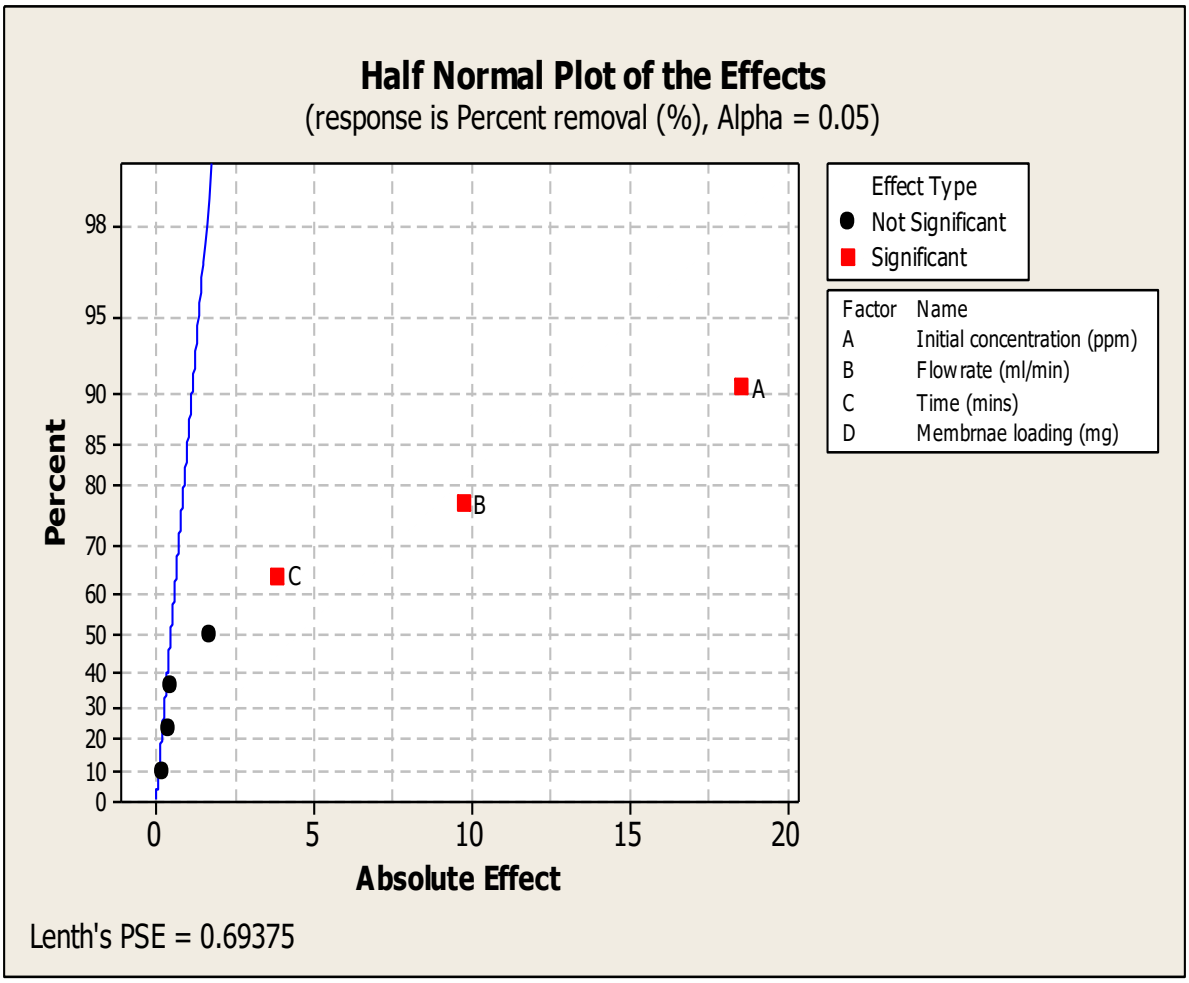

Figure 78: Half normal plot for percent removal of Hg (II) as obtained from Minitab 16

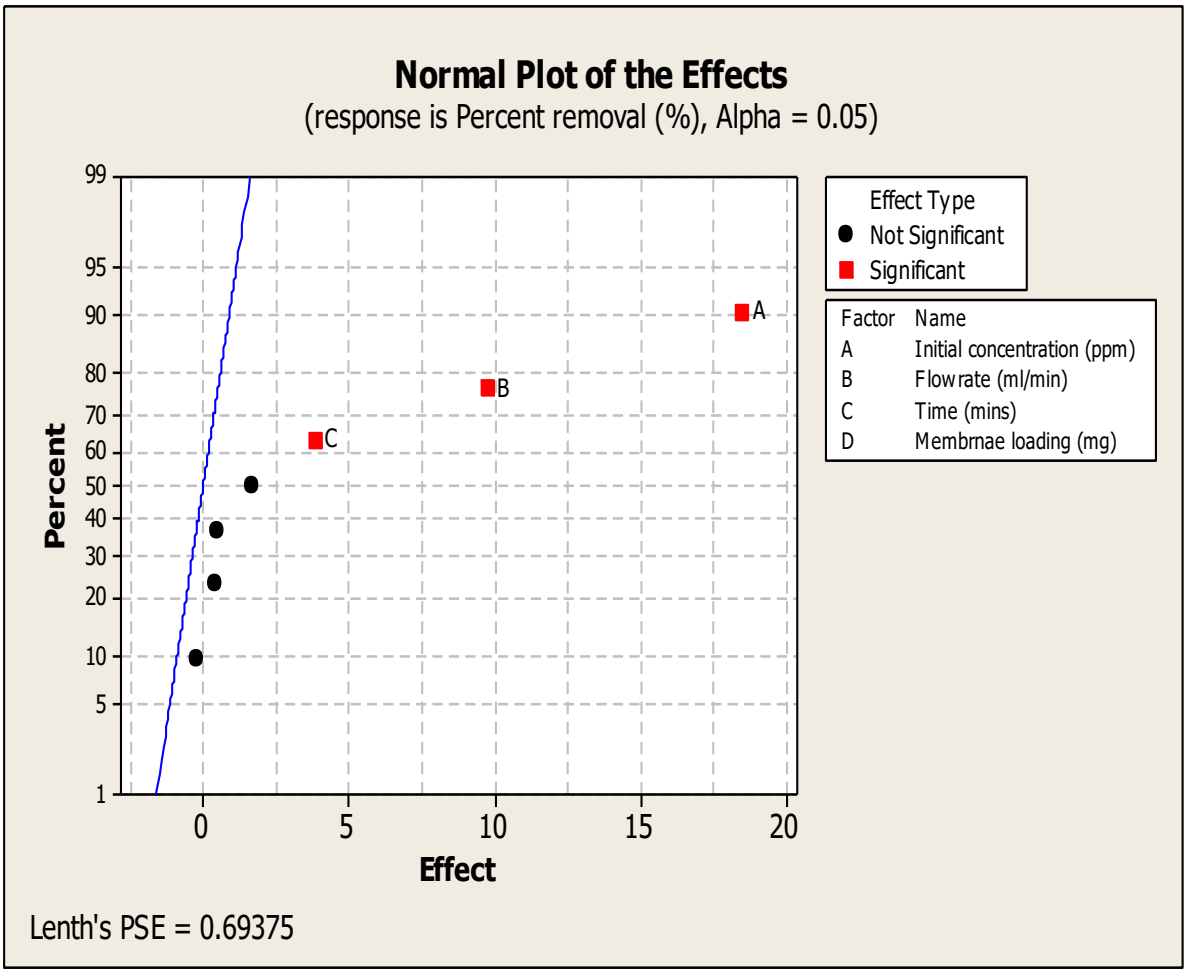

Figure 79: Main effect plot for percent removal of Hg (II) as obtained from Minitab 16

CHAPTER 5

CONCLUSIONS AND RECOMMENDATIONS

5.1 Conclusions

Overall, this research presents the biosynthesis of silver nanoparticles using extracts from basil leaves as well as the effects of various physico-chemical factors on the biosynthesis. It also proposes a method for the colorimetric detection of Hg (II) in an aqueous medium using unmodified silver nanoparticles. While the formation of biogenic synthesized silver nanoparticles is enhance by increased temperature, pH and time, maximum absorbance was obtained using 2mM concentration of the precursor and a 1:25 ratio of the broth concentration. The application of as-prepared silver nanoparticles in the detection of Hg (II) in water presents a simple and cost-effective detection method, especially in the absence of sophisticated instrumentation. For example, when silver nanoparticles were added to different concentrations of Hg (II), the color change could be detected using the naked eye or a UV-vis spectrophotometer. Furthermore, the selectivity of this method for detecting Hg (II) when other metallic cations are present was determine, and it was found that these biogenic synthesized AgNPs were both sensitive and selective. The better detection limit observed for these biogenic synthesized AgNPs, compared to detection limit for similar unmodified AgNPs may have arisen because of our choice of plant extract (basil), which allows for less nanoparticle aggolemeration and smaller particle size. Although the Hg (II) detection limit for these biogenic synthesized nanoparticles remains higher than the limits for chemically synthesized and modified silver nanoparticles used in

colorimetric Hg (II), our study still represents a step forward in the development of "green" chemistry to perform various chemical reactions and analysis.

Fe_2O_3 and nZVI were synthesized using myrtle and aloe vera plant extract respectively. The biosynthesized nanoparticles characterized using SEM shows that the biosynthesized NZVI are agglomerated while XRD result shows crystallinity of the synthesized nanoparticles. Further characterization was done using FTIR, EDX and TGA. The removal process was done in batch mode. The effects of contact time, agitation speed, pH and adsorbent dosage variation were investigated. The adsorbent shows good adsorption capacity to remove Hg (II) in water. The result also shows that pH, contact time, adsorbent dosage variation and agitation speed affects the removal of mercury (II) in water using Fe_2O_3 and NZVI. The results were evaluated using both Langmuir and Freundlich adsorption isotherm. The experimental data have higher R2 value for Langmuir adsorption isotherm and as such is considered homogeneous and monolayer according to Langmuir's adsorption. The results were also fitted to Pseudo second order and intraparticle diffusion kinetics models.

5.2 Recommendations

In order to scale up the research findings presented in this study. The following recommendations are made for subsequent studies;

I. Real water samples collected from different contaminated studies should be treated using similar adsorbent to ascertain the application of these adsorbents in real life situations

II. Different other environmental friendly polymer materials should also be tried. The use of other insoluble polymer membrane to support the adsorbent should be investigated.

III. Other biosynthesized nanoparticles should also be tried for the removal of Hg (II) from water

IV. Functionalization of the adsorbent presented in this study with biomaterials such as moringa oleifera can also be investigated.

REFERENCES

Ahmad, N., Sharma, S., Alam, M. K., Singh, V. N., Shamsi, S. F., Mehta, B. R., & Fatma, A. (2010). Rapid synthesis of silver nanoparticles using dried medicinal plant of basil. Colloids and Surfaces. B, Biointerfaces, 81(1), 81–6. http://doi.org/10.1016/j.colsurfb.2010.06.029

Allouche, J. (2013). Nanomaterials: A Danger or a Promise? (R. Brayner, F. Fiévet, & T. Coradin, Eds.). London: Springer London. http://doi.org/10.1007/978-1-4471-4213-3

Al-Saad, K. A., Amr, M. A., Hadi, D. T., Arar, R. S., Al-Sulaiti, M. M., Abdulmalik, T. A., … Kwak, J. C. (2012). Iron oxide nanoparticles : applicability for heavy metal removal from contaminated water, 45(2), 335–346.

Amin, M., Anwar, F., Janjua, M. R. S. A., Iqbal, M. A., & Rashid, U. (2012). Green Synthesis of Silver Nanoparticles through Reduction with Solanum xanthocarpum L. Berry Extract: Characterization, Antimicrobial and Urease Inhibitory Activities against Helicobacter pylori. International Journal of Molecular Sciences, 13(8), 9923–41. http://doi.org/10.3390/ijms13089923

Ashok, D. (2012). Rapid and green synthesis of silver nanoparticles using the leaf extracts of parthenium hysterophorus : a novel biological approach. international research journal of pharmacy, 3(2), 169–173.

Aslan K., Lakowicz, J.R., Geddes, C.D. (2004). Nanogold plasmon resonance based glucose sensing, Anal. Biochem. 330, 145–155.

Awwad, A. M., Salem, N. M., & Abdeen, A. O. (2013). Green synthesis of silver nanoparticles using carob leaf extract and its antibacterial activity. International Journal of Industrial Chemistry, (Figure 1), 2–7. Retrieved from http://www.industchem.com/content/4/1/29

Balaji, D. S., Basavaraja, S., Deshpande, R., Mahesh, D. B., Prabhakar, B. K., & Venkataraman, A. (2009). Extracellular biosynthesis of functionalized silver nanoparticles by strains of Cladosporium cladosporioides fungus. Colloids and Surfaces. B, Biointerfaces, 68(1), 88–92. http://doi.org/10.1016/j.colsurfb.2008.09.022

Bali, R., Razak, N., Lumb, a., & Harris, a. T. (2006). The synthesis of metallic nanoparticles inside live plants. 2006 International Conference on Nanoscience and Nanotechnology, 224–227. http://doi.org/10.1109/ICONN.2006.340592

Banerjee K., S. T. Ramesh, R. Gandhimathi, P. V Nidheesh, and K. S. Bharathi. (2012). A Novel Agricultural Waste Adsorbent , Watermelon Shell for the Removal of Copper from Aqueous Solutions. Iran. J. Energy Environ., vol. 3, no. 2, pp. 143–156.

Basavegowda, N., Sobczak-kupiec, A., Malina, D., Hs, Y., Keerthi, V., Chandrashekar, N.,

Liny, P. (2013). Plant mediated synthesis of gold nanoparticles using fruit extracts of ananas comosus (L .) (pineapple) and evaluation of biological activities, 4(5), 332–337. http://doi.org/10.5185/amlett.2012.9423

Bernalte, E., Marín Sánchez, C., & Pinilla Gil, E. (2011). Determination of mercury in ambient water samples by anodic stripping voltammetry on screen-printed gold electrodes. Analytica Chimica Acta, 689(1), 60–4. http://doi.org/10.1016/j.aca.2011.01.042

Bhatt, I., & Tripathi, B. N. (2011). Interaction of engineered nanoparticles with various components of the environment and possible strategies for their risk assessment. Chemosphere, 82(3), 308–17. http://doi.org/10.1016/j.chemosphere.2010.10.011

Bodaly, R. D., Rudd, W. M., & Flett, R. J. (1998). Effect of urban sewage treatment on total and methyl mercury concentrations in effluents. Biogeochemistry, 40(2-3), 279-291.

Bothra, S., Solanki, J. N., & Sahoo, S. K. (2013). Functionalized silver nanoparticles as chemosensor for pH, Hg2+ and Fe3+ in aqueous medium. Sensors and Actuators B: Chemical, 188, 937–943. http://doi.org/10.1016/j.snb.2013.07.111

Bothra, S., Solanki, J. N., Sahoo, S. K., & Callan, J. F. (2014). Anion-driven selective colorimetric detection of Hg 2+ and Fe 3+ using functionalized silver nanoparticles. RSC Advances, 4(3), 1341-1346.

Buzea, C., Pacheco, I. I., & Robbie, K. (2007). Nanomaterials and nanoparticles: Sources and toxicity. Biointerphases, 2(4), MR17. http://doi.org/10.1116/1.2815690

Chiarle, S., Ratto, M., & Rovattu, M. (2000). Mercury removal from water by ion exchange resins adsorption. Water Research, 34(11), 2971–2978. http://doi.org/10.1016/S0043-1354(00)00044-0

Chen, J. A., Zheng, A. Chen, Y. Gao, C. He, X. Kai, G. Wu, Y. Chen. (2007). A functionalized gold nanoparticles and Rhodamine 6G based fluorescent sensor for high sen- sitive and selective detection of mercury(II) in environmental water samples, Anal. Chim. Acta 599, 134–142.

Clercq, J. De. (2012). Removal of mercury from aqueous solutions by adsorption on a new ultra stable mesoporous adsorbent and on a commercial ion exchange resin. Int. J. Ind. Chem., vol. 3, no. 1, p. 1.

Coronado, E., Galan-Mascaros, J.R., Marti-Gastaldo,C., Palomares, E., Durrant, J.R. R. Vilar, M. Gratzel, M.K. Nazeeruddin. (2005). Reversible colorimetric probes for mercury sensing, J. Am. Chem. Soc. 127, 12351–12356.

Crespo-López, M. E., Macêdo, G. L., Pereira, S. I. D., Arrifano, G. P. F., Picanço-Diniz, D. L. W., do Nascimento, J. L. M., & Herculano, A. M. (2009). Mercury and human genotoxicity: critical considerations and possible molecular mechanisms. Pharmacological Research : The Official Journal of the Italian Pharmacological

Society, 60(4), 212–20. http://doi.org/10.1016/j.phrs.2009.02.011

Czaja, A. U., Trukhan, N., & Müller, U. (2009). Industrial applications of metal–organic frameworks. Chemical Society Reviews, 38(5), 1284-1293.

Das, S. K., Das, A. R., & Guha, A. K. (2007). A study on the adsorption mechanism of mercury on Aspergillus versicolor biomass. Environmental Science and Technology, 41(24), 8281–8287. http://doi.org/10.1021/es070814g

David W. Mazyck, A. M. H. and H. B. (2009). Aqueous Phase Mercury Removal: Strategies for a Secure Future Water Supply.

De Clercq, J. (2012). Removal of mercury from aqueous solutions by adsorption on a new ultra stable mesoporous adsorbent and on a commercial ion exchange resin. International Journal of Industrial Chemistry, 3(1), 1. http://doi.org/10.1186/2228-5547-3-1

Dehner, C., & Barton, L. (2010). Size-dependent bioavailability of hematite (α-Fe2O3) nanoparticles to a common aerobic bacterium. Environmental Science & …. Retrieved from http://pubs.acs.org/doi/abs/10.1021/es102922j

Dong, Y., Dong, W., Cao, Y., Han, Z., & Ding, Z. (2011). Preparation and catalytic activity of Fe alginate gel beads for oxidative degradation of azo dyes under visible light irradiation. Catalysis Today. Retrieved from http://www.sciencedirect.com/science/article/pii/S0920586111002446

Du, M., Zhang, Z. H., Zhao, X. J., & Xu, Q. (2006). Modulated preparation and structural diversification of ZnII and CdII metal-organic frameworks with a versatile building block 5-(4-pyridyl)-1, 3, 4-oxadiazole-2-thiol. Inorganic chemistry, 45(15), 5785-5792.

Dubey, S. P., Dwivedi, A. D., Lahtinen, M., Lee, C., Kwon, Y.-N., & Sillanpaa, M. (2013). Protocol for development of various plants leaves extract in single-pot synthesis of metal nanoparticles. Spectrochimica Acta Part A: Molecular and Biomolecular Spectroscopy, 103, 134–142. http://doi.org/10.1016/j.saa.2012.11.021

Durán, N., Marcato, P. D., Alves, O. L., Souza, G. I. H. De, & Esposito, E. (2005). Mechanistic aspects of biosynthesis of silver nanoparticles by several Fusarium oxysporum strains. Journal of Nanobiotechnology, 3, 8. http://doi.org/10.1186/1477-3155-3-8

Elumalai, E. K., Prasad, T. N. V. K. V, Hemachandran, J., & Therasa, S. V. (2010). Extracellular synthesis of silver nanoparticles using leaves of Euphorbia hirta and their antibacterial activities. Journal ofPharmaceutical Sciences and Research, 2(9), 549–554.

Fu, F., & Wang, Q. (2011). Removal of heavy metal ions from wastewaters: a review. Journal of Environmental Management, 92(3), 407–18. http://doi.org/10.1016/j.jenvman.2010.11.011

Geethalakshmi, R., & Sarada, D. V. L. (2010). Synthesis of plant-mediated silver nanoparticles using Trianthema decandra extract and evaluation of their anti microbial activities, 2(5), 970–975.

Giasuddin, A., Kanel, S., & Choi, H. (2007). Adsorption of humic acid onto nanoscale zerovalent iron and its effect on arsenic removal. Environmental Science & …. Retrieved from http://pubs.acs.org/doi/abs/10.1021/es0616534

Hadavifar, M., Bahramifar, N., Younesi, H., & Li, Q. (2014). Adsorption of mercury ions from synthetic and real wastewater aqueous solution by functionalized multi-walled carbon nanotube with both amino and thiolated groups. Chemical Engineering Journal, 237, 217-228

Hardani, K., Buazar, F., & Ghanemi, K. (n.d.). Removal of Toxic Mercury (II) from Water via Fe3O4/Hydroxyapatite Nanoadsorbent: An Efficient, Economic and Rapid Approach. Researchgate.net. Retrieved from https://www.researchgate.net/profile/Mohammad_Badri3/publication/274085722_Removal_of_Toxic_Mercury_(II)_from_Water_via_Fe_3_O_4_Hydroxyapatite_Nanoadsorbent_An_Efficient_Economic_and_Rapid_Approach_Citation/links/551668180cf2f7d80a373480.pdf

Holmes, P., James, K. a F., & Levy, L. S. (2009). Is low-level environmental mercury exposure of concern to human health? The Science of the Total Environment, 408(2), 171–82. http://doi.org/10.1016/j.scitotenv.2009.09.043

Hua Ming, Shujuan Zhang, Bingcai Pan, Weiming Zhang, Lu Lv, Quanxing Zhang. (2012). Heavy metal removal from water/wastewater by nanosized metal oxides: A review. Journal of Hazardous Materials. 211–212:317–331

Huang, C. C., & Chang, H. T. (2006). Selective gold-nanoparticle-based "turn-on" fluorescent sensors for detection of mercury (II) in aqueous solution. Analytical Chemistry, 78(24), 8332-8338.

Huang, J., Lin, L., Sun, D., Chen, H., Yang, D., & Li, Q. (2015). Bio-inspired synthesis of metal nanomaterials and applications. Chemical Society Reviews, 44, 6330–6374. http://doi.org/10.1039/c5cs00133a

Hussein, H. K., Abu-zinadah, O. A., Abdel, H., & El, S. (2011). Environmental assessment of ground water pollution by heavy metals and bioaccumulation of mercury residues in chicken tissues. African Journal of Biotechnology, 10(71), 16089–16100. http://doi.org/10.5897/AJB11.2694

Iravani, S., & Zolfaghari, B. (2013). Green synthesis of silver nanoparticles using Pinus eldarica bark extract. BioMed Research International, 2013, 639725. http://doi.org/10.1155/2013/639725

Jamil N., Munawar M. A., S. Badar, and Sidra-Tul-Muntaha. (2009). Biosorption of Hg(II) and Cd(II) from Waste Water by using Zea Mays Waste. J. Chem. Soc. Pakistan, vol. 31, no. 3.

Jesus M. de la Fuente, G. V. (2012). Nanobiotechnology. (G. V. Jesus M. de la Fuente, Ed.). Elsevier The Boulevard, Langford Lane, Kidlington, Oxford OX5 1GB, UK Radarweg 29, PO Box 211, 1000 AE Amsterdam, The Netherlands.

Jha, A. K., Prasad, K., & Prasad, K. (2009). A green low-cost biosynthesis of Sb2O3 nanoparticles. Biochemical Engineering Journal, 43(3), 303–306. http://doi.org/10.1016/j.bej.2008.10.016

Kanel, S., & Manning, B. (2005). Removal of arsenic (III) from groundwater by nanoscale zero-valent iron. Environmental Science & …. Retrieved from http://pubs.acs.org/doi/abs/10.1021/es048991u

Katok, K. V, Whitby, R. L. D., Fukuda, T., Maekawa, T., Bezverkhyy, I., Mikhalovsky, S. V, & Cundy, A. B. (2012). Hyperstoichiometric interaction between silver and mercury at the nanoscale. Angewandte Chemie (International Ed. in English), 51(11), 2632–5. http://doi.org/10.1002/anie.201106776

Ke, F., Qiu, L. G., Yuan, Y. P., Peng, F. M., Jiang, X., Xie, A. J., ... & Zhu, J. F. (2011). Thiol-functionalization of metal-organic framework by a facile coordination-based postsynthetic strategy and enhanced removal of Hg 2+ from water. Journal of hazardous materials, 196, 36-43.

Khalil, A. (2013). Antimicrobial Activity of Ethanolic Extracts of Ocimum basilicum leaf from Saudi Arabia. Biotechnology.

Khalil, M. M. H., Ismail, E. H., El-Baghdady, K. Z., & Mohamed, D. (2013). Green synthesis of silver nanoparticles using olive leaf extract and its antibacterial activity. Arabian Journal of Chemistry. http://doi.org/10.1016/j.arabjc.2013.04.007

Khan, N. A., Hasan, Z., & Jhung, S. H. (2013). Adsorptive removal of hazardous materials using metal-organic frameworks (MOFs): a review. Journal of hazardous materials, 244, 444-456.

Kim, I. B., & Bunz, U. H. (2006). Modulating the sensory response of a conjugated polymer by proteins: an agglutination assay for mercury ions in water. Journal of the American Chemical Society, 128(9), 2818-2819.

Kumar, K. V. (2007). Optimum sorption isotherm by linear and non-linear methods for malachite green onto lemon peel. Dyes and Pigments, 74(3), 595–597. http://doi.org/10.1016/j.dyepig.2006.03.026

Kutty, P. C. M., Nomani, A. A., Al-sulami, S., & Al-rabeh, A. (1995). Monitoring of trace metals in desalinated drinking water and their permissible levels. In IDA conference, Abu Dhabi (pp. 1180–1190). Al-Jubail 31951.

Lagergren, S. (1898). Zur theorie der sogenannten adsorption gelˆster stoffe, Kungliga Svenska Vetenskapsakademiens. Handlingar. 24 (4), 1-39. Microchemical Journal Environ. Sci. Technol. J. Colloid.

Lee, J.S., Han, M.S., Mirkin, C.A.(2007). Colorimetric detection of mercuric ion (Hg2+)

in aqueous media using DNA-functionalized gold nanoparticles, Angew. Chem. Int. Ed. 46, 4093–4096.

Leopold, K., Foulkes, M., & Worsfold, P. (2010). Methods for the determination and speciation of mercury in natural waters--a review. Analytica Chimica Acta, 663(2), 127–38. http://doi.org/10.1016/j.aca.2010.01.048

Lisha, K. P., & Pradeep, T. (2009, June). Towards a practical solution for removing inorganic mercury from drinking water using gold nanoparticles. Gold Bulletin, 42(2), 144–152. http://doi.org/10.1007/BF03214924

Liu, J., & Lu, Y. (2007). Rational Design of "Turn-On" Allosteric DNAzyme Catalytic Beacons for Aqueous Mercury Ions with Ultrahigh Sensitivity and Selectivity. Angewandte Chemie, 119(40), 7731-7734.

Liu, X., Tang, Y., Wang, L., Zhang, J., Song, S., Fan, C., & Wang, S. (2007). Optical detection of mercury (II) in aqueous solutions by using conjugated polymers and label-free oligonucleotides. Advanced Materials, 19(11), 1471-1474.

Malato, S., Fernández-Ibáñez, P., Maldonado, M. I., Blanco, J., & Gernjak, W. (2009). Decontamination and disinfection of water by solar photocatalysis: Recent overview and trends. Catalysis Today, 147(1), 1–59. http://doi.org/10.1016/j.cattod.2009.06.018

Maria, B. S., Devadiga, A., Kodialbail, V. S., & Saidutta, M. B. (2015). Synthesis of silver nanoparticles using medicinal Zizyphus xylopyrus bark extract. Applied Nanoscience, 5(6), 755-762.

Manahan, S. E. (2004). Environmental chemistry, eighth edition. CRC Press. Retrieved from http://www.amazon.co.uk/Environmental-chemistry-edition-Stanley-Manahan/dp/1566706335

Mazyck, David W.Hagan, A. M., & Byrne, H. (2009). Aqueous Phase Mercury Removal : Strategies for a Secure Future Water Supply Critical National Need Idea White Paper.

Meena A. K., G. K. Mishra, S. Kumar, and C. Rajagopal. (2004). Low-cost Adsorbents for the Removal of Mercury (11) from Aqueous Solution-A Comparative Study, vol. 54, no. 4, pp. 537–548.

Miretzky, P., & Cirelli, A. F. (2009). Hg (II) removal from water by chitosan and chitosan derivatives: a review. Journal of hazardous materials, 167(1), 10-23.

Mittal, A. K., Chisti, Y., & Banerjee, U. C. (2013). Synthesis of metallic nanoparticles using plant extracts. Biotechnology Advances, 31(2), 346–56. http://doi.org/10.1016/j.biotechadv.2013.01.003

Mohan D., Gupta V. , S. . Srivastava, and S. Chander. (2001). Kinetics of mercury adsorption from wastewater using activated carbon derived from fertilizer waste," Colloids Surfaces A Physicochem. Eng. Asp., vol. 177, no. 2–3, pp. 169–181.

MubarakAli, D., Thajuddin, N., Jeganathan, K., & Gunasekaran, M. (2011). Plant extract mediated synthesis of silver and gold nanoparticles and its antibacterial activity against clinically isolated pathogens. Colloids and Surfaces. B, Biointerfaces, 85(2), 360–5. http://doi.org/10.1016/j.colsurfb.2011.03.009

Murali Sastry, Absar Ahmad, M. I. K. and R. K. (2003). Biosynthesis of metal nanoparticles using fungi and actinomycete.pdf. Current Science, 85(2).

Nowack, B., & Bucheli, T. D. (2007). Occurrence, behavior and effects of nanoparticles in the environment. Environmental Pollution (Barking, Essex : 1987), 150(1), 5–22. http://doi.org/10.1016/j.envpol.2007.06.006

Namasivayam, C., & Kadirvelu, K. (1999). Uptake of mercury (II) from wastewater by activated carbon from an unwanted agricultural solid by-product: coirpith. Carbon, 37(1), 79-84.

Nwabanne, J., & Igbokwe, P. (2008). Kinetics and equilibrium modeling of nickel adsorption by cassava peel. J Eng Appl Sci. Retrieved from http://docsdrive.com/pdfs/medwelljournals/jeasci/2008/829-834.pdf

Pacheco, S., Medina, M., Valencia, F., & Tapia, J. (2006). Removal of Inorganic Mercury from Polluted Water Using Structured Nanoparticles, (March), 342–349.

Pan, J. T., Zhu, F., Kong, L., Yang, L. M., Tao, X. T., Tian, Y. P., ... & Yang, J. X. (2015). A simple pyridine-based colorimetric chemosensor for highly sensitive and selective mercury (II) detection with the naked eye. Chemical Papers, 69(4), 527-535.

Parham, H., Zargar, B., & Shiralipour, R. (2012). Fast and efficient removal of mercury from water samples using magnetic iron oxide nanoparticles modified with 2-mercaptobenzothiazole. Journal of Hazardous Materials, 205-206, 94–100. http://doi.org/10.1016/j.jhazmat.2011.12.026

Philip, D., & Unni, C. (2011). Extracellular biosynthesis of gold and silver nanoparticles using Krishna tulsi (Ocimum sanctum) leaf. Physica E: Low-Dimensional Systems and Nanostructures, 43(7), 1318–1322. http://doi.org/10.1016/j.physe.2010.10.006

Perry Iv, J. J., Perman, J. A., & Zaworotko, M. J. (2009). Design and synthesis of metal–organic frameworks using metal–organic polyhedra as supermolecular building blocks. Chemical Society Reviews, 38(5), 1400-1417.

Pilehrood, M., Heikkilä, P., & Harlin, A. (2012). Preparation of carbon nanotube embedded in polyacrylonitrile (pan) nanofibre composites by electrospinning process. AUTEX Research Journal. Retrieved from http://www.degruyter.com/view/j/aut.2012.12.issue-1/v10304-012-0001-0/v10304-012-0001-0.xml

Prathna T.C., L. M. N. C. A. M. R. and A. M. (2010). Biomimetics Learning from Nature. (A. Mukherjee, Ed.). InTech. http://doi.org/10.5772/198

Ramteke, C., Chakrabarti, T., Sarangi, B. K., & Pandey, R.-A. (2013). Synthesis of Silver

Nanoparticles from the Aqueous Extract of Leaves of Ocimum sanctum for Enhanced Antibacterial Activity. Journal of Chemistry, 2013, 1–7. http://doi.org/10.1155/2013/278925

Rao M. M., Reddy D. H. K. K., Venkateswarlu, P., and Seshaiah, K.. (2009). Removal of mercury from aqueous solutions using activated carbon prepared from agricultural by-product/waste.," J. Environ. Manage., vol. 90, no. 1, pp. 634–43.

Rao, G. P., Lu, C., & Su, F. (2007). Sorption of divalent metal ions from aqueous solution by carbon nanotubes: a review. Separation and Purification Technology, 58(1), 224-231.

Rastogi, L., & Arunachalam, J. (2011). Sunlight based irradiation strategy for rapid green synthesis of highly stable silver nanoparticles using aqueous garlic (Allium sativum) extract and their antibacterial potential. Materials Chemistry and Physics, 129(1-2), 558–563. http://doi.org/10.1016/j.matchemphys.2011.04.068

Rastogi, L., Sashidhar, R. B., Karunasagar, D., & Arunachalam, J. (2014). Gum kondagogu reduced/stabilized silver nanoparticles as direct colorimetric sensor for the sensitive detection of Hg^{2+} in aqueous system. Talanta, 118, 111–7. http://doi.org/10.1016/j.talanta.2013.10.012.

Rex, M., Hernandez, F.E., Campiglia, A.D. (2006). Pushing the limits of mercury sensors with gold nanorods, Anal. Chem. 78, 445–451.

Rivera-Utrilla J., M. Sánchez-Polo, V. Gómez-Serrano, P.M. Álvarez, M.C.M. Alvim-Ferraz, J.M. Dias. (2011). Activated carbon modifications to enhance its water treatment applications. An overview. Journal of Hazardous Materials, 187:1–23

Roquerol, F., J. Roquerol K. S., W. Sing, P. Llewellyn, G. Maurin (2014). Adsorption by powders and porous solids: Principles, Methodology and Application. 2nd Edition Elsevier UK.

Ros-Lis, J.V., Marcos, M.D., Máˇnez,R.M., K. Rurack, J. Soto. (2005). A regenerative chemo-dosimeter based on metal-induced dye formation for the highly selective and sensitive optical determination of Hg2+ ions, Angew. Chem. Int. Ed. 44 4405–4407.

Sahayaraj, K., & Rajesh, S. (2011). Bionanoparticles : synthesis and antimicrobial applications, 228–244.

Sahoo, S. K., Agarwal, K., Singh, a K., Polke, B. G., & Raha, K. C. (2010). Characterization of γ- and α-Fe 2 O 3 nano powders synthesized by emulsion precipitation-calcination route and rheological behaviour of α-Fe 2 O 3. Science And Technology, 2(8), 118–126. http://doi.org/10.4314/ijest.v2i8.63841

Sarfaraz Khan Marwat, Muhammed Aslam Khan, Fazal-ur-Rehman, Abdul Hakim Akbari, Muhammad Shoaib, M. A. S. (2011). Interpretation and Medicinal Potential of Ar-Rehan (Ocimum basilicum)-A Review.pdf. Journal of Agricultural and Environmental Science, 10(4).

Saware, K., Sawle, B., & Salimath, B. (2014). Biosynthesis and Characterization of Silver Nanoparticles using Ficus benghalensis Leaf Extract. … Journal of Research …. Retrieved from http://esatjournals.net/ijret/2014v03/i05/IJRET20140305158.pdf

Selin, N. E. (2009). Global Biogeochemical Cycling of Mercury: A Review. Annual Review of Environment and Resources, 34(1), 43–63. http://doi.org/10.1146/annurev.environ.051308.084314

Shadbad, M. J., Mohebbi, A., & Soltani, A. (2011). Mercury(II) removal from aqueous solutions by adsorption on multi-walled carbon nanotubes. Korean Journal of Chemical Engineering, 28(4), 1029–1034. http://doi.org/10.1007/s11814-010-0463-5

Skubal, L. R., & Meshkov, N. K. (2002). Reduction and removal of mercury from water using arginine-modified TiO 2, 148, 211–214.

Song, J. Y., Jang, H.-K., & Kim, B. S. (2009). Biological synthesis of gold nanoparticles using Magnolia kobus and Diopyros kaki leaf extracts. Process Biochemistry, 44(10), 1133–1138. http://doi.org/10.1016/j.procbio.2009.06.005

Song, J. Y., & Kim, B. S. (2009). Rapid biological synthesis of silver nanoparticles using plant leaf extracts. Bioprocess and Biosystems Engineering, 32(1), 79–84. http://doi.org/10.1007/s00449-008-0224-6

Sumesh, E., Bootharaju, M. S., Anshup, & Pradeep, T. (2011). A practical silver nanoparticle-based adsorbent for the removal of Hg2+ from water. Journal of Hazardous Materials, 189(1-2), 450–7. http://doi.org/10.1016/j.jhazmat.2011.02.061

Sundaram, P. A., Augustine, R., & Kannan, M. (2012). Extracellular biosynthesis of iron oxide nanoparticles by Bacillus subtilis strains isolated from rhizosphere soil. Biotechnology and Bioprocess Engineering, 17(4), 835–840. http://doi.org/10.1007/s12257-011-0582-9

Taha, M., & Ibrahim, A. (2014). Characterization of nano zero-valent iron (nZVI) and its application in sono-Fenton process to remove COD in palm oil mill effluent. Journal of Environmental Chemical Engineering. Retrieved from http://www.sciencedirect.com/science/article/pii/S2213343713002376

Tawabini, B. S., Al-Khaldi, S. F., Khaled, M. M., & Atieh, M. a. (2011). Removal of arsenic from water by iron oxide nanoparticles impregnated on carbon nanotubes. Journal of Environmental Science and Health. Part A, Toxic/hazardous Substances & Environmental Engineering, 46(3), 215–23. http://doi.org/10.1080/10934529.2011.535389

Vanaja, M., Gnanajobitha, G., Paulkumar, K., Rajeshkumar, S., Malarkodi, C., & Annadurai, G. (2013). Phytosynthesis of silver nanoparticles by Cissus quadrangularis: influence of physicochemical factors. Journal of Nanostructure in Chemistry, 3(1), 17. http://doi.org/10.1186/2193-8865-3-17

Vijayaraghavan, K., & Padmesh, T. (2006). Biosorption of nickel (II) ions onto Sargassum

wightii: application of two-parameter and three-parameter isotherm models. Journal of Hazardous

Wang, Z., & Cohen, S. M. (2009). Postsynthetic modification of metal–organic frameworks. Chemical Society Reviews, 38(5), 1315-1329.

Watts, M., Coker, V., & Parry, S. (2015). Biogenic nano-magnetite and nano-zero valent iron treatment of alkaline Cr (VI) leachate and chromite ore processing residue. Applied …. Retrieved from http://www.sciencedirect.com/science/article/pii/S088329271400300X

Yantasee, W., Warner, C. L., Sangvanich, T., Addleman, R. S., Carter, T. G., Wiacek, R. J., … Warner, M. G. (2007). Removal of heavy metals from aqueous systems with thiol functionalized superparamagnetic nanoparticles. Environmental Science & Technology, 41(14), 5114–9. Retrieved from http://www.ncbi.nlm.nih.gov/pubmed/17711232

Yardim, M. F., Budinova, T., Ekinci, E., Petrov, N., Razvigorova, M., & Minkova, V. (2003). Removal of mercury (II) from aqueous solution by activated carbon obtained from furfural. Chemosphere, 52(5), 835-841.

Yoon, S., Albers,A.E., Wong, A.P., Chang, C.J. (2005). Screening mercury levels in fish with a selective fluorescent chemosensor, J. Am. Chem. Soc. 127, 16030–16031.

Yu, W.-J., Hou, P.-X., Zhang, L.-L., Li, F., Liu, C., & Cheng, H.-M. (2010). Preparation and electrochemical property of Fe2O3 nanoparticles-filled carbon nanotubes. Chemical Communications (Cambridge, England), 46(45), 8576–8. http://doi.org/10.1039/c0cc02121k

Zahir, F., Rizwi, S. J., Haq, S. K., & Khan, R. H. (2005). Low dose mercury toxicity and human health. Environmental Toxicology and Pharmacology, 20(2), 351–60. http://doi.org/10.1016/j.etap.2005.03.007

Zhang, F.-S., Nriagu, J. O., & Itoh, H. (2004). Photocatalytic removal and recovery of mercury from water using TiO2-modified sewage sludge carbon. Journal of Photochemistry and Photobiology A: Chemistry, 167(2-3), 223–228. http://doi.org/10.1016/j.jphotochem.2004.06.001

Zhang, F.-S., Nriagu, J. O., & Itoh, H. (2005). Mercury removal from water using activated carbons derived from organic sewage sludge. Water Research, 39(2-3), 389–95. http://doi.org/10.1016/j.watres.2004.09.027

Zhao,Y.., Zhong, Z. (2006). Tuning the sensitivity of a foldamer-based mercury sensor by its folding energy, J. Am. Chem. Soc. 128, 9988–9989.

Zhou, W., He, W., Ma, J., Wang, M., Zhang, X., Yan, S., Tian, X., Sun, X., Han, X. (2009). Biosynthesis of mesoporous organic–inorganic hybrid Fe2O3 with high photocatalytic activity. *Materials Science and Engineering: C*, *29*(6), 1893–1896. http://doi.org/10.1016/j.msec.2009.02.019

Zhu, X.J., Fu, S.T., Wong, W.K., J.P. Guo, W.Y. Wong. (2006). A near-infrared-fluorescent chemodosimeter for mercuric ion based on an expanded porphyrin, Angew. Chem. Int. Ed. 45, 3150–3154.

Zohdi, N., Mahdavi, F., Abdullah, L. C., & Choong, T. S. Y. (2014). Environmental health Removal of boron from aqueous solution using magnetic carbon nanotube improved with tartaric acid, 1–12.

Vitae

Name	: **SALAWU OMOBAYO ADIO**
Nationality	: NIGERIAN
Date of Birth	:8/13/1989
Email	: saomobayonle@yahoo.com; saomobayonle@gmail.com
Address	: Centre for Water and Environment Development, Nigeria
Academic Background	B. Eng. Agricultural and Environmental Resources Engineering, University of Maiduguri, Nigeria, 2011.

SOME SUBMITTED ARTICLES

International Journal of Environmental Analytical Chemistry; Manuscript ID GEAC-2015-0385 “Biosynthesized Silver Nanoparticles; Study of the effect of physicochemical parameters and application as nanosensor in the colorimetric detection of Hg (II) in water” - **Accepted**

Patent Submission; Method for detecting Hg (II) in an aqueous solution. Docket Number: 453661US8